CHALMERS UNIVERSITY OF TECHNOLOGY
Gothenburg, Sweden
www.chalmers.se

CHALMERS UNIVERSITY OF TECHNOLOGY

PHD THESIS

Optical networks form the high-speed highways that carry digital information across the globe. As our world becomes more connected—through video streaming, remote work, cloud computing, and emerging smart services—these networks must handle ever-growing amounts of data. New architectural choices and network control methods are needed to accommodate such dynamic traffic efficiently, reliably, and at an acceptable cost. This thesis explores three key approaches.
First, it investigates programmable filterless optical networks, an architecture that removes costly optical filters from intermediate nodes. By dynamically tuning the spectrum and enabling flexible lightpath selection, operators can reduce infrastructure costs and energy consumption while meeting diverse service needs. Second, the thesis proposes intelligent spectrum defragmentation techniques—an automated way to reorganize spectrum allocations so that fewer small slots go unused. Third, it considers the optical signal quality and spectrum fragmentation when deciding how to route connections and assign resources, preventing service blocking.
Taken together, these approaches serve as building blocks for next-generation optical networks. They enable flexible resource provisioning, and automated operations—improving energy and cost efficiency. The solutions proposed in this thesis form a step toward automated, high-performance optical networks able to meet the rising demands of our increasingly digital society.

CHALMERS
UNIVERSITY OF TECHNOLOGY

EHSAN ETEZADI • Efficient and intelligent resource allocation in optical networks • 2025

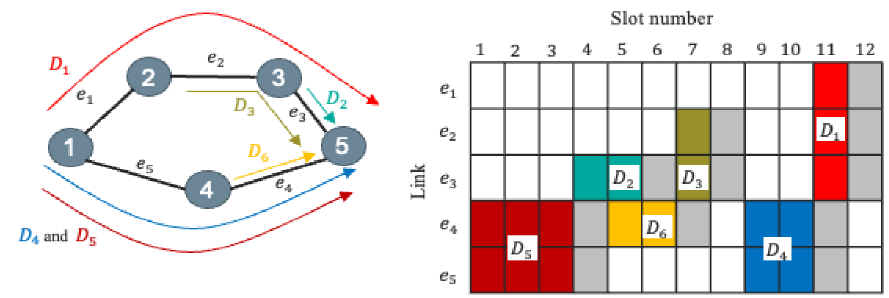

Efficient and intelligent resource allocation in optical networks

Electrical Engineering department, Chalmers University of Technology

EHSAN ETEZADI

DEPARTMENT OF ELECTRICAL ENGINEERING
CHALMERS UNIVERSITY OF TECHNOLOGY
Gothenburg, Sweden 2025
www.chalmers.se

THESIS FOR THE DEGREE OF DOCTOR OF PHILOSOPHY

Efficient and intelligent resource allocation in optical networks

Electrical Engineering department, Chalmers University of Technology

Ehsan Etezadi

Department of Electrical Engineering
Chalmers University of Technology
Gothenburg, Sweden, 2025

Efficient and intelligent resource allocation in optical networks
Electrical Engineering department, Chalmers University of Technology

Ehsan Etezadi
ISBN 978-91-8103-213-0

Acknowledgements, dedications, and similar personal statements in this thesis, reflect the author's own views.

Doktorsavhandlingar vid Chalmers tekniska högskola
Ny serie nr 5671
ISSN 0346-718X

Department of Electrical Engineering
Chalmers University of Technology
SE-412 96 Gothenburg, Sweden
Phone: +46 (0)31 772 1000

Printed by Chalmers Digital Printing
Gothenburg, Sweden, May 2025

Efficient and intelligent resource allocation in optical networks

Electrical Engineering department, Chalmers University of Technology

EHSAN ETEZADI
Department of Electrical Engineering
Chalmers University of Technology

Abstract

The exponential growth in bandwidth demand, driven by emerging network services with diverse requirements, necessitates a cost-efficient design and effective resource management in optical networks. This requires approaches that enhance network architecture flexibility, spectrum usage efficiency, and automation while maintaining low operational costs. The thesis addresses these challenges through three key contributions: developing a cost-efficient network planning approach, introducing machine learning-based approaches for dynamic resource reallocation, and extending resource management strategies to multi-band elastic optical networks (EONs) to improve spectrum usage efficiency.

To optimize resource utilization while maintaining network flexibility, the thesis studies programmable filterless optical networks (PFONs), an architecture that replaces conventional reconfigurable optical add-drop multiplexers with programmable optical white box switches. The routing, modulation format, and spectrum assignment problem in PFONs is formulated as an integer linear program aimed at minimizing spectrum and passive optical component usage. Simulation results show a 54% reduction in spectrum dissipation compared to passive filterless optical networks, while also achieving greater cost efficiency over conventional wavelength-switched optical networks.

A significant obstacle to efficient resource usage in dynamic single- and multi-band EONs is spectrum fragmentation (SF), where arrivals and departures of service requests leave stranded, unusable gaps in the available spectrum. To alleviate SF, we introduce DeepDefrag, a novel deep reinforcement learning-based framework designed to address spectrum defragmentation (SD) challenges. DeepDefrag dynamically determines appropriate timing for SD, selects connections to be reconfigured, and identifies suitable parts of the spectrum for reallocation. Through intelligent decision-making, DeepDefrag outperforms traditional heuristic algorithms, such as the older first-fit algorithm, by achieving a lower service blocking ratio (SBR) and minimizing the control overhead associated with SD.

To further extend resource management to multi-band EONs, where different achievable quality of transmission (QoT) levels across different bands exacerbate fragmentation, the thesis proposes a fragmentation- and QoT-aware routing, band, modulation format and spectrum assignment algorithm. The approach integrates proactive SD and traffic re-grooming to improve spectral efficiency. Simulations on three network topologies demonstrate a significant reduction in both SBR and spectrum fragmentation compared to QoT-only benchmarks, albeit with a slight increase in the average path length.

Keywords: Programmable filterless optical networks, Spectrum fragmentation, Proactive defragmentation, Multi-band elastic optical network

To my family

List of Publications

This thesis is based on the following publications:

[A] **Ehsan Etezadi**, Carlos Natalino, Christine Tremblay, Lena Wosinska, Marija Furdek, "Programmable Filterless Optical Networks: Architecture, Design and Resource Allocation". Published in IEEE/ACM Transactions on Networking, 2024.

[B] **Ehsan Etezadi**, Carlos Natalino, Renzo Diaz, Anders Lindgren, Stefan Melin, Lena Wosinska, Paolo Monti, Marija Furdek, "DeepDefrag: A deep reinforcement learning framework for spectrum defragmentation". IEEE Global Communications Conference (GLOBECOM), 2022.

[C] **Ehsan Etezadi**, Carlos Natalino, Renzo Diaz, Anders Lindgren, Stefan Melin, Lena Wosinska, Paolo Monti, Marija Furdek, "Deep reinforcement learning for proactive spectrum defragmentation in elastic optical networks [Invited]". Published in Journal of Optical Communications and Networking (JOCN), 2023.

[D] **Ehsan Etezadi**, Carlos Natalino, Vignesh Karunakaran, Renzo Diaz, Anders Lindgren, Stefan Melin, Achim Autenrieth, Lena Wosinska, Paolo Monti, Marija Furdek, "Demonstration of DRL-based intelligent spectrum management over a T-API-enabled optical network digital twin". 49th European Conference on Optical Communications (ECOC), 2023.

[E] **Ehsan Etezadi**, Farhad Arpanaei, Carlos Natalino, Lena Wosinska, Erik Agrell, Paolo Monti, David Larrabeiti, Marija Furdek, "Joint Fragmentation- and QoT-Aware RBMSA in Dynamic Multi-Band Elastic Optical Networks". 24th International Conference on Transparent Optical Networks (ICTON), 2024.

[F] **Ehsan Etezadi**, Farhad Arpanaei, Carlos Natalino, Erik Agrell, Paolo Monti, José Alberto Hernández, Marija Furdek, "Fragmentation- and QoT-Aware RBMSA with Spectrum Defragmentation in Dynamic Multi-Band Elastic Optical Networks". Submitted to the Journal of Lightwave Technology.

Other publications by the author, not included in this thesis, are:

[G] **Ehsan Etezadi**, Carlos Natalino, Renzo Diaz, Anders Lindgren, Stefan Melin, Lena Wosinska, Paolo Monti, Marija Furdek, "Proactive Spectrum Defragmentation Leveraging Spectrum Occupancy State Information". *23rd International Conference on Transparent Optical Networks (ICTON)*, Bucharest, Romania, 2023.

[H] Aryanaz Attarpour, **Ehsan Etezadi**, Memedhe Ibrahimi, Francesco Musumeci, Andrea Castoldi, Marija Furdek, Massimo Tornatore, "On the Benefits of Programmable FON for Low-cost OTN-over-WDM Metro Networks". *29th International Conference on Optical Network Design and Modeling (ONDM)*, Pisa, Italy, 2025.

Contents

Acknowledgments

Reaching the end of this Ph.D. journey has been one of the most challenging and rewarding experiences of my life, and I feel incredibly lucky to have had so many supportive people by my side throughout these years.

First and foremost, I would like to express my sincere gratitude to my main supervisor, Prof. Marija Furdek, for accepting me as a Ph.D. student and for all the professional guidance, kindness, and encouragement you have shown me throughout this journey. You've always been understanding, available for support, and it was easy to reach out to you, especially when things became difficult. And I've always appreciated your patience and trust. A big thank you to my co-supervisor, Dr. Carlos Natalino, for answering my questions especially on the technical aspects related to programming and implementation. Your clarity and responsiveness made a real difference throughout the process. I am grateful to Prof. Erik Agrell for the thoughtful hints you shared during my Ph.D.; they stayed with me and have a lasting impact. I'm also grateful to Prof. Paolo Monti for his valuable comments and feedback throughout my Ph.D., and his role as both my examiner and manager. I would also like to thank Prof. Lena Wosinska for all the rewarding collaboration and fruitful discussions. I am also grateful to everyone at the Optical Networks Unit for providing a friendly work environment.

I also extend my appreciation to all the collaborators I worked with during my Ph.D. A special thanks to Anders Lindgren, Stefan Melin, and Renzo Diaz from Telia for their collaborative spirit and practical insights. Thanks to Vignesh Karunakaran and Dr. Achim Autenrieth from Adtran for the productive discussions and knowledge sharing. I would also like to thank Dr. Mohit Chamania from Google Germany for the insightful collaboration. My sincere appreciation goes to Dr. Farhad Arpanaei, Prof. José Alberto Hernández and Prof. David Larrabeiti from Universidad Carlos III de Madrid for the engaging collaborations and valuable contributions. I would also like to thank Aryanaz Attarpour and Prof. Massimo Tornatore from Politecnico di Milano for the fruitful collaboration. Working with you all has significantly enriched my research experience.

I want to acknowledge the support of various projects, including Sweden's innovation agency VINNOVA, within the framework of the EUREKA cluster CELTIC-NEXT project AI-NET PROTECT (2020-03506), and Vetenskapsradet (2019-05008).

To my close friends, thank you for being there through it all. Your support meant more than you may know. You helped me feel at home here in Sweden, even during the difficult times. The laughs, conversations, and shared experiences made all the difference. And Firooz, thank you for being a great friend, a supportive flatmate throughout this journey, and for all the amazing meals you cooked and added comfort along the way.

And finally, my deepest thanks go to my family. Your unwavering support, encouragement, and unconditional love have carried me through every challenge. This accomplishment belongs to you as much as it does to me.

Acronyms

ASE:	amplified spontaneous emission
AoD:	architecture on demand
BF:	bigger-first
BVT:	bit-rate variable transponder
DFA:	doped fiber amplifier
DGE:	digital gain equalizer
DQN:	deep Q-Networks
DRL:	deep reinforcement learning
EDFA:	erbium-doped fiber amplifier
EGGN:	enhanced generalized Gaussian noise
EON:	elastic optical network
FF:	first-fit
FS:	fragmentation score
FSU:	frequency slot unit
FON:	filterless optical network
GSNR:	generalized signal to noise ratio
GN:	Gaussian noise
ILP:	integer linear program
ISRS:	inter-channel stimulated Raman scattering
JSO:	Jellyfish Search Optimization
LLF:	longer-lasting-first

LP:	lightpath
LPF:	longer-path-first
MB-EON:	multi-band elastic optical network
MDP:	Markov decision process
NN:	neural network
NoC:	number of cuts
No-SD:	no spectrum defragmentation
NTU:	normalized traffic unit
OB:	optical backplane
OF:	older-first
OF-FF:	older-first first-fit
OSNR:	optical signal-to-noise
PFON:	programmable filterless optical network
QoT:	quality of transmission
RBMSA:	routing, band, modulation format and spectrum assignment
RMSA:	routing, modulation and spectrum assignment
RMSCA:	routing, modulation, spectrum and core assignment
RL:	reinforcement learning
ROADM:	reconfigurable optical add-drop multiplexer
RS:	reallocation score
RSA:	routing and spectrum assignment
RWA:	routing and wavelength assignment

SA:	spectrum assignment
SBR:	service blocking ratio
SD:	spectrum defragmentation
SDM:	space division multiplexing
SE:	Shannon entropy
SF:	spectrum fragmentation
SFQA:	spectrum fragmentation- and QoT-aware
SNR:	signal-to-noise ratio
SPNB:	Spanish backbone
SSS:	spectrum-selective switches
T-API:	Transport API
TRx:	transceiver
TDFA:	thulium doped fiber amplifier
USB:	United States backbone
WDM:	wavelength division multiplexing
WSON:	wavelength-switched optical network
WSS:	wavelength selective switch
X-SD:	exhaustive spectrum defragmentation

Part I

Overview

CHAPTER 1

Introduction

The rapid growth of traffic and the increasing demand for bandwidth-intensive applications with dynamic behavior and stringent performance requirements have placed significant demands on modern optical transport networks. These networks must achieve high cost- and energy-efficiency, low latency, high capacity, reliability, flexibility, and scalability [1]. Meeting these requirements involves addressing complex challenges in optical network design and operation. First, the network architectures should be agile and flexible in order to efficiently adapt to varying traffic demands while maintaining low operational costs. Second, as network services become more dynamic and versatile, intelligent and automated resource management is essential to optimize resource allocation and enhance network efficiency. Finally, the spreading of transmission to bands beyond conventional introduces new challenges in spectrum fragmentation and dynamic resource provisioning, requiring efficient strategies to manage resources across different wavebands. The thesis addresses these challenges by proposing novel solutions in three key areas. First, it presents a cost-efficient network planning framework and proposes a RMSA approach to enhance spectrum utilization. Second, it develops machine learning-based approaches for dynamic resource reallocation, specifically leveraging reinforcement learning to automate spectrum defragmentation. Finally, it extends resource management strategies to multi-band networks, focusing on efficient service provisioning and fragmentation-aware resource allocation across different wavebands to maximize network capacity and performance. In the following, we briefly summarize the challenges addressed in this thesis.

The first line of research addressed in this thesis focuses on the design of flexible network architectures and cost-efficient resource assignment. Conventional wavelength-switched optical networks (WSONs) rely on reconfigurable optical add-drop multiplexers (ROADMs) to switch optical signals based on their wavelength. ROADMs use hard-wired components (e.g., wavelength-selective switches, passive couplers, or erbium-doped fiber amplifierss (EDFAs)) to support transparent optical switching and enable local add and drop of signals at the node. This hard-wired nature limits their architectural flexibility. In contrast, disaggregated optical white boxes, also referred to as architecture on demand (AoD) switches, introduce an unprecedented level of architectural flexibility and resource provisioning [2]. Unlike ROADMs, AoD switches do not have predefined interconnections between optical modules, but employ an optical backplane (OB), such as a piezoelectric space switch, to dynamically interconnect modules [3]. This adaptable architecture allows traffic-driven configuration, ensuring that each connection utilizes only the required modules. Consequently, AoD switches can swiftly adapt to traffic changes, scale network capacity efficiently, and seamlessly integrate upgrades. These characteristics help to improve cost effectiveness, energy efficiency, scalability, and network reliability, establishing AoD as an effective solution compared to conventional static ROADM architectures [2].

FONs are an alternative network architecture that relies entirely on passive optical components to broadcast signals, thus achieving high cost- and energy-efficiency [4]. Due to the absence of active switching and filtering, this architecture follows the drop-and-waste transmission, where optical signals propagate beyond their intended destination, and generate spectrum waste. Hence, FONs are typically characterized by low resource usage efficiency and lack of architectural flexibility [4].

To address these limitations and combine the strengths of AoD flexibility with FON simplicity, the programmable filterless optical network (PFON) architecture is introduced [5]. PFON maintains the gridless nature and simplified line-system design of FONs while incorporating the dynamic adaptability of AoD nodes. This integration allows for real-time reconfiguration of node architectures based on traffic demands, minimizing spectral waste caused by the drop-and-waste principle and improving the overall spectrum usage efficiency. An ILP model for the RMSA problem in PFONs is developed in [5], focused on minimizing spectrum usage while maintaining network performance. PFON planning in space-division multiplexed networks is studied in [6], and experimentally validated in [7]. However, cost-efficiency of PFONs remains an underexplored area. Efficient operation of PFONs requires optimized deployment of optical components such as passive splitters and couplers, EDFAs, and OB switches within AoD nodes, along with effective spectrum allocation strategies.

The second line of research explored in this thesis focuses on SF management in elastic optical networks (EONs). While PFON improves network architecture flexibility, SF remains a critical issue that persists regardless of node design. SF occurs when spectral resources become fragmented, creating small, non-contiguous gaps along the network links due to the dynamic establishment and teardown of optical connections [8]. These fragmented gaps are often insufficient to accommodate incoming service requests, leading to an increased service blocking ratio (SBR) and suboptimal spectrum utilization. To address this issue, spectrum defragmentation (SD) techniques are employed to reorganize spectral resources, consolidating smaller gaps into larger contiguous blocks [1]. This consolidation allows the network to accommodate a higher number of service requests and enhances spectrum usage efficiency. SD is a complex problem that requires answering three fundamental questions: When should SD be performed? Which connections should be reallocated? And to which spectrum should these connections be moved? In static traffic scenarios, minimizing fragmentation by reconfiguring a subset of connections has been proven to be an NP-complete problem [9]. The problem is exacerbated in dynamic traffic environments, where the continuous arrival and departure of connections lead to an ever-changing network state. Consequently, optimization techniques like ILPs often struggle to keep up with the computational demands of real-time SD in dynamic scenarios [10].

While SD has been shown to reduce the SBR, it also introduces a reconfiguration overhead, which is a concern for network operators [11]. This overhead typically involves terminating, reallocating, and reestablishing active connections, leading to increased computational complexity and operational costs.

The overhead depends on the frequency of SD operations and the number of connections reallocations in each cycle. Hence, the potential SBR improvement and the corresponding overhead should be considered jointly in the design of SD approaches. Existing SD strategies (e.g., [10]–[12]) often rely on static thresholds and deterministic policies, which are insufficient for addressing the complexities of dynamic network conditions. These conventional methods typically focus on only a subset of SD tasks, which limits their adaptability and effectiveness in dynamic and unpredictable traffic environments.

The third line of research in this thesis focuses on resource assignment and spectrum fragmentation management in multi-band elastic optical networks (MB-EONs), which are crucial for addressing the growing demands of modern communication systems. Proliferation of high-speed applications, such as video streaming, cloud services, and the internet of things, is pushing traditional C-band EONs to their limits [13]. MB-EONs address these limitations by using multiple wavelength bands, including L, S, E, O, and U bands [14]. This expanded spectrum increases data capacity and enables networks to handle diverse traffic patterns while preparing for future growth [15]. However, the shift from conventional routing, modulation and spectrum assignment (RMSA) in EONs to routing, band, modulation format and spectrum assignment (RBMSA) in MB-EONs introduces additional complexity due to the necessity of considering different wavelength bands, where the quality of transmission (QoT) of optical lightpaths varies due to nonlinear impairments. A major impairment is the inter-channel stimulated Raman scattering (ISRS), which causes power depletion from shorter to longer wavelengths in wavelength division multiplexing (WDM) systems, particularly when utilizing resources outside the traditional C-band [16]. The ISRS effects, combined with the dynamic nature of service requests, varying capacity demands, and wavelength continuity constraints, exacerbate the problems pertinent to RBMSA and SF.

Several algorithms have been developed to jointly address the challenges related to spectrum fragmentation and QoT maintenance in MB-EONs. Some of these algorithms tackle the RBMSA problem [17], [18], while others focus on proactive SD [19]. To the best of our knowledge, no existing work has accounted for all impairments, including the ISRS effects in amplified spontaneous emission (ASE) and non-linear interference (NLI) noise, while simultaneously integrating SF-aware resource allocation with proactive SD.

This thesis proposes innovative methods to address the challenges mentioned above regarding efficient and intelligent resource allocation in EONs. The specific research questions and the contributions of this thesis are summarized as follows.

1.1 Research Questions

Addressing architectural flexibility and dynamic spectrum management, along with physical layer impairment-aware and SF-aware resource allocation in EON, is critical for enhancing optical network scalability and spectrum usage efficiency. The thesis investigates three key aspects: development of an optimization framework for RMSA and PFON node design, implementation of intelligent SF management through deep reinforcement learning called Deep-Defrag, and design of fragmentation- and QoT-aware RBMSA strategies for MB-EONs. The following research questions are addressed:

- Q1: What are the trade-offs between spectrum usage efficiency and cost in PFONs? Can spectrum utilization and component costs be beneficially affected by joint optimization of total spectrum and optical component? How do these trade-offs compare to those in FONs and WSON-based networks, as a part of a broader perspective on the efficiency and cost implications across different optical networking architectures?

- Q2: How can machine learning-based approaches automate proactive SD? Can these algorithms simultaneously handle the timing, connection selection, and resource reallocation pertinent to an SD process? What are the trade-offs between SBR reduction and reconfiguration overhead in proactive SD?

- Q3: How can SF- and QoT-aware RBMSA algorithms improve spectrum usage efficiency and reduce service blocking in MB-EONs? What are the effects of integrating proactive SD with QoT-aware resource allocation on SF?

In the following subsection, we summarize the contributions of the thesis in relation to the research questions outlined above.

1.2 Thesis Contributions

The main contributions are categorized into three parts: cost-efficient planning of PFON, intelligent SD using DeepDefrag in EONs, and SF- and QoT-aware resource allocation in MB-EONs. The contributions are presented below along with a summary of related publications.

Programmable Filterless Optical Networks: Architecture, Design, and Resource Allocation

This study addresses research question Q1 by developing cost-efficient approaches for the design and planning of PFONs, focused on minimizing spectrum and passive component usage, the number of required EDFAs, and the size of switching matrices that serve as the optical backplane in each node. The RMSA problem for PFONs is formulated as an ILP model, with the objective of minimizing the total degree of deployed passive components and the highest used spectrum slot index. To address the scalability issues of the ILP in large networks, a two-step ILP formulation is proposed, providing near-optimal solutions at the significantly reduced execution time. Additionally, a heuristic algorithm is developed for the placement of EDFAs within nodes to compensate for intra-node losses, ensuring cost-efficient amplifier deployment.

Simulation results on two core and one regional network topology evaluate the performance of the proposed PFON solutions. The results presented in **Paper A** show that the proposed PFON architecture provides significant improvements compared to both passive FONs and WSONs. Specifically, compared to FONs, PFONs decrease the highest-used spectrum slot index by up to 64%, reduce spectrum waste by up to 44%, and lower the average extent of unwanted signal broadcasting in the network by up to 50%. Additionally, PFONs require only 16% of the total number of optical switches compared to WSONs and reduce the number of optical amplifiers at network nodes by up to 81%, albeit at the cost of increased spectrum usage.

The conclusion of the paper is that the programmable filterless architecture shows strong potential to provide agile and flexible solutions at a fraction of the cost of WSONs and significantly lower spectrum usage than FONs.

Proactive Spectrum Defragmentation in Elastic Optical Networks using Deep Reinforcement Learning

This study addresses research question Q2 by proposing DeepDefrag, a novel framework based on deep reinforcement learning (DRL) that automates SD in dynamic optical networks. DeepDefrag addresses several aspects of the SD problem in an integrated manner: determining the timing for defragmentation, selecting connections for reallocation, deciding on their order, and identifying target spectrum slots for reconfigured connections. The framework considers spectrum occupancy information and uses three fragmentation metrics—number of cuts (NoC), Shannon entropy (SE), and root of sum of squares (RSS)—as inputs to the decision-making process.

The results in **Paper B** show that DeepDefrag efficiently reduces the service blocking while requiring fewer defragmentation cycles and connection reallocations compared to state-of-the-art heuristic approaches. The results in **Paper C** further highlight the effectiveness of DeepDefrag, showing that its SBR performance approaches that of exhaustive methods while incurring significantly lower overhead. Moreover, DeepDefrag demonstrates strong adaptability to dynamic network conditions, maintaining high performance under varying traffic loads. **Paper D** presents the first experimental demonstration of DeepDefrag's capabilities in a real-world scenario, using the Open Networking Foundation T-API standard over a digital twin of an optical network. The experimental results confirm the potential of DeepDefrag to automate SD decisions by intelligently adapting to network conditions in real-time. The conclusion of these papers is that DeepDefrag provides an automated and flexible solution for SD, demonstrating its ability to enhance spectrum utilization while reducing service blocking and operational overhead in dynamic and realistic network environments.

Fragmentation- and QoT-Aware Resource Allocation in Dynamic Multi-Band Elastic Optical Networks

This study addresses research question Q3 by proposing innovative solutions for spectrum fragmentation- and QoT-aware (SFQA) RBMSA in dynamic MB-EONs. For the first time, a heuristic algorithm is developed that incorporates QoT parameters, such as the generalized signal to noise ratio (GSNR), alongside SF metrics, including the NoC and the RSS, into the decision-making framework for resource allocation problem. The proposed algorithm dynamically determines the paths and channels for service requests with the objective of maximizing spectrum usage efficiency. The algorithm is further extended by integrating proactive SD and traffic (re)grooming techniques to enhance network performance in terms of service blocking, referred to as *SFQA-defrag*. The results in **Paper E** show that the proposed SFQA RBMSA algorithm significantly reduces the SBR compared to benchmark algorithms, with improvements of up to 33.2%, albeit at a slight increase in the average path length of 4.4%. This demonstrates the algorithm's ability to effectively balance QoT and SF considerations. The results in **Paper F** highlight the effectiveness of combining the SFQA RBMSA algorithm with proactive SD, enabling the algorithm to address complex network scenarios by considering spectrum occupancy state and fragmentation information. The performance evaluation shows that *SFQA-defrag* outperforms traditional heuristic approaches, particularly those that consider only QoT indicators or SF metrics, in terms of SBR reduction. The results highlight the ability of the algorithm to manage QoT and SF challenges in dynamic MB-EONs, ultimately improving spectrum usage efficiency.

1.3 Thesis Outline

The thesis is organized as follows:

- Chapter 2 provides background information on resource management and node architecture in optical networks, routing and spectrum assignment (RSA) problem, and SF management in EONs.
- Chapter 3 focuses on PFONs, detailing their architecture, the proposed optimization algorithms, and performance evaluation, with a summary of cost and spectrum usage findings.
- Chapter 4 presents proactive SD, introducing the DeepDefrag framework, performance evaluation, and integration with the T-API standard.
- Chapter 5 addresses fragmentation- and QoT-aware RBMSA in MB-EONs, describing the system model, algorithms for resource allocation and SD, and performance analysis.

- Chapter 6 summarizes the key authors' contributions to the included papers.
- Chapter 7 concludes the thesis with final remarks and directions for future research.

CHAPTER 2

Background Information and Concepts

In this chapter, we present key concepts and background knowledge essential for understanding the research areas addressed in the thesis. The chapter begins by discussing various node architectures used in optical networks, including WSON, FON and PFON node architectures. Then, the resource allocation problem in elastic optical networks is introduced, covering both RSA and RBMSA scenarios. Finally, this chapter lays the foundation for understanding spectrum fragmentation management, defragmentation techniques, and the associated performance metrics, which are critical to the optimization goals of this research.

2.1 Optical Node Architecture

Node architecture plays a critical role in the design and operation of optical networks. Typically, optical nodes are responsible for key functions such as wavelength switching, which enables signals to be routed between input and output ports based on their wavelength; local add/drop functionality, which allows the insertion or extraction of specific wavelength channels at the node; and, in many cases, optical signal amplification, which compensates for losses introduced during transmission or within the node itself. Transponders serve as the interface between the electrical and optical layers, converting client signals to optical signals for transmission. Among various transponder types, bit-rate variable transponders (BVTs) are particularly important in EONs. BVTs can dynamically adjust key transmission parameters such as modulation format, enabling flexible and efficient use of the optical spectrum. This adaptability allows each lightpath to be tailored according to service requests and path conditions. For instance, shorter paths with higher signal quality may use high-order modulation, while longer paths may require more robust modulation [20].

This section overviews various node architectures, including WSON, FON and PFON nodes, highlighting their respective functionalities and trade-offs.

WSON Node Architecture

Figure 2.1 illustrates the architecture of a simple 2-degree WSON node [21]. In this architecture, the ROADM employs two wavelength selective switches (WSSs) in a route-and-select configuration. This setup enables precise signal filtering, ensuring that only the intended signals are dropped while the others are forwarded to the intended outgoing links. WSON nodes also host pre-amplifiers and boosters at their ingress and egress ports, respectively.

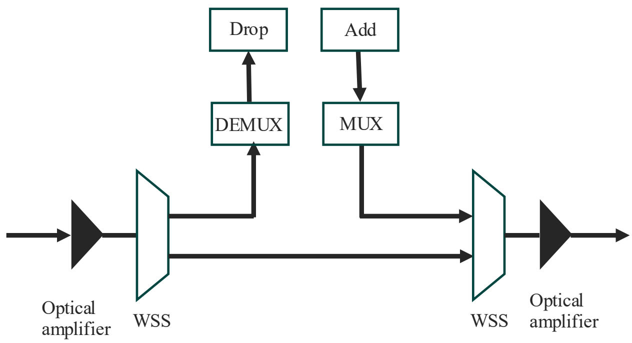

Figure 2.1: Architecture of a 2-degree WSON node

ROADMs are considered as the key enabling technology of modern optical networks, as they support flexible wavelength routing, enable dynamic reconfiguration, and allow for transparent signal switching without requiring optical-electrical-optical conversion. However, these advantages come at the cost of increased complexity and higher capital and operational expenditure, due to the reliance on active switching components.

Filterless Node Architecture

Filterless nodes, with architecture shown Fig. 2.2, represent a low-cost alternative to WSON nodes [21]. In these nodes, passive splitters and combiners replace the active WSSs, as well as the (de)multiplexers in the add-drop part, enabling gridless operation across the entire frequency band. The key operating principle in FONs is the "drop-and-waste" approach, where optical signals are broadcast to all output ports of a splitter, resulting in their propagation beyond their intended destination nodes. As there is no filtering functionality, coherent receivers at destination nodes are responsible for identifying and detecting the correct signals.

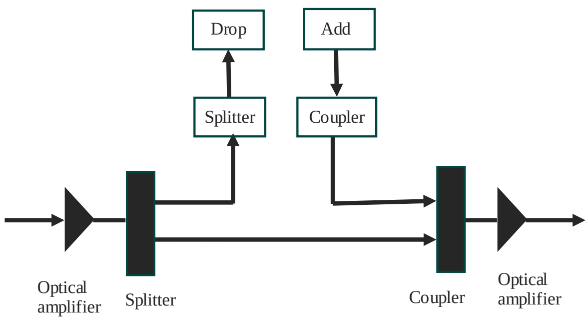

Figure 2.2: Architecture of a 2-degree passive filterless node

The passive design reduces both capital and operational expenditure through lower costs, reduced energy consumption, simplified maintenance, and higher availability [22]. However, filterless nodes also introduce several limitations. Spectrum waste arises from the broadcasting nature of the drop-and-waste principle, as unused copies of the signal propagate along unintended paths, unnecessarily occupying spectrum [6]. Additionally, the absence of filtering raises privacy concerns, since signals can be intercepted at unintended nodes, and imposes rigid structural constraints on the network, limiting flexibility in design and operation [23].

PFON Node Architecture

The optical white boxes feature a modular setup that enables dynamic arrangements of inputs, modules, and outputs through configurable cross-connections using an optical backplane (OB) [24]. This flexibility significantly enhances network adaptability by enabling programmable synthetic node architectures tailored to specific traffic requirements. Unlike conventional static designs, optical white box architectures avoid hardwired configurations, making them both scalable and resilient, as highlighted in recent studies [2]. PFONs leverage this flexible and modular architecture to combine the low-cost operation of filterless designs with the reconfigurability of white box nodes [5].

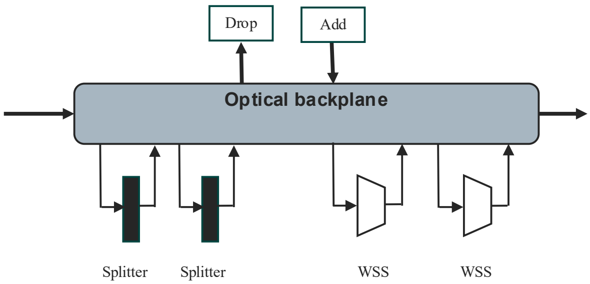

Figure 2.3: Architecture of a degree-2 PFON node

The PFON node architecture, shown in Fig. 2.3, highlights the configurable nature of the design. Flexibility is achieved through the OB, which enables direct interconnection between input and output fibers or routing through intermediate modules as required. Based on traffic requests, ingress and egress ports can either be connected directly via the OB or pass through optical components such as splitters, couplers, and WSSs. Unlike conventional FON nodes, PFON nodes do not require every ingress and egress ports to be equipped with splitters and couplers. Instead, these passive components are used selectively, depending on traffic requests and required functionalities. This design allows for the use of fewer and lower-degree passive components, which can help reduce insertion loss and lower the OB port utilization. However, the inclusion of passive devices introduces spectrum inefficiencies, leading to higher spectrum usage compared to WSON networks.

2.2 The RSA Problem in Optical Networks

Transparent optical networks, which operate without optical-electrical-optical conversions, establish end-to-end optical connections called lightpaths. These lightpaths carry upper-layer traffic, such as IP packets or Ethernet frames. The capacity of service requests, typically measured in Gbps, must be mapped onto optical transmission systems by selecting an appropriate modulation format, which determines the number of required spectrum slots. Setting up a lightpath involves computing a route from the source to the destination node and allocating spectrum resources. This process forms the foundation of the RSA problem in EONs [25].

The RSA problem is a fundamental part of elastic optical network design. Inputs include the network topology, a set of service requests, and their corresponding spectrum requirements in terms of the number of needed spectrum slots. The outputs of the problem are the routes and spectrum slots assigned to the requests. The RSA problem is subject to the following constraints:

1. **Spectrum continuity constraint**: The same spectrum slots must be allocated on all links traversed by a connection.

2. **Spectrum contiguity constraint**: The spectrum slots assigned to a single lightpath must be contiguous, i.e. adjacent.

3. **Non-overlapping spectrum constraint**: Lightpaths that share a common fiber must be assigned distinct and non-overlapping spectrum slots.

Static vs. Dynamic RSA

The RSA problem can be classified into two categories based on traffic scenarios: static and dynamic RSA [26]. In static, or offline, RSA, the service requests are known in advance, typically during the network planning phase. The most common objective in this scenario is to minimize the number of used spectrum slots or the total length of established paths. Dynamic RSA, on the other hand, deals with scenarios where connection requests arrive randomly over time, usually with unknown holding times. Since the full set of requests is not known beforehand, the objective shifts to minimizing the request blocking probability, that is the proportion of requests rejected due to resource unavailability. The static RSA problem is known to be NP-complete [27], making it computationally infeasible to find optimal solutions in polynomial time. In the dynamic scenario, the lack of complete demand knowledge further complicates finding optimal solutions.

Joint and Sequential RSA Problem

Solving the RSA problem involves addressing two sub-problems: routing and spectrum assignment. These can be tackled using either a one-step or a two-step approach. In the one-step (R & SA) approach, routing and spectrum assignment are addressed simultaneously for a set of service requests by formulating the problem as an optimization model, such as an ILP [28]. While ILP-based methods can yield optimal solutions, they are computationally intensive and do not scale for large networks. Heuristic methods, such as greedy randomized adaptive search procedure [29] and simulated annealing [30], are often employed to find near-optimal solutions within reasonable time bounds. The two-step (R + SA) approach decomposes the RSA problem into two independent sub-problems. First, the routing sub-problem determines a suitable path for service requests. Subsequently, the spectrum assignment sub-problem allocates the necessary spectrum slots along the selected route.

Routing in RSA often involves pre-computing multiple candidate paths between each source-destination pair. The fixed shortest path routing is the simplest method, where a single path is selected based on a specified cost function (e.g., link distance, hop count) between the source and destination nodes. The other widely used approach is fixed alternate routing [31], where k-shortest paths are computed using algorithms such as Yen's algorithm [32] or variants of Bellman-Ford [33]. These precomputed paths offer alternative options when the shortest path is unavailable, reducing the blocking ratio by increasing the chance of successful provisioning. Since these paths are computed in advance, no additional computational effort is required for path calculation during network provisioning.

The spectrum assignment sub-problem is commonly addressed using heuristics such as First Fit, Last Fit, or Random Fit to allocate spectrum slots [34]. In optical networks, spectrum is divided into discrete frequency slots, each indexed in ascending order from the lowest to the highest available frequency.

Among the available heuristics, First Fit is the most widely used due to its simplicity and efficiency in various scenarios [35]. This method assigns the first available set of contiguous spectrum slots according to their index, starting from the lowest. By prioritizing lower-indexed slots, First Fit generally leads to compact spectrum usage and helps minimize the highest-used spectrum index. However, it does not actively manage SF, potentially leaving small, unusable gaps scattered throughout the spectrum over time. On the other hand, the Last Fit algorithm selects the last available set of contiguous slots, aiming to preserve lower-indexed slots for future requests. Random Fit chooses any available set of contiguous slots randomly, avoiding deterministic patterns but potentially resulting in uneven resource utilization. Advanced techniques may consider load balancing or congestion-aware strategies to further optimize performance in terms of spectrum utilization.

A major advantage of EONs is the ability of optical transponders to adjust the transmission parameters, such as the modulation format, to match the bit rate and the reach requirements of individual service requests. This per-request adaptability improves spectrum usage efficiency but also introduces additional complexity in resource planning. Hence, the allocation of modulation formats must be carefully addressed to optimize performance and resource utilization. When the resource allocation problem includes the decision on the modulation format for each request, the RSA problem transforms to the RMSA problem [36]. One of the most important factors in modulation format assignment is transmission reach. Modulation formats with higher spectral efficiency allow more data to be transmitted within a given spectrum but are limited to shorter distances due to increased sensitivity to signal degradation. The RMSA problem is subject to an additional constraint ensuring that the selected modulation format is feasible for the assigned path length.

The Routing, Band, Modulation format and Spectrum Assignment (RBMSA) Problem

To meet increasing traffic demands that exceed the capacity of traditional C-band EONs, multi-band elastic optical networks (MB-EONs) extend spectrum utilization to additional bands such as L, S, and O [37]. By utilizing this broader spectral range, MB-EONs significantly increase network capacity. However, the use of multiple bands introduces new challenges related to band-dependent physical impairments, non-uniform hardware capabilities, and inter-band switching constraints [38].

To provision resources effectively in MB-EONs, the RBMSA problem must be addressed. This problem generalizes the RSA formulation by jointly determining a physical route, an optical band, a modulation format, and a contiguous and continuous set of spectrum slots for each service request. An essential aspect of the RBMSA problem is ensuring quality of transmission (QoT), which guarantees that the signal can be correctly received after traversing the selected path. QoT is influenced by factors such as transmission distance and band used, since different bands exhibit varying levels of attenuation and dispersion. To assess QoT, performance metrics like the optical signal-to-noise (OSNR) or generalized signal to noise ratio (GSNR) are commonly used. These metrics help determine whether a given lightpath meets the required signal quality threshold for reliable transmission [39].

2.3 Spectrum Fragmentation in Optical Networks

SF is a significant challenge in EONs, stemming from the dynamic provisioning and release of service requests. This process often results in non-contiguous free spectrum gaps within optical links, which are not big enough to accommodate new service requests. As a result, spectrum usage efficiency decreases, and blocking probability increases [40]. The root of the problem lies in the requirement for contiguous slots to satisfy spectrum continuity and contiguity constraints [8].

Figure 2.4 shows an example of service blocking due to SF. The network includes five nodes connected by five bi-directional links (Fig. 2.4a), each with 12 available spectrum slots. Figure 2.4b shows the network's occupancy state, where several connections, denoted by $D_1 - D_6$, are already established. We assume that one spectrum slot is used as a guard band between adjacent connections on a link. The effect of SF can be illustrated as follows: for the given state of the network, if an incoming service request arrives with node 1 as the source and node 5 as the destination, requiring four spectrum slots, it cannot be accommodated. This occurs despite sufficient capacity being available along the route 1→2→3→5, as the required slots on links e_1, e_2 and e_3 are scattered and not contiguous.

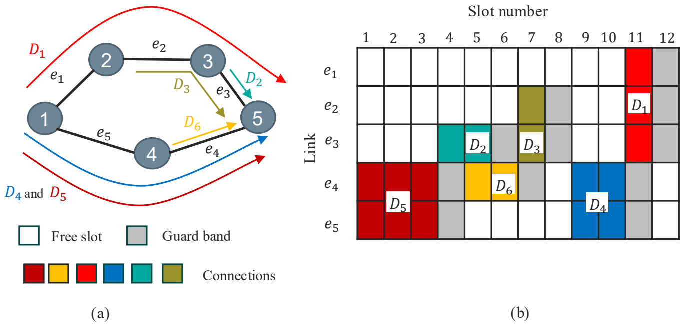

Figure 2.4: A simple network example (a), and the spectrum occupancy state (b)

Spectrum Fragmentation Metrics

The extent of spectrum fragmentation can be gauged by different metrics. A better metric value typically indicates more efficient resource usage with fewer gaps between occupied slots. These metrics help network operators monitor and optimize optical spectrum usage to achieve high performance and efficiency.

Various metrics have been introduced in the literature to evaluate SF. Utilization entropy measures the randomness of spectrum usage, with higher values indicating greater fragmentation [41]. The external SF metric compares the largest contiguous free spectrum block to the total size of all free fragments, offering a direct measure of fragmentation [42]. Spectrum compactness calculates the difference between the highest and lowest occupied slot indices, reflecting how tightly spectrum resources are packed [43], while the number of cuts [44] refers to the count of links along a selected connection path that have adjacent free spectrum slots available.

Equations (2.1) and (2.2) define the Shannon entropy (SE) [45] and the root of sum of squares (RSS) [42] metrics, respectively, which are used in this thesis. These metrics offer insights into fragmentation levels, where higher SE values indicate an exacerbated SF, and higher RSS values suggest an improved SF. The notation is defined as follows: e is the link index, S is the total number of slots per link, $b_i^{free}(e)$ is the size of the i^{th} free spectrum block on the link e, and N is the number of free spectrum blocks. Figure 2.5 illustrates the calculation of the SE and RSS values based on the spectrum assignment state for link e_3 of the example network provided in Fig. 2.4.

$$f_{SE}(e) = -\sum_{i=1}^{N} \frac{b_i^{free}(e)}{S} \ln \frac{b_i^{free}(e)}{S} \tag{2.1}$$

$$f_{RSS}(e) = \frac{\sqrt{\sum_i^N (b_i^{free}(e))^2}}{\sum_i^N b_i^{free}(e)} \tag{2.2}$$

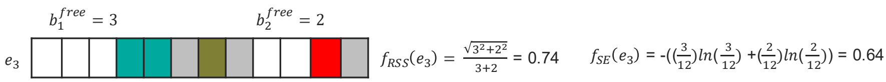

Figure 2.5: Calculation of the SE and RSS values for link e_3.

Fragmentation Management in EONs

Effective spectrum management techniques are essential to address SF, ensuring higher spectrum utilization and reducing the blocking probability. There are two main approaches to addressing SF. The first approach incorporates information about fragmentation into the resource allocation process. When determining routes and spectrum slots, these methods consider the fragmentation level of the candidate solutions (i.e., path and spectrum slot options) using various SF metrics, and select the best path and spectrum slots accordingly. These methods are referred to as fragmentation-aware resource allocation [44].

The second approach is SD, which reorganizes fragmented slots to create larger contiguous blocks for incoming service requests. SD approaches can generally be categorized into reactive and proactive methods [40]. Reactive SD is triggered when incoming service requests are blocked due to insufficient contiguous spectrum. In contrast, proactive SD attempts to prevent blocking by either monitoring network performance metrics and applying predefined thresholds to trigger SD, or by executing SD periodically, regardless of the network state. SD can be further classified based on whether it involves connection rerouting or solely reallocates spectrum resources [1]. Techniques that include rerouting tend to achieve greater fragmentation reduction at the cost of higher computational overhead. Another critical classification distinguishes between hitless and non-hitless SD approaches [46]. Hitless SD ensures that ongoing traffic remains uninterrupted during the defragmentation process. Techniques like push-pull retuning temporarily expand the occupied spectrum to encompass both the original and the target slots before shrinking it to the target spectrum range [47]. Similarly, make-before-break approaches establish a new connection on the target route and spectrum before releasing the original one, thus minimizing disruption [1]. These techniques effectively prevent disruptions at the optical layer, but they may still cause temporary interruptions at higher protocol layers, depending on the rerouting approach.

CHAPTER 3

Programmable Filterless Optical Networks: Architecture, Design, and Resource Allocation

Tailored design and optimization of optical networks are critical to meeting the growing traffic demands in a cost-efficient way. PFONs represent a promising technological solution that balances the architectural simplicity and low cost of passive architectures with the higher spectrum usage efficiency typically achieved in WSONs.

This chapter proposes ILP-based methods for cost-efficient planning of PFONs, focusing on minimizing the usage of spectrum and optical components. To address scalability, we introduce a two-step ILP formulation to achieve near-optimal solutions with reduced computation time. We then evaluate the performance of the proposed PFON planning framework across various network topologies and traffic loads, and compare results with benchmark architectures, such as FON and WSON. Key performance metrics include maximum frequency slot unit (FSU) usage, spectrum waste, and the number and degree of deployed passive optical couplers, highlighting the resource usage efficiency of the proposed approaches. This chapter is written based on **Paper A**.

3.1 Literature Review

Passive FONs have been extensively studied since their inception in [48], with theoretical and experimental research validating their feasibility for core, metro, and submarine networks. Early work on FONs focused on static RSA and fiber tree connectivity [49], [50], while later studies introduced elastic FONs [51] and heuristic approaches for survivable RSA with dedicated path protection. Dynamic provisioning [52] and control plane designs, such as path computation element [53], further expand FON applications. Pilot deployments of FONs were conducted in Croatia in 2012 and Germany in 2014 [54]. Recent efforts have explored FONs for metropolitan networks, leveraging bidirectional transmission [55] and extended spectrum use through the C+L band [56]. Techno-economic studies [57], [58] highlight their cost advantages over WSONs.

The PFON concept, introduced to mitigate FON limitations, combines optical white boxes with filterless architectures [5]. PFONs enhance flexibility and reduce spectrum waste caused by drop-and-waste transmission. Early studies focused on traffic-adaptive reconfiguration of programmable optical switches in PFONs to minimize the spectrum consumption [59]. To utilize additional spatial dimensions to eliminate unwanted signal splitting, [6] proposed to combine PFONs with space division multiplexing (SDM) technology. A heuristic algorithm for inter-core crosstalk-aware routing, modulation format, spectrum and core allocation (RMSCA) in PFONs is proposed [60].

Optical white boxes are pivotal to PFONs, enabling unprecedented flexibility in nodal architecture design and provisioning [2]. Studies have shown their benefits for switching, scalability, and energy efficiency [61], as well as their role in reducing network downtime through self-healing [62]. Cost-efficient planning of AoD-based networks has been explored for static [63], multi-hour [64], and dynamic traffic [65]. In all of these studies, optical white boxes are employed to construct AoD structures, where the optical backplane interconnect active components. However, this work focuses on PFON architectures using passive components and amplifiers for node loss compensation without filtering. We employ an ILP framework to jointly optimize spectrum and component usage, reducing the number of EDFAs and the size of OB switch matrices.

3.2 RMSA and Node Design for PFON

Figure 3.1 illustrates the effect of route selection on the number of deployed passive components, comparing two valid PFON configurations that serve a set of connections labeled $d_1 \check{} d_8$, with a focus on the configuration of node 3. When multiple connections share the same incoming link to a node but are directed to different outputs, they require splitting at the ingress port. For example, in Fig. 3.1a, connections d_1, d_2 and d_3 arrive at node 3 from the same link but are routed to different outgoing links, requiring splitting. Conversely, if connections come from different incoming links and are directed to the same outgoing link, coupling is required. For instance, in Fig. 3.1a, d_3 and d_6 enter node 3 from different links (1–3 and 2–3, respectively) but are routed to the same outgoing link. To achieve this, their signals must be coupled before leaving the node.

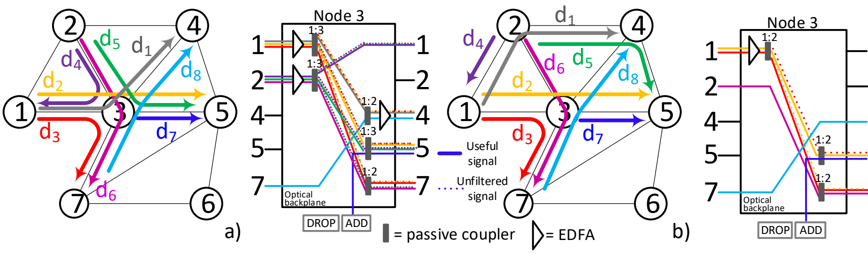

Figure 3.1: The impact of connection routing in PFON networks on the architecture of node 3 and the necessary amplifiers (a) without and (b) with trying to minimize signal splitting/coupling at node 3. Reprinted from **Paper A**, ©2024 IEEE.

Connection routing has a direct impact on the need for splitters/couplers and their degrees. Efficient route selection can reduce the number and the degree of splitters and couplers required at node 3, as shown in Fig. 3.1b. Additionally, the number of amplifiers required within node 3 is reduced in the routing solution shown in 3.1b compared to that in 3.1a. Detailed calculations for determining the need for amplifier usage are provided in **Paper A**. This example also illustrates the impact of routing on spectrum waste. In Fig. 3.1a, more unfiltered signals continue to propagate beyond their destinations and unnecessarily occupy the corresponding spectrum slots. In contrast, the routing in Fig. 3.1b leads to fewer unfiltered signals and thus lower spectrum waste. Finally, the routing choices also affect the OB switch size, which depends on the total number of ports of the deployed components.

3.3 Optimization Models for PFONs

The proposed PFON resource allocation approach aims at minimizing component and spectrum usage. Given a physical network topology, represented as a graph $G(V, E)$, where V is a set of nodes and E a set of links, and a set of traffic demands D, the problem involves finding a physical route, selecting an appropriate modulation format, and assigning the required spectrum slots to each demand. Additionally, node architectures must be configured to support the routing solutions, including the number and the degree of passive couplers. The problem is constrained by the spectrum continuity and contiguity requirements, ensuring that each demand uses contiguous and consistent spectrum slots on all links along its path, without overlap between useful or unfiltered signals caused by the drop-and-waste transmission. The objective of spectrum assignment is to minimize the highest utilized FSU index in the network, and the total degree of passive splitters and couplers deployed.

To tackle the resource planning challenges in PFONs, we formulated two ILP-based optimization approaches. The first model is a single-step ILP that simultaneously addresses the RMSA sub-problems, while minimizing the passive component degrees. While this approach provides optimal solutions for smaller networks, it becomes computationally prohibitive for larger network instances.

To enhance scalability, we propose a two-step ILP. The first step solves routing with the objective of minimizing a cost function that combines two factors: an estimate of the highest used FSU index and the total degree of passive components. In this step, spectrum continuity and contiguity constraints are not required. Instead, the estimated highest used FSU index is derived, considering both the spectrum occupied by active transmissions and the spectrum consumed by unfiltered signals traversing each link. The second step assigns spectrum based on the routing decisions fixed in the previous step. The objective is to minimize the highest used FSU index in the network while ensuring that the assigned spectrum satisfies continuity, contiguity, and non-overlapping constraints. This step allocates contiguous slots to each demand and ensures that overlapping between useful and unfiltered signals is avoided.

Upon solving the RMSA problem using the ILP formulations, the placement of EDFAs is determined by calculating the total loss experienced by each connection at each node and deploying amplifiers where needed to compensate for these losses. This study focuses specifically on the design of the node architecture, emphasizing the placement of amplifiers within nodes for managing node losses. It is assumed that the optical line system is already in place and optimized for span loss management, with launch channel power kept below the threshold for nonlinear effects. Details of the ILP formulations and their complexity analysis, along with the amplifier placement algorithm, are provided in **Paper A**.

3.4 Performance Evaluation

We evaluate the single-step and two-step ILP formulations for cost-efficient PFON design based on the spectrum and component usage. Spectrum usage is analyzed in terms of the highest used FSU index and the portion of spectrum wasted due to the drop-and-waste transmission. Component usage is assessed by the number and degree of passive couplers, the number of EDFAs, and the maximum size of the OB switch matrix.

The evaluations are performed through simulations on the German and Italian backbone networks, as well as a realistic regional network referred to as Reference Network 1 [66]. Each link consists of a single fiber per direction, supporting 320 FSUs, with additional fibers deployed if capacity is exceeded. Links are pre-equipped with line amplifiers to manage span losses, spaced evenly as described in [67]. The analysis considers multi-period scenarios with increasing traffic across 5 periods for the German and Italian networks and 3 periods for Reference Network 1. Traffic is distributed non-uniformly among node pairs, with all volume combined into a single demand for each source-destination pair.

We assume full reconfigurability between traffic periods, meaning that the ILP model is solved independently for each period. Smaller problem instances, such as the German topology under lighter traffic loads, are evaluated first to compare the single-step (PF-RSA) and two-step (PF-R+SA) ILPs. We use the Gurobi 7.5 solver on a server with 4 CPUs, 2.1 GHz Intel Xeon processors, and 128 GB RAM.

Table 3.1: Summary of Optimization Models

Abbreviation	Model
FON	Filterless optical networks solution
WSON-RSA	Single-step ILP solution for WSON
WSON-R+SA	Two-step ILP solution for WSON
PF-RSA	Single-step ILP solution for PFON
PF-R+SA	Two-step ILP solution for PFON
PF-SM-RSA	Spectrum minimizing single-step ILP solution for PFON
PF-SM-R+SA	Spectrum minimizing two-step ILP solution for PFON

Larger problem instances are analyzed to compare the PFON solutions to FON and WSON benchmarks. WSON solutions (WSON-RSA and WSON-R+SA) are derived by modifying the ILP to exclude PFON-specific variables and constraints. FON solutions are obtained heuristically for scalability, as detailed in [68]. Additionally, we compare multi-criteria PFON solutions to spectrum-minimization-only solutions, which disregards component usage. A summary of all models and their abbreviations is provided in Table 3.1.

Single-step and Two-step ILP Comparison

To evaluate the quality of sub-optimal solutions obtained by the two-step ILP formulation, we compare them with the optimal solutions obtained by the single-step ILP. Due to the high computational complexity of the single-step approach, optimal results are feasible only for smaller problem instances with lower traffic loads. For this analysis, we use the German network topology with a reduced traffic matrix, accommodating 21 connection requests and a total traffic volume of 43.5 Tbit/s under the highest load.

Figure 3.2a shows the highest FSU index used by both approaches for PFON and WSON architectures. On average, the optimal PF-RSA solution achieves only 1.6% lower maximum FSU usage than the sub-optimal two-step PF-R+SA approach. For the spectrum minimization variant, the gap is 1.7% for the PFON (PF-SM-RSA vs. PF-SM-R+SA), and 2.8% for the WSON architecture (WSON-RSA vs. WSON-R+SA). These results demonstrate the ability of the two-step ILP model to deliver high-quality solutions that closely approximate the optimal ones.

Figure 3.2b highlights the total degree of passive devices required by the single-step and two-step ILPs. Both approaches show nearly identical performance, with less than 1% difference on average for all traffic periods. Notably, single-objective models that only minimize spectrum usage (e.g., PF-SM-RSA) do not consider the passive component degrees and therefore result in higher total degrees compared to multi-objective models. While the spectrum-only minimizing ILPs achieves 7% lower maximum FSU usage on average, they lead to a 16% increase in the degree of passive components compared to multi-objective formulations. Details about the execution time of these ILP formulations are available in **paper A**.

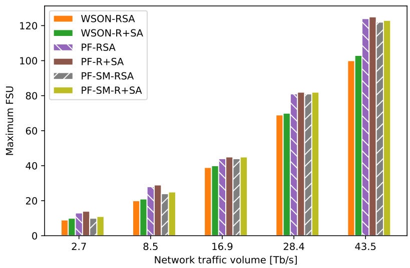

(a) Maximum used frequency slot unit (FSU)

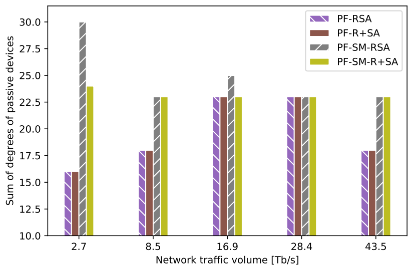

(b) Sum of the degrees of passive devices

Figure 3.2: Single-step (RSA) and two-step (R+SA) ILP comparison for 21 traffic demands in the German network. Reprinted from **Paper A**, ©2024 IEEE.

Comparison of PFONs, FONs and WSONs

Figure 3.3 illustrates the maximum FSU index for different designs under varying traffic loads, where PFON architectures demonstrate significant spectrum savings compared to FONs. For the German network, PF-R+SA and PF-SM-R+SA use 43% and 45% less spectrum, respectively. In the Italian network, both approaches achieve a 38% reduction, while for the Reference 1 network, they provide reductions of 59% and 64%, respectively. On the other hand, compared to the WSON solutions, the PF-R+SA and PF-SM-R+SA schemes exhibit spectrum usage overheads of 43% and 42% for the German network, 66% and 65% for the Italian network, and 66% and 61% for Reference 1, respectively. These results reflect the impact of network connectivity on the algorithm performance. In the low-connected Reference 1 topology, FONs suffer from high spectrum usage due to the limited routing flexibility, giving PFONs a significant advantage. In contrast, in highly connected networks like the German topology, PFONs benefit from flexible configurations and route selection, reducing the spectrum overhead compared to WSONs.

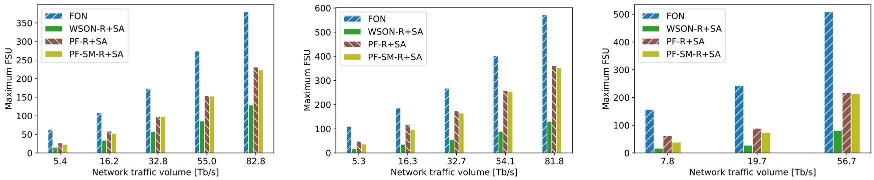

(a) German network **(b)** Italian network **(c)** Reference network 1

Figure 3.3: The maximum used frequency slot unit (FSU) for the three networks. Reprinted from **Paper A**, ©2024 IEEE.

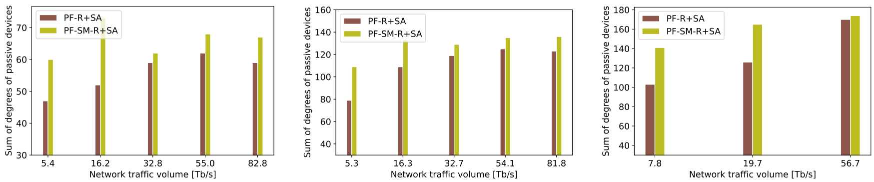

(a) German network **(b)** Italian network **(c)** Reference network 1

Figure 3.4: The average sum of the degrees of passive couplers deployed in the three networks over all traffic periods. Reprinted from **Paper A**, ©2024 IEEE.

Figure 3.4 shows the component usage in terms of the total degree of used passive couplers. In the German network, PF-R+SA reduces the sum of the coupler degrees by 16% compared to PF-SM-R+SA, while maintaining only a 5% difference in the maximum used FSU index across all traffic periods. For the Italian and Reference 1 networks, PF-R+SA reduces the total coupler degrees by 14% and 17% compared to PF-SM-R+SA, respectively, with spectrum usage overheads of only 7% and 10%. These findings demonstrate that joint optimization of spectrum and component usage effectively reduces spectrum waste without significantly impacting the maximum FSU usage.

The detailed numerical comparison of these approaches, including metrics such as spectrum waste, the average unintended recipient metric, the total number of amplifiers used at the nodes, and the sizes of OB switches, is provided in **Paper A**. Additionally, **Paper A** includes an analysis of a scenario without reconfiguration between traffic periods, modeling cases where network operators prefer to avoid complete reprogramming of optical nodes.

3.5 Summary

The chapter presents a design framework for programmable filterless optical network (PFON) that integrates routing, modulation, and spectrum assignment with node design optimization, formulated as an integer linear program (ILP) to minimize spectrum and component usage. To overcome the high complexity of the ILP, the problem is decomposed into two consecutive steps, enabling near-optimal solutions in significantly reduced computation time. Compared to passive filterless optical network (FON), the proposed PFON architecture reduces the highest frequency slot unit index by up to 64%, decreases spectrum waste by up to 44%, and lowers unwanted signal broadcasting by up to 50%. Compared to conventional wavelength-switched optical network (WSON), PFON utilizes only 16% of the optical switches, increases spectrum usage moderately, and reduces the number of amplifiers at network nodes by up to 81% compared to both FON and WSON. This highlights the potential of the PFON architecture to obtain flexible solutions while significantly reducing WSON costs and FON spectrum consumption.

CHAPTER 4

Proactive Spectrum Defragmentation in Elastic Optical Networks Using Deep Reinforcement Learning

The growing traffic demands and dynamic service patterns lead to inefficient spectrum utilization and higher service blocking rates, posing strain on the optical network operation. To address this, network operators are looking for intelligent strategies that can improve spectrum usage efficiency by reducing SF and making better use of the available spectrum. This chapter introduces DeepDefrag, a deep reinforcement learning (DRL)-based framework for proactive spectrum defragmentation (SD) in dynamic EONs. After a brief literature review, we begin by describing the architecture of DeepDefrag. We then explain the core aspects of the strategy, including DRL-based decision-making. Performance evaluation highlights the effectiveness of DeepDefrag in reducing the SBR and minimizing operational overhead. Finally, we demonstrate the effectiveness of DeepDefrag using a Transport API (T-API)-enabled digital twin, which mirrors real network behavior and enables real-time simulation of connectivity services. This chapter is written based on **Paper B**, **Paper C**, and **Paper D**.

4.1 Literature Review

Various approaches, including mathematical optimization models, heuristic algorithms, and machine learning (ML) techniques, have been extensively explored to address SF challenges in EONs. Among these, ILP formulations have been employed for SD due to their ability to deliver mathematically optimal solutions. For instance, an ILP model for proactive parallel SD is introduced in [10], offering optimal results but at the cost of significant computational complexity. In contrast, heuristic algorithms are prominent because of their ability to provide near-optimal solutions with substantially lower computational overhead. Approaches like Older-First, Bigger-First, Longer-Lasting-First, and Longer-Path-First guide spectrum reallocation based on service attributes such as age, size, holding time, and path length [11]. These algorithms often incorporate the First-Fit spectrum assignment policy for efficient reallocation. In [69], various SD heuristic algorithms, including Lowest-Slot-Index-First and Holding-Time-Aware, are evaluated based on metrics such as blocking probability, entropy, and bandwidth fragmentation ratio. The study in [70] introduces two approaches: a reactive disruptive scheme and a proactive non-disruptive scheme, both leveraging the holding time of existing connections to reduce the SBR.

More recently, ML techniques have emerged as a robust tool for addressing SD. Unsupervised machine learning techniques have been applied to spectrum defragmentation, such as in the clusterization-driven spectrum rearrangement algorithm [71], which groups lightpaths based on their features to rearrange the spectrum without rerouting. In [72], a two-dimensional rectangular packing model is employed to optimize spectrum allocation and minimize SF, with traffic demands predicted using Elman neural networks (NNs). In [19], a proactive SD scheme tailored for C + L band systems is proposed, leveraging machine learning to prioritize reducing the SF index while maintaining the QoT. A recent study employs DRL for on-demand, reactive SD [73]. In this framework, when a service request cannot be accommodated, a DRL agent selects one of the pre-defined schemes that increase the size of the fragmented spectrum to accommodate blocked services.

Despite these efforts, proactive SD that relies on DRL techniques remains underexplored. Current DRL models often fail to address all critical aspects of SD simultaneously, including decisions on when to perform SD, which connections to reallocate, and how to assign spectrum to reconfigured connections.

There is a need for intelligent strategies capable of dynamically selecting appropriate reconfiguration actions throughout the network's lifetime while effectively adapting to evolving network conditions. This study also considers the important trade-off between the benefits of spectrum defragmentation and the operational overhead it introduces, which is a critical factor for network operators.

4.2 The DeepDefrag Model

Figure 4.1 provides an overview of the DeepDefrag scheme, which manages SD cycles under dynamic traffic conditions. When a connection departs, the scheme evaluates the need for initiating an SD cycle. If an SD cycle is triggered, DeepDefrag identifies a connection for reconfiguration, determines a suitable spectrum allocation, and repeats this process until the SD cycle concludes.

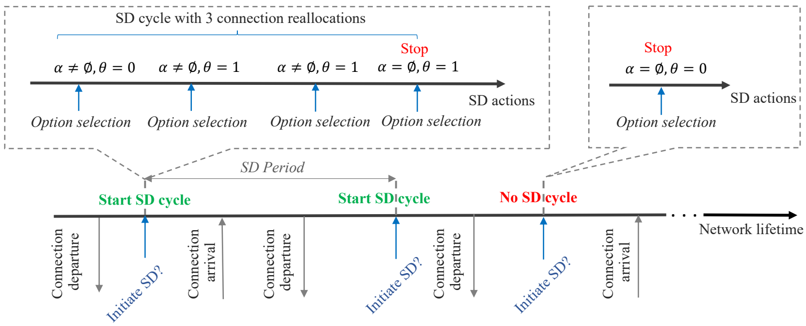

Figure 4.1: The decisions taken and implemented by the DeepDefrag scheme during network operation. Reprinted with permission from Paper **Paper C**, ©Optica Publishing Group.

The inset on the left of Fig. 4.1 presents an example SD cycle involving three reallocations. The SD process is modeled using two variables: θ, which serves as a control flag indicating whether there is an active, ongoing SD cycle ($\theta = 1$) or not ($\theta = 0$), and α, which represents the action chosen by the agent. The value of α can correspond to the index of a connection selected for reconfiguration or $\varnothing$, signaling a stop action. When an SD cycle starts, θ is initially 0, and a connection is reallocated ($\alpha \neq \varnothing$). DeepDefrag may then decide to continue with reallocations ($\theta = 1, \alpha \neq \varnothing$) or to terminate the cycle ($\theta = 1, \alpha = \varnothing$). The provided example illustrates two additional reallocations followed by termination. Only one connection is reconfigured at a time, as concurrent reconfiguration of multiple connections is not supported. The period between consecutive SD cycles is referred to as the SD period. DeepDefrag may also opt not to initiate an SD cycle after a connection departs, as shown in the right inset of Fig. 4.1, where no action is taken ($\theta = 0, \alpha = \varnothing$).

DeepDefrag evaluates all connections as potential candidates for reallocation and examines various spectrum reassignment possibilities. To identify relocation options, the algorithm first hypothetically excludes the currently considered connection from the spectrum grid, i.e., assumes that it does not occupy any slots. It then identifies all available spectrum blocks that can accommodate the connection, where each option implies relocation to the start of a free block.

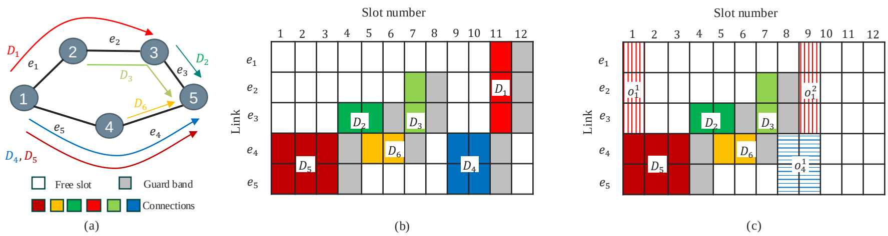

Figure 4.2: A network example serving six connections (a). The spectrum occupancy state (b). Different options for spectrum reallocation (c). Reprinted with permission from **Paper C**, ©Optica Publishing Group.

Figure 4.2 illustrates the SD options for a simple network example with five nodes and five links, each supporting a total of 12 spectrum slots. The considered network snapshot includes six established connections, labeled D_1 to D_6. The routes of these connections are shown in Fig. 4.2a, and the spectrum assignment state for each link is presented in Fig. 4.2b. Fig. 4.2c depicts the reallocation options for connections D_1 and D_4. Other options exist for additional connections, but are not shown in the figure for simplicity. For connection D_1, originally occupying slot 11, there are two candidate blocks that can be considered for its reallocation: slots 1–3 and 9–12, denoted as options o_1^1 and o_1^2. There is only one reallocation option for connection D_4, denoted by o_4^1, corresponding to the only free block (slots 8–12) along the links included its path. By combining the event model from Fig. 4.1 with the options introduced in Fig. 4.2, a DRL agent can be designed to effectively solve the SD problem.

4.3 DRL Modeling and Implementation

The DeepDefrag framework utilizes DRL to perform proactive SD. DRL is an ML approach designed to address control problems, where an agent learns to take actions by interacting with its environment to maximize a cumulative reward. These problems are often formulated as Markov decision processs (MDPs). This section details the MDP model for DeepDefrag, focusing on the observation space, action space, and reward function.

Observation Space

The DeepDefrag observation space offers the agent a detailed representation of the current network state and available reallocation options. This design allows the agent to learn about the network dynamics and make informed decisions. The observation space of DeepDefrag is composed of multiple components. The state representation for the reallocation option j of connection D_i is denoted by S_{ij}, which is defined as follows:

$$S_{ij} =< s_i, d_i, a_i, n_i, l_i, f_i, t_i, c_i, F_{RSS}, F_{SE}, f_{ij}, t_{ij}, c_{ij}, F_{RSS}^{ij}, F_{SE}^{ij} > ,$$

where s_i, d_i, b_i, and a_i denote the source, destination, requested bit rate, and arrival time of connection, respectively. l_i represents the number of links along the path allocated to the connection, f_i is the starting spectrum slot currently assigned to the connection, t_i is the total number of available slots along the path, and c_i indicates the number of cuts along the connection's path.

The metrics for the current network state, RSS and SE, are denoted by F_{RSS} and F_{SE}, respectively. For reallocation option j of connection D_i, the parameters include the new candidate starting slot f_{ij}, the number of spectrum cuts c_{ij}, and the size of the used free spectrum block t_{ij}. Additionally, assuming that D_i is reallocated to option j, the updated RSS and SE metrics are denoted by F_{RSS}^{ij} and F_{SE}^{ij}.

As an example, the state for option o_4^1 in Fig. 4.2c is defined as follows:

$$\begin{aligned} S_{41} = \langle s_4 = 1, d_4 = 5, a_4, n_4 = 2, l_4 = 2, f_4 = 9, t_4 = 2, c_4 = 2, \\ F_{RSS} = 1.7, F_{SE} = 0.48, f_{41} = 8, t_{41} = 5, c_{41} = 1, \\ F_{RSS}^{41} = 1.82, F_{SE}^{41} = 0.4\rangle \end{aligned} \tag{4.1}$$

Action Space

The action space defines all actions which the agent can execute within a given environment. As described in the previous sections, the agent selects one of the available options at each decision step in the DeepDefrag environment. The set of possible actions is represented as $\mathbb{J}$. Each action is defined by the tuple $\langle D_i, f_{ij}\rangle$, which specifies the connection and the new starting spectrum slot for the selected option. Additionally, the set $\mathbb{J}$ includes the $\varnothing$ action, representing either the termination of an ongoing SD cycle or the decision not to initiate a new one.

Reward Function

In DRL, the reward function is a key component that evaluates the impact of the agent's actions by assigning a numerical score based on the current state of the environment and the actions performed. In the initial design of the reward function, as described in **Paper B**, the primary objective is to minimize the SBR. The function encourages the agent to reduce the SBR by adopting it as the main term $(1 - SBR)$ in the reward. The design of the reward function evolves further in **Paper C** to address small variations in SBR more effectively and enhance the agent's learning efficiency, as defined in (4.2).

$$r_i = \begin{cases} -\frac{\log_{10} SBR}{3} & \theta \in \{0,1\} \wedge \alpha {=} \varnothing \\ -\frac{\log_{10} SBR}{3} - Ps - Pe & \theta = 0 \wedge \alpha \neq \varnothing \\ 1 + \frac{\log_{10}(F_{RSS}^{ij} - F_{RSS})}{3} - Pe & \theta = 1 \wedge \alpha \neq \varnothing \end{cases}, \tag{4.2}$$

Here, the logarithm of the SBR is introduced to amplify the sensitivity to minor changes in blocking probability. This design strongly penalizes even a slight increase in the SBR. To limit the overhead of SD, penalties are applied for initiating SD cycles (P_s) and reallocating connections (P_e). Specifically, when an SD cycle is initiated by reallocating a connection, both penalties are applied. Additionally, during an ongoing SD cycle, each connection reallocation is penalized to discourage excessive operations. These penalty values can be adjusted based on the costs incurred by network operators. During ongoing SD cycles, the reward function evaluates the improvement in the network fragmentation state using the RSS metric. A higher RSS value reflects reduced spectrum fragmentation. The reward function calculates the difference in the RSS metric before and after reconfiguration to assess the benefit of the reallocation. A logarithmic function is applied to this difference, ensuring that even small improvements in the RSS metric significantly impact the reward value. To balance the reward components and facilitate efficient agent learning, the logarithmic terms are normalized using a factor of 3, ensuring that the reward values remain within a range of 0 to 1. This normalization helps prevent excessively large or small reward values and allows penalties to be set proportionally to other reward components.

DRL Training and Implementation

We utilize the deep Q-Networks (DQN) algorithm [74] to develop the policy for the proposed SD approach. The DQN algorithm aims to optimize long-term rewards by estimating state-action values, referred to as Q-values, through a deep neural network (NN). These Q-values indicate the expected reward associated with each state-action pair. To compute the Q-values, an NN is employed, which takes the network state S_t as input, and outputs predicted state-action values for all possible actions. Further details of the training phase are provided in **Paper C**.

The training is conducted offline, ensuring that it does not interfere with network operations. In the prediction phase of the DQN, the trained model is used to predict the best action for a given state. This phase involves only a straightforward NN inference, making the time required for inference negligible compared to other network events. Ideally, new experiences gathered during operation are included in memory and used to further refine and improve the agent over time.

We used Optical RL-Gym [75] to develop the DRL agent, a toolkit built on the principles of the OpenAI Gym [76]. Optical RL-Gym offers a comprehensive set of optical network environments for efficiently setting up, training, and testing various DRL agent configurations. For the DeepDefrag toolkit, we further extend the built-in use cases provided by Optical RL-Gym by introducing basic concepts of SD, such as reallocating connections and calculating SF metrics.

4.4 Performance Evaluation

We conducted simulations under dynamic traffic conditions to evaluate the performance of the DeepDefrag scheme. The evaluation employed performance metrics such as the SBR, number of connection reallocations, and number of SD cycles. Two network topologies are used: NSFNET with 14 nodes and 22 links, and the German topology with 50 nodes and 88 links. The details of the simulation settings can be found in **Paper C**. In **Paper B**, we considered an early-stage deployment of DeepDefag, where the reward function and observation space did not include SF metrics. The results presented in this section are based on Paper C, which evaluated a refined version of DeepDefrag for different scenarios.

The performance of DeepDefrag is compared with three heuristic approaches: older-first first-fit (OF-FF), exhaustive spectrum defragmentation (X-SD), and no spectrum defragmentation (No-SD). OF-FF prioritizes reconfiguring the longest-running connections, while X-SD represents a heuristic lower bound for SBR by reallocating all connections upon each departure. Both methods use a first-fit (FF) spectrum allocation policy to determine the target spectrum slots. No-SD serves as a baseline with no defragmentation. OF-FF is evaluated in two configurations to facilitate a fair comparison: one where its defragmentation overhead matched that of DeepDefrag and another where it achieved a similar SBR as DeepDefrag. Notably, X-SD achieved the lowest SBR among all approaches by reallocating an unlimited number of connections, but this came at the expense of significantly higher operational overhead. The DeepDefrag agent is evaluated with two penalty sets for defragmentation: (0.8, 0.1) and (0.3, 0.05). These penalties reflect the higher cost of initiating SD cycles compared to reallocating connections. Network operators can fine-tune the penalty values to align with their specific operational priorities.

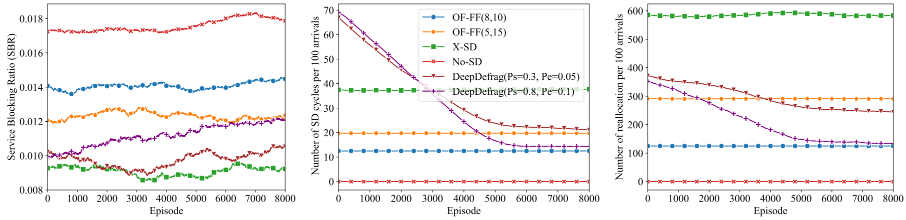

(a) Service blocking ratio (SBR) **(b)** Number of SD cycles per 100 arrivals **(c)** Number of reallocations per 100 arrivals

Figure 4.3: Performance of the considered spectrum defragmentation schemes for the NSFNET network topology. Reprinted with permission from **Paper C**, ©Optica Publishing Group.

Figure 4.3 showcases the performance of the described SD schemes for the NSFNET topology, highlighting the benefits of DeepDefrag. As illustrated in Fig. 4.3a, the *X-SD* approach achieves the strongest SBR reduction, outperforming the No-SD scheme by 49%. This demonstrates the potential gains of proactive SD algorithms. Figures 4.3b and 4.3c provide insights into the number of SD cycles and connection reallocations per 100 arrivals for each strategy. Compared to No-SD, DeepDefrag significantly reduces the SBR upon the convergence of the DRL agent, lowering it by 32% for the (0.8, 0.1) penalty configuration, and by 38.6% for the (0.3, 0.05) one. To simplify the analysis, the configuration (0.8, 0.1) is the only one used in the remainder.

OF-FF is evaluated in two configurations. In the first configuration, OF-FF(5, 15), the SD period is set to 5 connection departures, and up to 15 reallocations are allowed per SD cycle. This configuration achieves SBR values comparable to DeepDefrag, allowing for a comparison of their defragmentation overheads. The second configuration, denoted by OF-FF(8, 10), sets the value of the SD period to 8 departures and allows for up to 10 reallocations per cycle. It matches the defragmentation overhead of DeepDefrag, enabling a comparison of their SBR performance. On average, OF-FF(8, 10) and OF-FF(5, 15) obtain 20.2% and 29.4% lower SBR values than No-SD, respectively. However, DeepDefrag outperforms OF-FF(8, 10) by reducing the SBR by 15.8% while maintaining the same overhead. X-SD achieves 23.3% lower SBR than DeepDefrag but incurs significantly higher defragmentation overhead.

Figure 4.3b reveals that DeepDefrag triggers 14.1 SD cycles per 100 arrivals on average, a 29.5% reduction compared to OF-FF(5, 15). Similarly, Figure 4.3c shows that DeepDefrag reallocates 132 connections per 100 arrivals, which is 56% fewer than OF-FF(5, 15). These results indicate that DeepDefrag achieves a promising balance between reducing SBR and minimizing the defragmentation overhead.

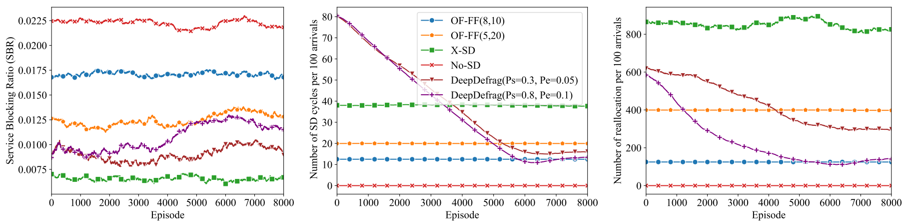

(a) Service blocking ratio (SBR) **(b)** Number of SD cycles per 100 arrivals **(c)** Number of reallocations per 100 arrivals

Figure 4.4: Performance of the considered spectrum defragmentation schemes for the German network topology. Reprinted with permission from **Paper C**, ©Optica Publishing Group.

Figure 4.4 illustrates the performance of the evaluated schemes for the German topology, where DeepDefrag also outperforms the benchmark heuristics. In this topology, X-SD obtains 69.5% lower SBR than No-SD, whereas DeepDefrag, using the (0.8, 0.1) penalty configuration, achieves a 50% reduction in SBR compared to No-SD. Compared to OF-FF(8, 10), which has a similar defragmentation overhead, DeepDefrag reduces the SBR by 34.8%. Furthermore, DeepDefrag achieves a comparable SBR performance to OF-FF(5, 20) while reducing the number of SD cycles and connection reallocations by 34.1% and 75%, respectively, as shown in Figs. 4.4b and 4.4c. The training progression depicted in the figures highlights DeepDefrag's capability to reduce SD overhead after 5,500 episodes for the NSFNET topology and 6,000 episodes for the German topology. The analysis of the two topologies indicates that DeepDefrag adapts effectively to different network scenarios, with a more prominent impact on the German topology due to its higher traffic variability and complexity.

4.5 Integration with T-API for Practical Network Implementation

To observe how the DRL-based SD module improves spectrum utilization in realistic scenarios, we demonstrated the integration of the DeepDefrag module with a digital twin of an optical network that supports T-API [77]. This represents the first instance of combining DRL-based defragmentation with a T-API-enabled optical network, showcasing the module's capability to manage spectrum dynamically and intelligently in a carrier-grade environment.

Workflow of the Demo

Figure 4.5 outlines the workflow of the proposed demonstration, showcasing the interaction between the SD module and the T-API-enabled optical network digital twin. The first phase focuses on data collection and analysis, where the SD module periodically communicates with the digital twin to gather up-to-date information on connectivity services and the network topology. Through T-API messages, the module retrieves essential details such as unique identifiers of active connectivity services. This data is used by the DRL agent to assess the network state and determine whether to initiate an SD cycle.

Once the DRL agent decides to initiate an SD cycle, the second phase begins, focusing on spectrum defragmentation. The agent selects specific connectivity services for reallocation and identifies suitable target spectrum slots while ensuring the paths of the connections remain unchanged. This process adopts a break-before-make strategy, where the selected service is first removed using T-API messages and then re-established with updated spectrum allocations. The agent iteratively executes this procedure until it determines that the SD cycle is complete. By integrating these two phases, the system dynamically improves spectrum utilization in real time, aligning SD decisions with the current network conditions. This structured workflow ensures operational stability while achieving intelligent and adaptive spectrum management.

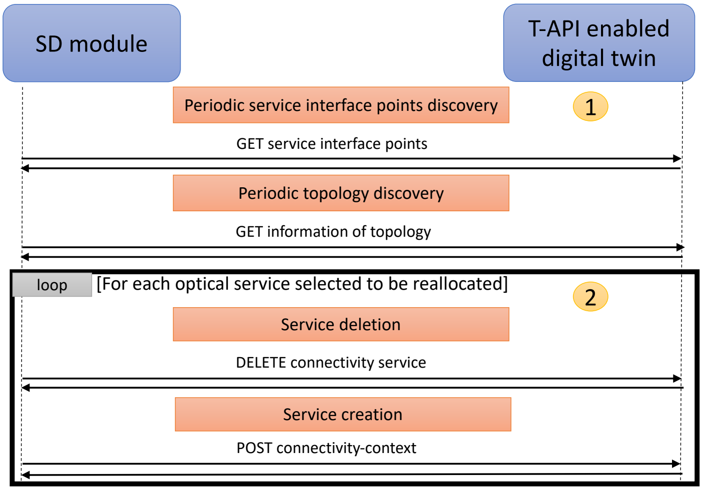

Figure 4.5: Communication between the SD module and the digital twin. Reprinted from **Paper D**.

Demonstration Implementation

Figure 4.6 illustrates the deployment setup used in this demonstration. The setup involves several interconnected components working together to achieve real-time SD. The SD module is implemented in Python and employs the Optical RL-Gym framework to simulate network operations. The digital twin mirrors the optical network by replicating each element as a virtual instance, ensuring the simulation environment closely resembles a real-world network. The digital twin operates under a production-grade software-defined networking (SDN) controller, with T-API managing the northbound communication and NETCONF handling the southbound communication. The DRL agent, which drives the SD decisions, is pre-trained offline to improve spectrum usage. During operation, the SD module interacts with the digital twin to exchange information and execute SD decisions in real-time. This interaction follows the T-API specification version 2.1, ensuring compatibility with multi-vendor environments. The demonstration also includes a dashboard for visualizing the network state, allowing users to observe fragmented spectrum grids, track SD cycles, and monitor various performance metrics.

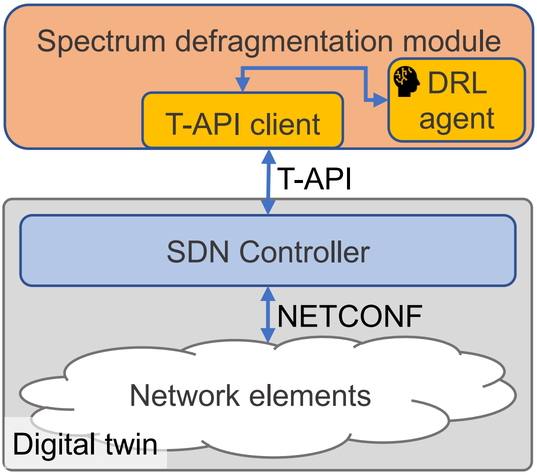

Figure 4.6: Demonstrator architecture. Reprinted from **Paper D**.

4.6 Summary

This chapter introduces DeepDefrag, a deep reinforcement learning (DRL)-based framework for proactive spectrum defragmentation (SD) in elastic optical networks. DeepDefrag jointly addresses the key aspects of the SD process, including when to perform defragmentation, which connections to reallocate and in what order, and how to assign new spectrum resources. By leveraging spectrum occupancy information using spectrum fragmentation metrics, DeepDefrag effectively learns to adapt its decisions to dynamic network conditions. Simulation results show that DeepDefrag significantly reduces the SBR while requiring fewer SD cycles and connection reallocations compared to existing heuristic algorithms. Finally, this chapter presents the first experimental demonstration of DRL-based SD integrated with a T-API-enabled optical network digital twin. This real-time experiment showcases DeepDefrag's ability to interact with standard network interfaces and make intelligent SD decisions in a carrier-grade optical network.

CHAPTER 5

Spectrum Fragmentation- and QoT-Aware Resource Allocation in Dynamic Multi-Band Elastic Optical Networks

This chapter presents a spectrum fragmentation (SF)- and quality of transmission (QoT)-aware routing, band, modulation format and spectrum assignment (RBMSA) algorithm with proactive spectrum defragmentation (SD) for multi-band elastic optical networks (MB-EONs), referred to as *SFQA-defrag*. The proposed method jointly considers QoT level of the lightpaths and SF metrics to ensure efficient resource allocation. Additionally, we introduce a proactive SD strategy to mitigate SF before it leads to service blocking. Performance evaluations across multiple network topologies demonstrate significant improvements in service blocking ratio (SBR) and spectrum utilization compared to conventional heuristics. This chapter is written based on **Paper E** and **Paper F**.

5.1 Literature Review

Recent research on MB-EONs has addressed challenges related to resource allocation, SF, and inter-channel stimulated Raman scattering (ISRS) effects. Various studies have proposed ISRS-aware RBMSA strategies to optimize spectrum usage efficiency while mitigating ISRS interference. One approach introduces an ISRS impact-reduced RBMSA algorithm for C+L-band EONs, optimizing spectrum allocation while minimizing ISRS effects [78]. Another study employs a deep neural network-assisted QoT estimator to predict the optical signal-to-noise ratio (SNR), enhancing spectrum allocation efficiency [79]. Additionally, a statistical interference noise prediction model is developed for C+L-band EONs, enabling single- and multi-period network planning [80]. While fragmentation management has been extensively studied in C-band EONs [81], [82], existing models often rely on fixed reach and capacity assumptions due to limited low-complexity QoT estimation techniques. Few works address fragmentation in multi-band networks, with some focusing on fragmentation-aware resource allocation and others on defragmentation. Q-learning-based routing has been applied to C+L-band EONs, considering fiber impairments such as ISRS while using first-fit, last-fit, and exact-fit allocation strategies [17]. Other studies explore SNR-aware resource allocation and survivability-focused RBMSA to balance SNR and spectrum usage efficiency, while reducing SF and service disruptions caused by link failures [18], [83]. Existing approaches for spectrum defragmentation in multi-band networks include adaptive bandwidth defragmentation algorithms [84] and machine learning-based QoT-aware SD schemes, which minimize SF while maintaining QoT during spectrum retuning [19]. Despite these advances, prior works incorporate QoT-awareness either with SF-aware resource allocation or with proactive SD. They do not fully integrate the two aspects while addressing ISRS in amplified spontaneous emission and nonlinear interference noise.

5.2 System Model and Physical Layer Assumption

In this study, we consider a dynamic MB-EON consisting of a set of nodes and links, where service requests continuously arrive and depart over time. Data transmission takes place across predefined channels in the C, L, and S bands.

Each channel comprises six frequency slots and is associated to a dedicated BVT, allowing for independent modulation. For each service request, a source-destination path is selected, along with one or more channels that together meet the required bit rate. Because each channel is handled by a separate BVT, the assigned channels do not need to be contiguous along the path. However, the assigned channels must remain consistent across all links of the selected path due to the spectrum continuity constraint.

Each node is equipped with C+L+S-band ROADMs and BVTs that support dynamic add/drop operations across bands. In-line amplification is achieved using EDFAs for the C and L bands and thulium doped fiber amplifiers (TDFAs) for the S band, with digital gain equalizers ensuring optimal power levels per span. The ability of BVTs to operate at variable transmission rates enables traffic (re-)grooming directly at the optical layer. This allows multiple lower-bit-rate service requests between the same source and destination to be aggregated onto existing lightpaths with available capacity, thereby reducing the need for establishing new lightpaths.

For physical layer modeling, we estimate the QoT using the GSNR, which accounts for both linear and nonlinear impairments, including ISRS. The GSNR is computed using an enhanced generalized Gaussian noise model for any lightpath from an arbitrary source to an arbitrary destination in the network [85], [86]. Subsequently, for each of the K shortest paths, the highest supported modulation format for every channel along the path is pre-calculated by comparing the estimated GSNR of each channel to the modulation format thresholds defined in the literature [87]. The modulation format levels range from $m = \{1, 2, 3, 4, 5, 6\}$, corresponding to bit rates from 100 Gbps to 600 Gbps. For instance, a value of 6 for a given channel means that the channel can support up to 600 Gbps. Further details on end-to-end GSNR calculations for lightpaths can be found in **Paper E**.

Finally, to monitor and manage fragmentation, we use two metrics, RSS and NoC, that evaluate SF across network links [88]. Since spectrum contiguity is not required in our model, we adjust these metrics to assess fragmentation across adjacent links only. A higher NoC value and a lower RSS value both indicate greater SF in the network. Hence, we aim at reducing the NoC and increasing the RSS values.

5.3 The Spectrum Fragmentation- and QoT-Aware (SFQA) RBMSA Algorithm with Spectrum Defragmentation (SD)

In this section, we present the proposed *SFQA-defrag* algorithm for dynamic MB-EONs. The section is structured into two parts: the first outlines the RBMSA algorithm, while the second introduces the proactive SD algorithm.

Joint Spectrum Fragmentation- and QoT-Aware (SFQA) RBMSA

The core idea of the *SFQA* RBMSA algorithm is to reduce the SBR by jointly considering QoT and SF during path and channel selection. For each service request, the algorithm prioritizes paths and channels that support the highest possible modulation format while also minimizing SF.

The algorithm executes in three main phases. First, it attempts to serve the incoming service request through traffic grooming. For each path, it examines the already established channels and evaluates their modulation format levels to determine whether the cumulative remaining capacity can satisfy the requested bit rate. If such channels are found, the service is accommodated without establishing new physical channels. If grooming is not possible, the algorithm proceeds to the second phase, where it calculates the fragmentation score (FS) for all candidate paths and their available channels with the goal of establishing a new channel. Finally, in the third phase, it selects the best path and channels based on both the modulation format level and the computed FS values.

Figure 5.1 provides an illustrative example of the *SFQA* algorithm in a simple network scenario where two alternative paths are considered for each incoming service request. Figure 5.1a shows a network with four nodes (v_1–v_4) and five links (e_1–e_5). Each link supports six channels (c_1–c_6). The network currently carries five active services (d_1–d_5), with their channel assignments shown in the right side of the figure. Note that some channels are fully occupied, while others have spare capacity available for incoming service requests.

Figure 5.1b illustrates the logic of the *SFQA* algorithm. The modulation format level for each path–channel pair is denoted by $M(p, c)$. The blacked-out parts in each channel indicate portions that are unusable due to limitations

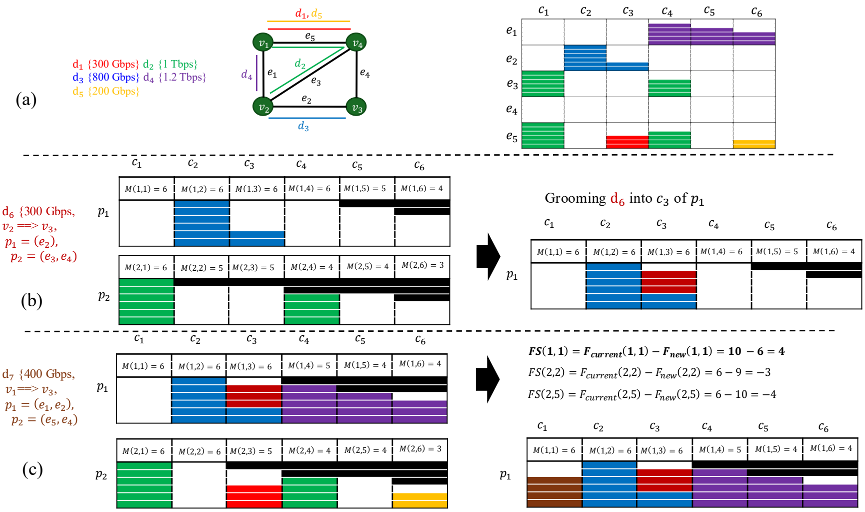

Figure 5.1: A simple network example supporting five services (a), provisioning a new service via traffic grooming by SFQA algorithm (b), and establishing a new lightpath (c).

on the modulation format. For example, if the modulation level is 4, only four of the six portions are usable, and the remaining two are shown in black. When service request d_6 arrives, requiring 300 Gbps, the algorithm first checks for traffic grooming. For the two candidate paths, denoted by p_1 and p_2, it inspects the occupied channels to determine if their cumulative remaining capacity can accommodate d_6. Starting from the first candidate $p_1 = (e_2)$, the algorithm identifies channel c_3 as the channel with sufficient remaining capacity, which allows the service request to be established without activating a new channel.

Figure 5.1c presents the arrival of service request d_7, requiring 400 Gbps from v_1 to v_3. There are two paths available: $p_1 = (e_1, e_2)$ and $p_2 = (e_5, e_4)$. However, neither has an established channel with enough capacity to accommodate d_7. Hence, a new physical channel is needed, and the second phase of the algorithm initiates. Channel c_1 on p_1 and channels c_2 and c_5 on p_2 are available. The algorithm then calculates the FS for each channel by simulating a scenario where the channel is assigned to d_7. This involves computing the difference between the current fragmentation value ($F_{current}$) and the estimated value (F_{new}) if that channel were used. The right side of Fig. 5.1c presents these calculations based on the NoC metric as the SF target. For example, for channel c_1 on path p_1, the fragmentation score is computed as $FS(1,1) = F_{\text{current}}(1,1) - F_{\text{new}}(1,1) = 4$. This score reflects the reduction in SF if c_1 is assigned to d_7.

In the final phase, the algorithm determines the most suitable path and channels for the service request. Candidates are first ranked by the highest modulation format available across their channels. If they share the same highest modulation format level, they are further ranked by the FS of their channels. In this example, c_1 on p_1 and c_2 on p_2 offer the same highest modulation format level, so c_1 on p_1 is selected due to its superior FS.

QoT-aware Spectrum Defragmentation Algorithm

The proposed defragmentation algorithm starts SD cycles either at regular intervals or when a performance indicator threshold is reached. The main objective of this algorithm is to reorganize service channels, which is a term we use to refer to channels currently assigned to active services. The algorithm focuses on the channels whose reallocation yields the most significant reduction of SF. It considers the reallocation of individual service channels rather than entire services, since a service may occupy multiple non-contiguous channels that can be reallocated independently.

The algorithm comprises three phases. First, it performs traffic re-grooming by merging partially filled channels to free up a service channel. In the second phase, the algorithm identifies the best service channel for reallocation. Finally, the algorithm seeks the best target channel to which the selected service channel is reassigned.

Figure 5.2 illustrates an example of an SD cycle for the same network topology shown in Figure 5.1, after accommodating service requests d_6 and d_7. In the first phase, the algorithm iterates through all active services and their associated channels, attempting to identify another occupied channel along the same path that can be merged through re-grooming. As shown in Figure 5.2a, Services d_5 and d_1 share the same path, and channel c_3 has sufficient capacity to accommodate d_5. Consequently, the service channel of d_5 is consolidated to channel c_3. As a result, c_6, the original service channel of d_5 is released.

In the second phase, the algorithm identifies the best service channel candidates for reallocation (Fig. 5.2b). In this example, service channels c_4 and

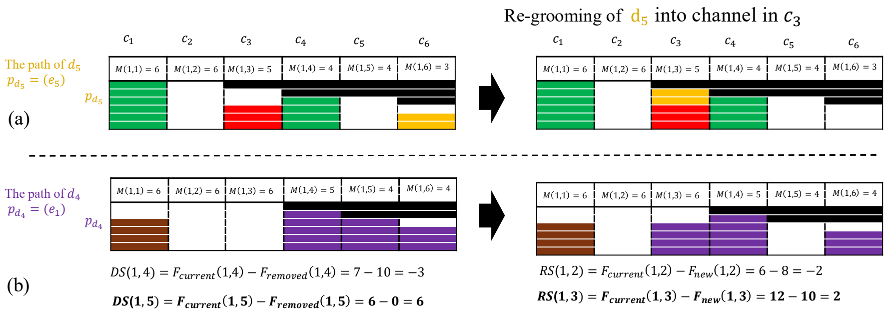

Figure 5.2: An example of defragmentation done via traffic re-grooming (a), and by reallocating a service channel (b). Reprinted from **Paper F**.

c_5, which support d_4, are evaluated. The defragmentation score (DS) is computed for each channel by hypothetically removing them and assessing the change in the SF metric before ($F_{current}$) and after ($F_{removed}$) their removal. The DS is calculated for both options based on the NoC metric. In this case, $DS(1,4)$ and $DS(1,5)$ correspond to the potential reduction in the NoC metric if channels c_4 and c_5 are hypothetically removed. Based on the computed scores, c_5 is identified as the most beneficial candidate for reallocation in terms of fragmentation reduction.

The third phase involves determining the most suitable target channel for reallocation by evaluating all available channels along the path of d_4. Channels c_2 and c_3 are free and considered as potential targets. For each candidate target channel, the algorithm calculates the reallocation score (RS), which measures the change in SF obtained by moving the service channel c_5 to that channel. As shown on the right-hand side of Fig. 5.2b, the RS is computed for both options (channels c_2 and c_3) based on the NoC metric, ultimately selecting c_3 as the target channel. The details of the algorithms along with the pseudocodes is provided in **Paper F**.

5.4 Performance Evaluation

This study investigates resource allocation in multi-band EONs spanning the C, L, and S bands, totaling a bandwidth of 20 THz, with 6 THz each for the C and L bands, and 8 THz for the S band. The spectrum is partitioned into

268 channels, each 75 GHz wide (6 $\times$ 12.5 GHz spectrum slots), including 400 GHz guard bands separating adjacent bands. The analysis is based on simulations on three network topologies: the Japanese backbone (JPNB) with 12 nodes and 17 links, the United States backbone (USB) with 14 nodes and 22 links, and the Spanish backbone (SPNB) with 30 nodes and 56 links [89]. The network employs six modulation formats: PM-BPSK to PM-64QAM operating at 64 Gbaud, supporting bit rates from 100 Gbps to 600 Gbps, with modulation granularity set at 100 Gbps. The parameter K, representing the number of pre-computed shortest paths, is fixed at 3. Service requests are uniformly generated between nodes with bit rates ranging from 50 Gbps to 600 Gbps, with a 50 Gbps granularity. The load is adjusted to achieve a SBR between 0.01% and 1% when employing the proposed *SFQA-defrag* algorithm.

This thesis evaluates two variants of the *SFQA* algorithm, distinguished by the choice of the SF metric. The variant using the NoC metric is denoted as *SFQA-NoC*, while the one based on the RSS metric is named *SFQA-RSS*. When the RBMSA algorithm is integrated with proactive SD, the corresponding versions are denoted as *SFQA-defrag-NoC* and *SFQA-defrag-RSS*. The SD period is fixed at 10 service request arrivals, and the maximum number of allowed reallocations per SD cycle is set to $N = 10$.

To assess the performance of the proposed algorithm, we compare it with three benchmark algorithms: *QA*, which considers only the QoT of the channels during resource assignment and always selects the highest modulation format available [89], *FA-NoC* and *FA-RSS*, which are fragmentation-aware only, and rely on the two respective fragmentation metrics, and *SAP*, a baseline approach that first selects the shortest path and then identifies the channel that supports the highest modulation format along that path. For all methods, when identical modulation formats or SF metrics are encountered, channels at the lowest frequency are prioritized.

Figures 5.3a, 5.3b, and 5.3c present the SBR results under varying traffic loads for the JPNB, USB, and SPNB topologies, respectively. The results demonstrate that the *QA* strategy consistently outperforms *SAP* by 23.7%, 19%, and 10% for the JPNB, USB, and SPNB topologies, respectively, indicating performance improvements obtained through the prioritization of physical-layer impairments in path selection. The results further indicate that *FA-NoC* and *FA-RSS*, which incorporate only SF metrics into the decision-making process, also outperform *SAP* for all topologies.

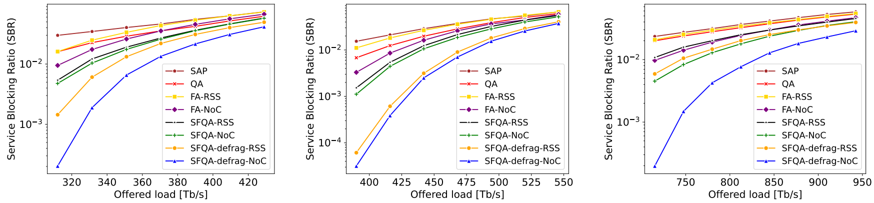

(a) JPNB topology **(b)** USB topology **(c)** SPNB topology

Figure 5.3: The service blocking ratio (SBR) for the three considered topologies. Reprinted from **Paper F**.

The *SFQA* algorithm, which jointly considers QoT and SF, achieves superior performance compared to all benchmark algorithms. The *SFQA-NoC* version of the algorithm slightly outperforms *SFQA-RSS*, and significantly surpasses *QA* and *FA-NoC* by 23% and 24% on average across all traffic loads for the JPNB topology. A similar trend is observed for the USB topology, where *SFQA-NoC* outperforms *QA* and *FA-NoC* by 28% and 19% on average, with performance levels close to *SFQA-RSS*. However, a different trend emerges for the SPNB topology, where *SFQA-NoC* outperforms *SFQA-RSS* by 22%. Additionally, in the SPNB topology, *SFQA-NoC* outperforms the *QA* and *FA-NoC* algorithms by 39% and 22%, respectively. The overall superior performance of the *SFQA* algorithms over *QA* highlights the benefits of incorporating spectrum occupancy state information into the path and channel selection processes. Also, joint consideration of both QoT and SF metrics leads to more informed routing and allocation decisions, resulting in improved resource utilization compared to strategies focused on one single aspect.

Figure 5.3 further illustrates the SBR performance of *SFQA-defrag-RSS* and *SFQA-defrag-NoC*, which combine RBMSA with proactive defragmentation. These enhanced versions outperform their non-defragmentation counterparts. Specifically, for the JPNB topology, *SFQA-defrag-NoC* and *SFQA-defrag-RSS* achieve 41.2% and 20% improvements over *SFQA-NoC* and *SFQA-RSS*, respectively. The USB topology shows comparable improvements of 43% and 41%, while in the SPNB topology, the respective improvements are 44% and 18%.

The impact of different SF metrics on the performance of the proposed algorithms, in terms of SBR, can be assessed by comparing *SFQA-defrag-RSS* and *SFQA-defrag-NoC*, as illustrated in Figure 5.3. For all three topologies, *SFQA-defrag-NoC* consistently outperforms *SFQA-defrag-RSS*, indicating that the NoC metric is better suited than RSS for capturing SF in MB-EONs where services are allocated over discrete channels. The detailed numerical comparison of these approaches, including performance metrics such as average path length, GSNR, and defragmentation overhead, is provided in **Paper F**.

5.5 Summary

This chapter proposes a heuristic algorithm for the routing, band, modulation format and spectrum assignment problem in multi-band elastic optical network, incorporating both quality of transmission-awareness and spectrum fragmentation (SF) metrics. The algorithm integrates proactive spectrum defragmentation (SD) with traffic grooming for new service requests and regrooming during SD cycles to improve spectrum usage efficiency.

Simulation results on three realistic topologies show that the proposed approach achieves a significant reduction in service blocking ratio up to 44% on average compared to benchmark methods. This improvement comes at the cost of a modest increase in average path length, which is observed to rise by up to 13%. This observation highlights the importance of jointly incorporating physical-layer impairments and spectrum fragmentation into the resource allocation process, rather than relying solely on one of them.

CHAPTER 6

Summary of included papers

This chapter provides a summary of the included papers.

6.1 Paper A

Ehsan Etezadi, Carlos Natalino, Christine Tremblay, Lena Wosinska, Marija Furdek
Programmable Filterless Optical Networks: Architecture, Design and Resource Allocation
Published in IEEE/ACM Transactions on Networking,
vol. 32, no. 2, pp. 1096-1109. 2024

This paper presents a cost-efficient planning approach for PFON, aiming to minimize spectrum usage, the degree of deployed couplers, the number of required EDFAs, and the size of OB switching matrices. The RMSA problem in PFONs is formulated as an ILP with the objective of minimizing both spectrum resource usage and the total degree of passive components. To address scalability issues associated with ILP, a two-step formulation is introduced, enabling near-optimal solutions for larger problem instances within a short execution time. Additionally, a heuristic algorithm is proposed for EDFA placement, calculating the total loss experienced by each connection at each node and deploying amplifiers accordingly for intra-node loss compensation. The study focuses on amplifier placement within nodes for managing internal losses, assuming that the optical line system is pre-deployed and optimized for span loss compensation. Furthermore, the study explores cost trade-offs associated with incorporating AoD-enabled programmability in filterless networks, evaluating spectrum resource usage alongside OB switch and amplifier costs. A detailed simulation analysis on two core and one regional network topology under varying traffic loads demonstrates the strong potential of PFONs to strike a balance between spectrum usage efficiency and equipment cost.

Ehsan Etezadi (EE) developed the ILP formulation, performed the simulation, analyzed the results, and wrote the paper. Marija Furdek (MF) proposed the research idea, formulated the problem, and contributed to the writing of the system model and analysis. Carlos Natalino (CN) contributed to the implementation and analysis. Lena Wosinska (LW) and Christine Tremblay (CT) contributed to the analysis. All authors reviewed and revised the paper.

6.2 Paper B

Ehsan Etezadi, Carlos Natalino, Renzo Diaz, Anders Lindgren, Stefan Melin, Lena Wosinska, Paolo Monti, Marija Furdek
DeepDefrag: A deep reinforcement learning framework for spectrum defragmentation
2022 IEEE Global Communications Conference, GLOBECOM 2022 - Proceedings, p. 3694-3699,
Rio de Janeiro, Brazil, Dec. 2022

Motivated by the need for automating complex networking tasks, this paper introduces DeepDefrag, a novel DRL-based framework that efficiently manages all aspects of the SD process. DeepDefrag determines the good timing and composition of SD actions, including the number of reconfigurations, their execution order, and the target spectrum allocation for affected connections. The proposed framework dynamically adapts to the network state, ensuring appropriate decision-making while aligning with operator priorities, such as minimizing the number of connection reallocations. Its performance is evaluated through extensive simulations, demonstrating that DeepDefrag outperforms the state-of-the-art heuristic OF-FF across multiple performance metrics.

EE formulated the problem, developed the DeepDefrag framework, performed the simulation, analyzed the results, and wrote the paper. MF, CN, Paolo Monti (PM), and LW proposed the research idea and contributed to the problem formulation and analysis. Renzo Diaz (RD), Anders Lindgren (AL), and Stefan Melin (SM) provided inputs from Telia company and contributed to the analysis. All authors reviewed and revised the paper.

6.3 Paper C

Ehsan Etezadi, Carlos Natalino, Renzo Diaz, Anders Lindgren, Stefan Melin, Lena Wosinska, Paolo Monti, Marija Furdek
Deep reinforcement learning for proactive spectrum defragmentation in elastic optical networks [Invited]
Published in IEEE/Optica Journal of Optical Communications and Networking (JOCN),
vol. 15, no. 10, pp. 86-96.

The DeepDefrag framework in **Paper B** only considered a limited subset of connections for reconfiguration and did not incorporate spectrum occupancy state in its decision-making process. This paper extends DeepDefrag by including all network connections as potential reconfiguration candidates, integrating comprehensive spectrum occupancy information with multiple fragmentation metrics, and refining the reward function for a more comprehensive evaluation of SD actions. Additionally, this paper examines the impact of different penalty models representing SD overhead and assesses how varying traffic loads influence performance. The improved DeepDefrag framework is compared against heuristic algorithms from the literature, with simulation results showing that it achieves SBR values near an approximated heuristic lower bound obtained through exhaustive defragmentation. We also demonstrate that, unlike preconfigured approaches such as OF-FF, DeepDefrag dynamically adapts to traffic fluctuations, learning optimal policies based on current network conditions, enabling it to make more efficient decisions, continuously optimize spectrum utilization, and improve overall network performances.

EE formulated the problem, proposed ideas, performed the simulation, analyzed the results, and wrote the paper. MF, CN, PM, and LW contributed to the idea generation, problem formulation and analysis. RD, AL, and SM provided inputs from Telia company and contributed to the analysis. All authors reviewed and revised the paper.

6.4 Paper D

Ehsan Etezadi, Carlos Natalino, Vignesh Karunakaran, Renzo Diaz, Anders Lindgren, Stefan Melin, Achim Autenrieth, Lena Wosinska, Paolo Monti, Marija Furdek
Demonstration of DRL-based intelligent spectrum management over a T-API-enabled optical network digital twin
49th European Conference on Optical Communications (ECOC), Glasgow, Scotland, Oct. 2023

In this demonstration, we develop a novel defragmentation module that leverages standard T-API messages to implement SD decisions made by the DeepDefrag DRL agent. We demonstrate the module's capabilities through an interactive dashboard, allowing users to configure network operation settings, monitor the fragmented network state, observe DRL-driven SD decisions, and analyze their execution within a carrier-grade digital twin.

EE formulated the problem, developed the dashboard, and wrote the paper. CN contributed to implementation and idea generation. MF, PM, and LW contributed to the problem formulation and analysis. RD, AL, and SM provided inputs from Telia company and contributed to the analysis. Vignesh Karunakaran and Achim Autenrieth provided T-API interface. All authors reviewed and revised the paper.

6.5 Paper E

Ehsan Etezadi, Farhad Arpanaei, Carlos Natalino, Lena Wosinska, Erik Agrell, Paolo Monti, David Larrabeiti, Marija Furdek
Joint Fragmentation- and QoT-Aware RBMSA in Dynamic Multi-Band Elastic Optical Networks
24th International Conference on Transparent Optical Networks (ICTON),
Bari, Italy, Jul. 2024

In this paper, we propose, for the first time, a heuristic algorithm for SFQA RBMSA in C+L+S-band dynamic MB-EONs. The algorithm jointly considers two different SF metrics along with the GSNR levels of available channels across multiple candidate paths. A comprehensive performance evaluation is conducted, comparing the proposed approach against existing heuristic algorithms from the literature. The results demonstrate that the SFQA algorithm outperforms approaches that consider only the QoT of the channels, achieving superior results in terms of SBR.

EE formulated the problem, proposed ideas, performed the simulation, analyzed the results, and wrote the paper. MF, CN, PM, Erik Agrell (EA) and LW contributed to the analysis. Farhad Arpanaei (FA) and David Larrabeiti provided the physical layer model. All authors reviewed and revised the paper.

6.6 Paper F

Ehsan Etezadi, Farhad Arpanaei, Carlos Natalino, Erik Agrell, Paolo Monti, José Alberto Hernández, Marija Furdek
Fragmentation- and QoT-Aware RBMSA with Spectrum Defragmentation in Dynamic Multi-Band Elastic Optical Networks
Submitted to the Journal of Lightwave Technology in May 2025
.

In this paper, we enhance the SFQA RBMSA algorithm from **Paper E** by integrating it with proactive SD, creating a more efficient approach for C+L+S-band MB-EONs. In addition to QoT- and fragmentation-aware RBMSA, we incorporate traffic grooming to optimize incoming requests, and traffic regrooming during SD cycles to further improve spectrum utilization. To evaluate the effectiveness of the proposed approach, we conduct extensive performance analyses across three network topologies under different traffic loads, and compare the results against existing heuristic algorithms. The findings demonstrate that SFQA with proactive SD significantly reduces SBR, outperforming algorithms that consider only QoT or SF metrics.

EE formulated the problem, proposed ideas, performed the simulation, analyzed the results, and wrote the paper. MF, CN, PM, and EA contributed to the analysis. FA and Jose Alberto Hernandez provided the physical layer model. All authors reviewed and revised the paper.

CHAPTER 7

Concluding Remarks and Future Work

The approaches proposed in this thesis address some of the timely and relevant problems related to the flexibility of optical network architecture and resource usage efficiency in forward-looking scenarios. Despite the demonstrated benefits of the proposed techniques, these challenges remain relevant and open additional directions for future extensions, summarized as follows.

This study introduces a detailed design framework for programmable filterless optical network (PFON) architecture, leveraging coherent elastic transmission and optical white box switches. The routing, modulation format, and spectrum assignment problem is addressed jointly with the node architecture design and formulated as an integer linear program aimed at minimizing both spectrum usage and the degree of passive coupler deployment. The PFON architecture demonstrates advantages over traditional passive filterless optical networks, showing improvements in spectrum usage efficiency and a reduction in unnecessary signal broadcasting. Compared to conventional wavelength-switched optical networks, the PFON design significantly reduces the number of switches and amplifiers. These findings confirm the potential of programmable filterless architectures to provide scalable, cost-effective, and flexible solutions for future optical network deployments.

In this thesis, we have investigated PFONs under static traffic conditions. However, with the emergence of new services characterized by highly dynamic traffic patterns and the advancements in network function virtualization, it becomes essential to explore the operation of PFONs in dynamic environments. The new services can be realized as service chains, where traffic flows are processed through a sequence of virtualized network functions running on different servers. In such scenarios, a PFON must support adaptive and flexible service provisioning to handle dynamic and heterogeneous traffic demands. Future research should focus on the integration of intelligent service chaining frameworks with programmable optical nodes to fully exploit the potential of PFONs for efficient, scalable, and resilient service provisioning in next-generation optical networks.

Regarding the dynamic network scenarios, this thesis proposes DeepDefrag, a deep reinforcement learning-based framework for proactive spectrum defragmentation (SD). DeepDefrag determines efficient SD strategies by incorporating spectrum fragmentation (SF) metrics into its decision-making process. Simulation results demonstrate that DeepDefrag significantly improves service blocking ratio (SBR) performance while reducing the overhead associated with defragmentation operations. Additionally, the framework adapts effectively to varying network load conditions, continuously refining its decisions to maintain good network performance. However, the current approach focuses solely on reassigning spectrum along the same path without considering connection rerouting. Integrating rerouting strategies alongside spectrum reallocation could offer substantial improvements in managing SF. Future research should investigate the combined impact of rerouting and reallocation in dynamic network environments, carefully assessing the trade-offs between operational complexity, reconfiguration overhead, and potential SD gains.

Finally, this study extends to evaluate SF management in multi-band elastic optical networks (MB-EONs), which are crucial for addressing the growing demands of modern communication systems. It proposes a heuristic algorithm for routing, band, modulation format, and spectrum assignment in MB-EONs, incorporating quality of transmission-awareness and fragmentation metrics. By further integrating proactive SD, the proposed approach demonstrates significant improvements in SBR and spectrum utilization for multiple network topologies. The results highlight that joint consideration of spectrum occupancy and physical-layer impairments during resource allocation leads to better performance than relying on either one of them. However, this study does not explore the cost and energy consumption considerations across different spectral bands. In particular, the cost and energy efficiency of transponders, amplifiers, and switching equipment should be further analyzed to provide a more comprehensive evaluation of MB-EONs designs. Future work could extend the proposed framework to consider these aspects.

References

[1] B. C. Chatterjee, S. Ba, and E. Oki, "Fragmentation problems and management approaches in elastic optical networks: A survey," *IEEE Communications Surveys & Tutorials*, vol. 20, no. 1, pp. 183–210, 2017.

[2] N. Amaya, G. Zervas, and D. Simeonidou, "Introducing node architecture flexibility for elastic optical networks," *Journal of Optical Communications and Networking*, vol. 5, no. 6, pp. 593–608, 2013.

[3] Polatis, *Series 6000n network optical switch*, 2022.

[4] E. Archambault, N. Alloune, M. Furdek, *et al.*, "Routing and spectrum assignment in elastic filterless optical networks," *IEEE/ACM Transactions On Networking*, vol. 24, no. 6, pp. 3578–3592, 2016.

[5] M. Furdek, A. Muhammad, G. Zervas, N. Alloune, C. Tremblay, and L. Wosinska, "Programmable filterless network architecture based on optical white boxes," in *2016 International Conference on Optical Network Design and Modeling (ONDM)*, IEEE, 2016, pp. 1–6.

[6] A. Muhammad, M. Furdek, G. Zervas, and L. Wosinska, "Filterless networks based on optical white boxes and sdm," in *ECOC 2016; 42nd European Conference on Optical Communication*, VDE, 2016, pp. 1–3.

[7] G. M. Saridis, B. J. Puttnam, R. S. Luis, *et al.*, "Experimental demonstration of a flexible filterless and bidirectional sdm optical metro/inter-dc network," in *ECOC 2016; 42nd European Conference on Optical Communication*, VDE, 2016, pp. 1–3.

[8] Y. Yin, H. Zhang, M. Zhang, *et al.*, "Spectral and spatial 2d fragmentation-aware routing and spectrum assignment algorithms in elastic optical networks," *Journal of Optical Communications and Networking*, vol. 5, no. 10, A100–A106, 2013.

[9] S. Ba, B. C. Chatterjee, and E. Oki, "Defragmentation scheme based on exchanging primary and backup paths in 1+ 1 path protected elastic optical networks," *IEEE/ACM Transactions on Networking*, vol. 25, no. 3, pp. 1717–1731, 2017.

[10] M. Zhang, C. You, and Z. Zhu, "On the parallelization of spectrum defragmentation reconfigurations in elastic optical networks," *IEEE/ACM Transactions on Networking*, vol. 24, no. 5, pp. 2819–2833, 2015.

[11] J. Comellas, L. Vicario, and G. Junyent, "Proactive defragmentation in elastic optical networks under dynamic load conditions," *Photonic Network Communications*, vol. 36, no. 1, pp. 26–34, 2018.

[12] D. Moniz, A. Eira, A. de Sousa, and J. Pires, "On the comparative efficiency of non-disruptive defragmentation techniques in flexible-grid optical networks," *Optical Switching and Networking*, vol. 25, pp. 149–159, 2017.

[13] W. Klaus, P. J. Winzer, and K. Nakajima, "The role of parallelism in the evolution of optical fiber communication systems," *Proceedings of the IEEE*, vol. 110, no. 11, pp. 1619–1654, 2022.

[14] T. Hoshida, V. Curri, L. Galdino, *et al.*, "Ultrawideband systems and networks: Beyond c+ l-band," *Proceedings of the IEEE*, vol. 110, no. 11, pp. 1725–1741, 2022.

[15] F. Arpanaei, J. M. Rivas-Moscoso, I. De Francesca, *et al.*, "Enabling seamless migration of optical metro-urban networks to the multi-band: Unveiling a cutting-edge 6d planning tool for the 6g era," *Journal of Optical Communications and Networking*, vol. 16, no. 4, pp. 463–480, 2024.

[16] P. Poggiolini, "A generalized gn-model closed-form formula," *arXiv preprint arXiv:1810.06545*, 2018.

[17] J. L. Ravipudi and M. Brandt-Pearce, "Impairment-and fragmentation-aware dynamic routing, modulation and spectrum allocation in c+ l band elastic optical networks using q-learning," *Optical Switching and Networking*, vol. 47, p. 100 717, 2023.

[18] Y. Liu, N. Feng, L. Shen, J. Lv, D. Yan, and J. Zhao, "Fragmentation and isrs-aware survivable routing, band, modulation, and spectrum allocation algorithm in multi-band elastic optical networks," *Applied Sciences*, vol. 14, no. 11, p. 4755, 2024.

[19] R. K. Jana, B. C. Chatterjee, A. P. Singh, *et al.*, "Machine learning-assisted nonlinear-impairment-aware proactive defragmentation for c+ l band elastic optical networks," *Journal of Optical Communications and Networking*, vol. 14, no. 3, pp. 56–68, 2021.

[20] S. J. Ben Yoo, "Elastic optical networking architecture, system, and technologies," in *2014 Asia Communications and Photonics Conference (ACP)*, 2014, pp. 1–1.

[21] O. Ayoub, O. Karandin, M. Ibrahimi, A. Castoldi, F. Musumeci, and M. Tornatore, "Tutorial on filterless optical networks," *Journal of Optical Communications and Networking*, vol. 14, no. 3, pp. 1–15, 2021.

[22] C. Tremblay, P. Littlewood, M. P. Bélanger, L. Wosinska, and J. Chen, "Agile filterless optical networking," in *2017 International Conference on Optical Network Design and Modeling (ONDM)*, IEEE, 2017, pp. 1–4.

[23] Q. Lv and Z. Zhu, "On the multilayer planning of filterless optical networks with otn encryption," *IEEE/ACM Transactions on Networking*, vol. 31, no. 6, pp. 2529–2544, 2023.

[24] P. Castoldi, A. Giorgetti, A. Sgambelluri, *et al.*, "Optical white box: Modeling and implementation," in *2018 20th International Conference on Transparent Optical Networks (ICTON)*, IEEE, 2018, pp. 1–4.

[25] B. C. Chatterjee, N. Sarma, and E. Oki, "Routing and spectrum allocation in elastic optical networks: A tutorial," *IEEE Communications Surveys & Tutorials*, vol. 17, no. 3, pp. 1776–1800, 2015.

[26] X. Wan, N. Hua, and X. Zheng, "Dynamic routing and spectrum assignment in spectrum-flexible transparent optical networks," *Journal of Optical Communications and Networking*, vol. 4, no. 8, pp. 603–613, 2012.

[27] M. M. R. Villamayor-Paredes, L. V. Maidana-Benítez, J. Colbes, and D. P. Pinto-Roa, "Routing, modulation level, and spectrum assignment in elastic optical networks. a route-permutation based genetic algorithms," *Optical Switching and Networking*, vol. 47, p. 100 710, 2023.

[28] J. H. Capucho and L. C. Resendo, "Ilp model and effective genetic algorithm for routing and spectrum allocation in elastic optical networks," in *2013 SBMO/IEEE MTT-S International Microwave & Optoelectronics Conference (IMOC)*, IEEE, 2013, pp. 1–5.

[29] T. A. Feo and M. G. Resende, "Greedy randomized adaptive search procedures," *Journal of global optimization*, vol. 6, pp. 109–133, 1995.

[30] R. Chibante, *Simulated annealing: theory with applications*. BoD–Books on Demand, 2010.

[31] H. Zang, J. P. Jue, B. Mukherjee, *et al.*, "A review of routing and wavelength assignment approaches for wavelength-routed optical wdm networks," *Optical networks magazine*, vol. 1, no. 1, pp. 47–60, 2000.

[32] J. Y. Yen, "Finding the k shortest loopless paths in a network," *management Science*, vol. 17, no. 11, pp. 712–716, 1971.

[33] D. Cavendish and M. Gerla, "Internet qos routing using the bellmanford algorithm," in *High Performance Networking: IFIP TC-6 Eighth International Conference on High Performance Networking (HPN '98) Vienna, Austria, September 21–25, 1998*, Springer, 1998, pp. 627–646.

[34] I. Olszewski, "Spectrum allocation policy in elastic optical networks," *International Journal of Electronics and Telecommunications*, vol. 63, no. 4, pp. 423–429, 2017.

[35] G. N. Rouskas, "First-fit: A universal algorithm for spectrum assignment," in *GLOBECOM 2023-2023 IEEE Global Communications Conference*, IEEE, 2023, pp. 2123–2128.

[36] K. Christodoulopoulos, I. Tomkos, and E. A. Varvarigos, "Elastic bandwidth allocation in flexible ofdm-based optical networks," *Journal of Lightwave Technology*, vol. 29, no. 9, pp. 1354–1366, 2011.

[37] S. Hosseini, I. de Miguel, R. J. D. Barroso, *et al.*, "Multi-band elastic optical networks: Overview and recent contributions from the iotalentum project," in *International Symposium on Distributed Computing and Artificial Intelligence*, Springer, 2023, pp. 467–472.

[38] N. Sambo, A. Ferrari, A. Napoli, *et al.*, "Provisioning in multi-band optical networks," *Journal of Lightwave Technology*, vol. 38, no. 9, pp. 2598–2605, 2020.

[39] A. Napoli, N. Costa, J. K. Fischer, *et al.*, "Towards multiband optical systems," in *Photonic Networks and Devices*, Optica Publishing Group, 2018, NeTu3E–1.

[40] R. Wang and B. Mukherjee, "Provisioning in elastic optical networks with non-disruptive defragmentation," *Journal of Lightwave Technology*, vol. 31, no. 15, pp. 2491–2500, 2013.

[41] X. Wang, Q. Zhang, I. Kim, P. Palacharla, and M. Sekiya, "Utilization entropy for assessing resource fragmentation in optical networks," in *Optical Fiber Communication Conference*, Optica Publishing Group, 2012, OTh1A–2.

[42] D. Amar, E. Le Rouzic, N. Brochier, J.-L. Auge, C. Lepers, and N. Perrot, "Spectrum fragmentation issue in flexible optical networks: Analysis and good practices," *Photonic Network Communications*, vol. 29, pp. 230–243, 2015.

[43] X. Yu, J. Zhang, Y. Zhao, *et al.*, "Spectrum compactness based defragmentation in flexible bandwidth optical networks," in *OFC/NFOEC*, IEEE, 2012, pp. 1–3.

[44] Y. Yin, M. Zhang, Z. Zhu, and S. B. Yoo, "Fragmentation-aware routing, modulation and spectrum assignment algorithms in elastic optical networks," in *2013 Optical Fiber Communication Conference and Exposition and the National Fiber Optic Engineers Conference (OFC/NFOEC)*, IEEE, 2013, pp. 1–3.

[45] P. Lechowicz, M. Tornatore, A. Włodarczyk, and K. Walkowiak, "Fragmentation metrics and fragmentation-aware algorithm for spectrally/spatially flexible optical networks," *Journal of Optical Communications and Networking*, vol. 12, no. 5, pp. 133–145, 2020.

[46] M. Zhang, Y. Yin, R. Proietti, Z. Zhu, and S. B. Yoo, "Spectrum defragmentation algorithms for elastic optical networks using hitless spectrum retuning techniques," in *2013 Optical Fiber Communication Conference and Exposition and the National Fiber Optic Engineers Conference (OFC/NFOEC)*, IEEE, 2013, pp. 1–3.

[47] Y. Aoki, X. Wang, P. Palacharla, *et al.*, "Dynamic and flexible photonic node architecture with shared universal transceivers supporting hitless defragmentation," in *European Conference and Exhibition on Optical Communication*, Optica Publishing Group, 2012, We–3.

[48] C. Tremblay, F. Gagnon, B. Chatelain, E. Bernier, and M. P. Belanger, "Filterless optical networks: A unique and novel passive wan network solution," *IEICE proceedings series*, vol. 49, no. 12P-7, 2007.

[49] É. Archambault, D. O'Brien, C. Tremblay, F. Gagnon, M. P. Bélanger, and É. Bernier, "Design and simulation of filterless optical networks: Problem definition and performance evaluation," *Journal of Optical Communications and Networking*, vol. 2, no. 8, pp. 496–501, 2010.

[50] B. Jaumard, Y. Wang, and D. Coudert, "Dantzig–wolfe decomposition for the design of filterless optical networks," *Journal of Optical Communications and Networking*, vol. 13, no. 12, pp. 312–321, 2021.

[51] Z. Xu, C. Tremblay, E. Archambault, *et al.*, "Flexible wavelength assignment in filterless optical networks," *IEEE Commun. Lett*, vol. 19, no. 4, pp. 565–568, 2015.

[52] P. Littlewood, M. P. Bélanger, C. Tremblay, M. Nooruzzaman, and N. Alloune, *Network resource optimization based on time-varying traffic in optical networks*, US Patent 10,623,126, Apr. 2020.

[53] G. Mantelet, C. Tremblay, D. V. Plant, P. Littlewood, and M. P. Bélanger, "Pce-based centralized control plane for filterless networks," *IEEE Communications Magazine*, vol. 51, no. 5, pp. 128–135, 2013.

[54] A. Clauberg, "Ipv6 deployment in germany and croatia," *online: http://www.ipv6observatory. eu/wp-content/uploads/2012/11/01-06-Axel-Clauber1.pdf*, 2012.

[55] D. Uzunidis, M. Presi, A. Sgambelluri, F. Paolucci, A. Stavdas, and F. Cugini, "Bidirectional single-fiber filterless optical networks: Modeling and experimental assessment," *Journal of Optical Communications and Networking*, vol. 13, no. 6, pp. C1–C9, 2021.

[56] F. Paolucci, R. Emmerich, A. Eira, *et al.*, "Disaggregated edge-enabled c+ l-band filterless metro networks," *Journal of Optical Communications and Networking*, vol. 12, no. 3, pp. 2–12, 2019.

[57] O. Karandin, O. Ayoub, F. Musumeci, M. Tornatore, *et al.*, "A techno-economic comparison of filterless and wavelength-switched optical metro networks," in *Proceedings of International Conference of Transparent Optical Networks*, 2020, pp. 1–4.

[58] P. Pavon-Marino, F.-J. Moreno-Muro, M. Garrich, *et al.*, "Techno-economic impact of filterless data plane and agile control plane in the 5g optical metro," *Journal of Lightwave Technology*, vol. 38, no. 15, pp. 3801–3814, 2020.

[59] O. Ayoub, F. Fatima, A. Bovio, F. Musumeci, and M. Tornatore, "Traffic-adaptive re-configuration of programmable filterless optical networks," in *ICC 2020-2020 IEEE International Conference on Communications (ICC)*, IEEE, 2020, pp. 1–6.

[60] V. Abedifar and M. Eshghi, "Routing, modulation format, spectrum and core allocation in space-division-multiplexed programmable filterless networks," *Optical fiber technology*, vol. 49, pp. 37–49, 2019.

[61] M. Džanko, M. Furdek, B. Mikac, G. Zervas, E. Hugues-Salas, and D. Simeonidou, "Synthesis, resiliency and power efficiency of function programmable optical nodes," in *2015 13th International Conference on Telecommunications (ConTEL)*, IEEE, 2015, pp. 1–8.

[62] M. Džanko, M. Furdek, G. Zervas, and D. Simeonidou, "Evaluating availability of optical networks based on self-healing network function programmable roadms," *Journal of Optical Communications and Networking*, vol. 6, no. 11, pp. 974–987, 2014.

[63] M. Furdek, M. Dzanko, N. Skorin-Kapov, and L. Wosinska, "Planning of optical networks based on programmable roadms," in *Asia Communications and Photonics Conference*, Optica Publishing Group, 2015, AM3G–1.

[64] M. Furdek, M. Dzanko, M. Matani, I. Boric, L. Wosinska, and B. Mikac, "Multi-hour network provisioning utilizing function programmable roadms," in *2015 17th International Conference on Transparent Optical Networks (ICTON)*, IEEE, 2015, pp. 1–4.

[65] A. Muhammad, G. Zervas, N. Amaya, D. Simeonidou, and R. Forchheimer, "Introducing flexible and synthetic optical networking: Planning and operation based on network function programmable roadms," *Journal of Optical Communications and Networking*, vol. 6, no. 7, pp. 635–648, 2014.

[66] N. Sambo, P. Castoldi, A. D'Errico, *et al.*, "Next generation sliceable bandwidth variable transponders," *IEEE Communications Magazine*, vol. 53, no. 2, pp. 163–171, 2015.

[67] M. Ibrahimi, O. Ayoub, F. Musumeci, *et al.*, "Minimum-cost optical amplifier placement in metro networks," *Journal of Lightwave Technology*, vol. 38, no. 12, pp. 3221–3228, 2020.

[68] É. Archambault, N. Alloune, M. Furdek, *et al.*, "Routing and spectrum assignment in elastic filterless optical networks," *IEEE/ACM Trans. Netw.*, vol. 24, no. 6, pp. 3578–3592, Dec. 2016.

[69] S. Fernández-Martínez, B. Baran, and D. P. Pinto-Roa, "Spectrum defragmentation algorithms in elastic optical networks," *Optical Switching and Networking*, vol. 34, pp. 10–22, 2019.

[70] S. K. Singh and A. Jukan, "Efficient spectrum defragmentation with holding-time awareness in elastic optical networks," *Journal of Optical Communications and Networking*, vol. 9, no. 3, B78–B89, 2017.

[71] S. Trindade and N. L. Da Fonseca, "Machine learning for spectrum defragmentation in space-division multiplexing elastic optical networks," *IEEE Network*, vol. 35, no. 1, pp. 326–332, 2020.

[72] Y. Xiong, Y. Yang, Y. Ye, and G. N. Rouskas, "A machine learning approach to mitigating fragmentation and crosstalk in space division multiplexing elastic optical networks," *Optical Fiber Technology*, vol. 50, pp. 99–107, 2019.

[73] R. Li, R. Gu, W. Jin, and Y. Ji, "Learning-based cognitive hitless spectrum defragmentation for dynamic provisioning in elastic optical networks," *IEEE Communications Letters*, vol. 25, no. 5, pp. 1600–1604, 2021.

[74] V. Mnih, "Playing atari with deep reinforcement learning," *arXiv preprint arXiv:1312.5602*, 2013.

[75] C. Natalino, T. Magalhães, F. Arpanaei, *et al.*, "Optical networking gym: An open-source toolkit for resource assignment problems in optical networks," *Journal of Optical Communications and Networking*, vol. 16, no. 12, G40–G51, 2024.

[76] G. Brockman, "Openai gym," *arXiv preprint arXiv:1606.01540*, 2016.

[77] ONF, *Tr-547, functional requirements for transport api*, https://opennetworking.org, Jul. 2020.

[78] L. Shen, N. Feng, Y. Liu, *et al.*, "Isrs impact-reduced routing, modulation, band, and spectrum allocation algorithm in c+ l-bands elastic optical networks," *Optical Fiber Technology*, vol. 82, p. 103 640, 2024.

[79] R. K. Jana, B. C. Chatterjee, A. P. Singh, *et al.*, "Quality-aware resource provisioning for multiband elastic optical networks: A deep-learning-assisted approach," *Journal of Optical Communications and Networking*, vol. 14, no. 11, pp. 882–893, 2022.

[80] M. Mehrabi, H. Beyranvand, M. J. Emadi, and F. Arpanaei, "Efficient statistical qot-aware resource allocation in eons over the c+ l-band: A multi-period and low-margin perspective," *Journal of Optical Communications and Networking*, vol. 16, no. 5, pp. 577–592, 2024.

[81] R. Wang and B. Mukherjee, "Spectrum management in heterogeneous bandwidth optical networks," *Optical Switching and Networking*, vol. 11, pp. 83–91, 2014.

[82] R. Zhu, S. Li, P. Wang, and J. Yuan, "Time and spectrum fragmentation-aware virtual optical network embedding in elastic optical networks," *Optical Fiber Technology*, vol. 54, p. 102 117, 2020.

[83] Y. Teng, H. Yang, Q. Yao, *et al.*, "Srs-proactive-aware resource allocation based on all-optical wavelength converters in c+ l band optical networks," *Journal of Lightwave Technology*, 2024.

[84] J. Liu, Z. Xi, and R. Gu, "Adaptive cross-layer bandwidth defragmentation for multi-band optical network," in *2023 Asia Communications and Photonics Conference/2023 International Photonics and Optoelectronics Meetings (ACP/POEM)*, IEEE, 2023, pp. 1–5.

[85] P. Poggiolini and M. Ranjbar-Zefreh, "Closed form expressions of the nonlinear interference for uwb systems," in *2022 European Conference on Optical Communication (ECOC)*, IEEE, 2022, pp. 1–4.

[86] M. R. Zefreh and P. Poggiolini, "A gn-model closed-form formula supporting ultra-low fiber loss and short fiber spans," *arXiv preprint arXiv:2111.04584*, 2021.

[87] F. Arpanaei et al., "Enabling seamless migration of optical metro-urban networks to the multi-band: Unveiling a cutting-edge 6D planning tool for the 6G era," *Journal of Optical Communications and Networking*, vol. 16, no. 4, pp. 463–480, 2024.

[88] M. Quagliotti et al., "Spectrum fragmentation metrics and their use in optical channel allocation algorithms," in *Fotonica*, 2017, pp. 1–4.

[89] F. Arpanaei, M. R. Zefreh, Y. Jiang, *et al.*, "Synergizing hyper-accelerated power optimization and wavelength-dependent qot-aware cross-layer design in next-generation multi-band eons," *arXiv preprint arXiv:2411.02911*, 2024.

Part II

Papers

PAPER A

Programmable Filterless Optical Networks: Architecture, Design and Resource Allocation

Ehsan Etezadi, Carlos Natalino, Christine Tremblay, Lena Wosinska, Marija Furdek

Published in IEEE/ACM Transactions on Networking,
vol. 32, no. 2, pp. 1096-1109. 2024

The layout has been revised.

Abstract

Filterless optical networks (FONs) are a cost-effective optical networking technology that replaces reconfigurable optical add-drop multiplexers, used in conventional, wavelength-switched optical networks (WSONs), by passive optical splitters and couplers. FONs follow the *drop-and-waste* transmission scheme, i.e., broadcast signals without filtering, which generates spectrum waste. Programmable filterless optical networks (PFONs) reduce this waste by equipping network nodes with programmable optical white box switches that support arbitrary interconnections of passive elements. Cost-efficient PFON solutions require optimal routing, modulation format and spectrum assignment (RMSA) to connection requests, as well as optimal design of the node architecture. This paper presents an optimization framework for PFONs. We formulate the RMSA problem in PFONs as a single-step integer linear program (ILP) that jointly minimizes the total spectrum and optical component usage. As RMSA is an NP-complete problem, we propose a two-step ILP formulation that addresses the RMSA sub-problems separately and seeks sub-optimal solutions to larger problem instances in acceptable time. Simulation results indicate a beneficial trade-off between component usage and spectrum consumption in proposed PFON solutions. They use up to 64% less spectrum than FONs, up to 84% fewer active switching elements than WSONs, and up to 81% fewer optical amplifiers at network nodes than FONs or WSONs.

1 Introduction

To support the immense traffic growth and enable scalable on-demand provisioning of service requests, optical networks must deliver great adaptability in a cost- and resource-efficient manner. Agile and flexible optical networking can be achieved in different ways through different technological solutions. The most relevant functionalities enabling adaptable optical networks refer to programmability and reconfigurability of optical switches and edge terminals, which can then be combined into diverse solutions with different trade-offs between performance and cost.

In conventional WSONs, nodes deploy ROADMs with hard-wired constituent components that support transparent switching of optical signals based on their wavelength, as well as local add and drop at the node. An unprecedented level of flexibility in nodal architecture design and network provisioning is provided by disaggregated optical white boxes, also referred to as AoD or function programmable switches [1]. Unlike hard-wired ROADMs, white boxes do not interconnect optical modules (e.g., wavelength-selective switches, passive couplers or EDFAs) in a fixed manner. Instead, the modules are interconnected via an OB (e.g., piezoelectric space switch [2]). This allows to efficiently satisfy the traffic requirements (every connection uses only the required modules) and enables swift reconfiguration in order to accommodate traffic changes, scale capacity, or upgrade the network. Consequently, AoD brings benefits in terms of cost- and energy-efficiency, scalability, and network reliability compared to their ROADM-based counterpart [1].

Filterless optical networks (FONs) have been proposed as a low-cost solution for agile optical networking [3], and accepted as a viable technological solution for deployments in core and metro networks with feasibility demonstrated through several pilot trials. Nodes in FONs use only passive components (i.e., optical couplers and splitters) to broadcast signals, without any active switching or filtering. These passive interconnects result in a set of passive fiber trees that carry signals across the network, while tunable elastic coherent transmitters and receivers at the edge nodes support agile operation [4].

Transmission in FONs follows the drop-and-waste principle, where signals are broadcasted to all links in the fiber tree downstream of the source node and continue to propagate along the links beyond the destination node due to the absence of filtering. The inherently gridless arhitecture and the absence of active switching components bring major advantages of FONs in terms of cost-effectiveness, reliability and energy-efficiency [3]. However, these benefits come at the expense of higher spectrum usage due to the *drop-and-waste* transmission, as well as a rigid physical structure with no architectural flexibility.

To mitigate the drawbacks and combine the benefits of filterless networking with the advantages of optical white boxes, a PFON architecture based on

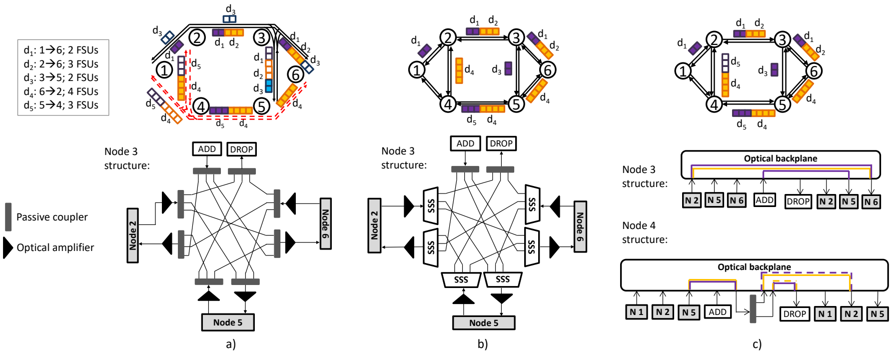

Figure 1: An illustrative example of (a) passive filterless, (b) conventional wavelength-switched, and (c) programmable filterless optical network architecture supporting five connection requests, along with the configuration of representative nodes shown below.

optical white boxes was proposed in [5]. The underlying idea of PFONs is to keep the gridless nature and line system simplifications enabled by filterless networking while introducing node architecture flexibility supported by AoD nodes. Such flexibility enables better adaptation of the nodal configuration to the traffic demands, yielding lower dissipation of spectrum due to the *drop-and-waste* transmission. The PFON architecture is illustrated in Fig. 1 through comparison to FON and WSON, using a simple network example with 6 nodes and 5 communication demands denoted by d_1 to d_5.

Fig. 1a depicts a fully passive filterless solution where two passive fiber trees (shown with the full black and the dashed red lines, respectively) connect the nodes. The details of the internal structure are shown for node 3 below the network example and are analogous for all other nodes. Each node comprises passive splitters and couplers. The nodes also host amplifiers at each ingress and egress port, referred to as pre-amplifiers and boosters, respectively. The absence of filtering implies that a copy of each signal present at the input port of a passive splitter also appears on all of its output ports. The color-filled squares denote the FSUs occupied by the useful signals, while the empty ones represent the unfiltered, wasted slots. As the example illustrates, FONs suffer from a significant waste of spectrum and privacy issues due to the broadcasting and *drop-and-waste* transmission.

Fig. 1b depicts a ROADM-based WSON architecture, and a characteristic nodal setup with spectrum-selective switchess (SSSs) in route&select configuration (shown for node 3 in the lower part of the figure). Naturally, this architecture does not suffer from any spectrum waste as all nodes filter the signals, but it is associated with a much higher cost of the nodes. As in FONs, WSON nodes also host a pre-amplifier and a booster at each ingress and egress port, respectively. Note that both FON and WSON nodes may host additional amplifiers at their *add* and *drop* sections. However, in our study, we focus only on the pass-through functionalities and do not consider the dimensioning of the *add* and *drop* segments.

The PFON architecture supporting the given set of demands is shown in Fig. 1c. Compared to Fig. 1a, PFON wastes less spectrum for unfiltered channels, implying a greater possibility of spectrum reuse than in FONs. The reduction in spectrum use is particularly noticeable on link 3–5, where the PFON uses 4 times fewer FSUs than the FON architecture. The detailed setup of nodes 3 and 4, shown in the bottom part of the figure, illustrates how the nodal architecture can be configured in a flexible manner, as per traffic requirements. AoD nodes support node bypass, often referred to as fiber switching, where an input and an output fiber are directly connected via the OB. In node 3, this allows for d_1 and d_2 to be sent from the incoming port from node 2 directly to the outgoing port towards node 6, while d_3 is added towards node 5. In node 4, fiber switching is not possible and d_4 and d_5 must be split before being directed to their corresponding output ports. Due to the absence of filtering, parts of each signal remain present on both split copies, represented by dashed lines. However, compared to the FON solution, fewer splitters/couplers are used and their degree is lower. Combined with fiber switching, this translates to a lower insertion loss and a lower number of used OB ports.

The existence of unfiltered signals and a lack of pre-defined nodal architecture in PFONs require tailored network design approaches. For a given physical topology of the optical network comprising nodes that host optical white box switches, interconnected with optical fiber links, and a given set of connection demands, the problem of designing a PFON considered in this paper comprises two intertwined sub-problems:

- Solving the RMSA problem for the offered traffic, taking into account the presence of unfiltered signals due to the *drop-and-waste* transmission.

The RMSA problem is proven to be NP-complete already in WSONs [6], and is exacerbated by the presence of unfiltered signals.

- Determining the architecture of the nodes, i.e., the number and the type of components (passive couplers and EDFAs) to be deployed at the nodes, as well as the OB interconnections to support the required processing of the traffic.

In [5], we carried out a preliminary study of the PFON architecture and formulated an ILP for the RMSA problem in PFONs with the objective to minimize spectrum usage. Planning of PFONs based on SDM was investigated in [7], while their feasibility was verified experimentally in [8]. However, cost-efficiency of the new architecture has not been studied so far. Low-cost, energy-efficient solutions require efficient use of active optical equipment at network nodes, i.e., EDFAs and OB switches in the AoD nodes, as well as high spectrum usage efficiency. Both of these parameters are strongly affected by the signal splitting. Splitting, combined with the absence of filtering, is the mechanism that generates spectrum waste. Splitting losses, which are a function of the splitter and coupler degrees, significantly contribute to the losses experienced by the signals inside PFON nodes, creating the need for EDFA deployment at nodes. Moreover, the required OB switch size (and the resulting cost) is directly proportional to the number and the degree of components it interconnects.

Therefore, in this work we extend upon our preliminary study from [5] and develop cost-efficient PFON planning approaches aimed at minimizing spectrum usage, the degree of deployed couplers, the number of required EDFAs, and the required size of the OB switching matrices. We formulate the RMSA problem for PFONs as an ILP with the objective to minimize the total degree of the deployed passive components and spectrum resource usage. The RMSA problem is NP-complete [6], so it is often decomposed into its constituent subproblems of routing, modulation format and spectrum assignment, as in, e.g., [9]. To avoid ILP scalability issues, we propose a two-step ILP formulation that allows finding near-optimal solutions for larger problem instances under short execution time. Furthermore, we propose a heuristic algorithm for the placement of EDFAs that computes the total loss experienced by each connection at each node and deploys the EDFAs required for intra-node loss compensation. We focus on the placement of amplifiers inside the nodes for node loss management purpose, assuming that the optical line system is already deployed and optimized for span loss management.

Our primary objective is to study the cost trade-offs related to the introduction of AoD-enabled programmability to filterless networks in terms of spectrum resource usage, as well as the OB switch and amplifier costs. A detailed simulation analysis carried out on two core and one regional network topology with varying total traffic indicates a strong potential of PFONs to achieve a favorable trade-off between spectral resource usage and equipment cost. The PFON architecture uses up to 64% less spectrum and up to 81% fewer EDFAs than the FON and WSON solutions with hard-wired node structure. On the other hand, PFON uses up to 66% more spectrum than WSON architecture, but reduces the need for optical switching equipment by up to 84% as it only uses 1 optical switch matrix per node instead of an SSS at each input and each output port of all ROADM nodes (considering route&select configuration).

The remainder of the paper is organized as follows. Section 2 reviews the related work on passive filterless networks and AoD as PFON enabling technologies. Section 3 presents the details of our proposed PFON design approaches whose performance is analyzed in Section 4, while Section 5 concludes the paper.

2 Related Work

2.1 Filterless Optical Networking

Since their original proposal in [10], passive filterless optical networks have been extensively studied through theoretical and experimental analysis. A detailed account of the FON concept, architecture, and design can be found in [11], along with an early validation of the FON physical-layer performance in [12]. Since then, extensive design and performance verification studies have established FONs as a viable option for cost-efficient core, metro and submarine networks.

The majority of the initial literature on FONs focused on their applications in core networks, addressing aspects related to design, resource assignment and operation. The problems of defining the node connectivity in the form of passive fiber trees and the static version of the RSA problem for fixed optical grid were addressed in [11], [13] for unprotected design, while [14] investigated

1+1 dedicated optical layer protection. Elastic FONs were introduced in [15], along with a heuristic approach for survivable RMSA with dedicated path protection. An in-depth study of the RMSA problem in FONs was carried out in [3] by developing an ILP formulation and a heuristic approach based on genetic algorithm (GA). Dynamic connection provisioning in FONs was addressed in [16] for terrestrial networks, while [17] investigated the resource savings benefits of dynamic connection reconfiguration under periodic traffic in filterless submarine networks. A control plane design based on path computation element (PCE) was proposed in [18]. Trial deployments in pilot networks based on FONs were carried out in Croatia (2012) and Germany (2014) [19]. Vendor-interoperable FONs interfaces were proposed and experimentally evaluated in [20], indicating great potential of this technology for open line systems.

Telecom operators' search for cost-efficient solutions that satisfy the proliferating traffic in metropolitan areas has been fueling the recent interest in filterless metro networks. [21] introduced a FON architecture for metro applications and developed a physical-layer model to assess their capacity and scalability. A FON node architecture that exploits bidirectional transmission over a single fiber was proposed in [22]. [23] proposed to double the capacity of filterless metro optical networks by exploiting the full C+L band, and implemented and validated extensions of the OpenConfig YANG model to support the C+L band FON transmission. Techno-economic aspects of filterless metro network solutions were studied in [24] and [25]. [24] defined a FON cost model and analyzed the savings with respect to WSONs, while [25] investigated SDN as a dynamic and agile control plane for FONs.

In [26], the authors investigated the problem of virtual service chaining in filterless optical metro networks for dynamic traffic using a heuristic algorithm. [27] defined the problem of survivable virtual network mapping (SVNM) in FONs, highlighting the differences from SVNM in WSONs and jointly solving the problems of fiber tree setup and SVNM with an ILP formulation. The work was extended in [28] by studying virtual network embedding with virtual link protection in FONs, while trying to minimize the network cost in terms of equipment and overall spectrum consumption.

Driven by the operators' interest to reduce equipment costs, the problem of amplifier placement in FONs has received substantial interest from different research groups lately. A GA-based approach for placing boosters, inline amplifiers, and pre-amplifiers in FONs with the objective of minimizing amplifiers cost by considering QoT parameters was proposed in [29]. In [30], the authors developed algorithms for the allocation of amplifiers and transponders and RSA in the open-source Net2Plan framework. The above efforts show that filterless networking is a widely considered solution with relevant applications in practical scenarios. A recent encompassing tutorial on FONs can be found in [31].

Upon the proposal of the PFON concept in [5], a limited number of studies evaluated them towards FONs and WSONs in terms of resource usage and cost. The authors in [32] proposed a traffic-adaptive exhaustive-search algorithm for re-configuration of programmable optical switches in PFONs, with the sole objective of minimizing the overall spectrum consumption. In order to avoid spectrum waste generated by the *drop-and-waste* transmission, [7] proposed to combine PFONs with SDM technology where additional spatial dimensions are utilized to eliminate undesirable signal splitting. A heuristic algorithm for the routing, modulation format, spectrum, and core allocation (RMSCA) problem in programmable filterless SDM networks was proposed in [33], considering also the effect of inter-core crosstalk. Compared to the aforementioned approaches, we provide an ILP optimization framework for joint minimization of component usage and spectrum consumption in PFONs. We present a single-step joint optimization approach that obtains optimal solutions for smaller problem instances. Apart from considering spectrum usage, as in the existing models in the literature, our optimization approach considers the component cost as well, and aims at reducing the number of required EDFAs and the required size of the switch matrices in AoD nodes by minimizing the degree of the deployed passive couplers.

2.2 Optical White Boxes

Optical white boxes were proposed as a technological solution allowing for unprecedented flexibility in nodal architecture design and network provisioning [1]. The work in [1] analyzed the switching, routing and architectural flexibility of this technology, and experimentally demonstrated its feasibility and benefits. Procedures for synthesizing the nodal architecture to support a given traffic mapping between input and output ports of the node can be found in [34], [35]. The related analysis of scalability, power consumption and cost indicates a decrease in the number of used optical backplane ports and the resulting cost and power consumption due to aggregation of channels into fiber-switched port pairs that only use the optical backplane and bypass all other optical components in the node.

Cost-efficient network planning approaches for white box-based elastic networks under static and dynamic traffic were proposed in [36]. Their common objective is to dimension network nodes and perform RMSA for connection requests so as to minimize the number of used components. The impact of optical white box deployment to the availability of connections in the network was evaluated in [37], showing a strong reduction in network downtime due to the support of self-healing of node component failures. Cost-effective planning of AoD-based networks under static, multi-hour and dynamic traffic has been addressed in [38], [39], and [36], respectively. [40] investigated physical-layer implications of AoD and proposed OSNR-aware procedures for nodal architecture composition. Advantages of AoD have been demonstrated in terms of scalability [36], energy efficiency [35], network reliability [37] and resilience [41].

Note that in all of these studies, optical white boxes were used to create complex AoD ROADM structures, where the optical backplane interconnects other active components such as SSSs, amplifiers, or sub-wavelength switches. However, in this paper we assume that the optical backplane uses only passive components to split or couple signals between different ports when necessary, as well as optical amplifiers for node loss compensation, without using any filtering components.

3 PFON Design: RMSA and Node Setup

3.1 Problem Definition

The RMSA problem in programmable filterless networks based on white boxes with the objective of minimizing spectrum usage, the need for amplifier deployment inside nodes, and the required OB switch matrix size can be formally defined as follows. Given a physical topology represented by a graph $\mathcal{G}(\mathcal{V}, \mathcal{E})$ comprising a set of nodes $\mathcal{V}$ and a set of links $\mathcal{E}$, and a set of traffic demands D, we must find a physical route through the network, select a modulation format and assign the appropriate number of spectrum slots to each demand. Moreover, we must determine the architecture of each node capable of sup-

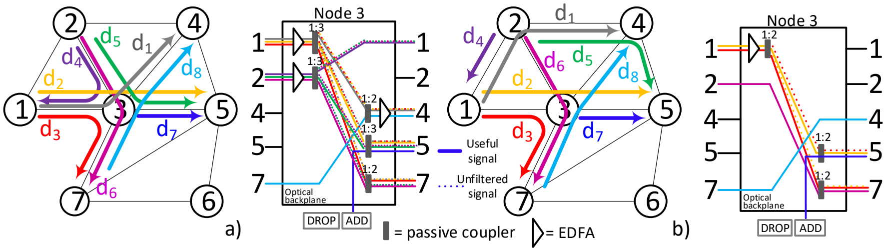

Figure 2: The impact of connection routing in programmable filterless networks on the architecture of node 3 and the necessary amplifiers without (a) and with trying to minimize signal splitting/coupling at node 3 (b).

porting the devised routing solution by configuring an appropriate number and degree of passive couplers, and compensate for the incurred losses with EDFAs. When solving the RMSA problem, the spectrum continuity and contiguity constraints must hold, implying that a demand must use the same, adjacent, spectrum slots along all links included in its path, and there can be no spectrum overlapping among channels that carry useful signals and other useful or unfiltered signals generated due to *drop-and-waste* transmission. In our proposed approach, the objective of minimizing spectrum usage is modeled by minimizing the highest used FSU index in the network. The objective of reducing the component usage is modeled by minimizing the total degree of passive splitters/couplers deployed in the network.

3.2 Illustrative Example

The impact of route selection on the degree of deployed passive components and the subsequent need for amplification is illustrated in Fig. 2 for two valid PFON solutions that serve a set of connections denoted with d_1–d_8, with a focus on the configuration of the central node 3.

The choice of routes used for each demand determine the necessary splitters and couplers. If connections d_i and d_j share the same incoming link to node v but are directed to different outputs, they need to be split at the ingress port. This is the case for, e.g., d_1, d_2 and d_3 in Fig. 2a, where a copy of each signal appears as unfiltered at the outgoing links of node 3 traversed by the other two connections. Analogously, if the two connections use the same outgoing link towards node u but arrive at node v via different incoming links, they

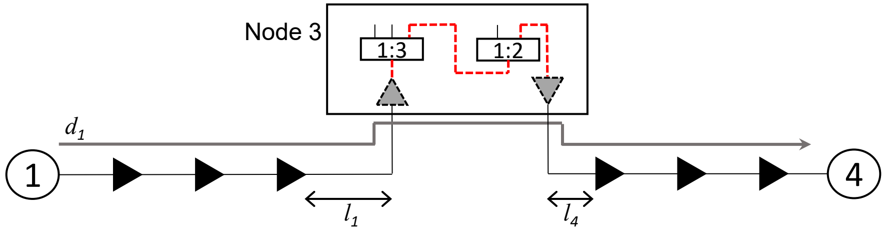

Figure 3: A detailed view of components traversed by connection d_1 inside PFON node 3. The amplifiers inside the node, shown in gray color, are deployed as needed, depending on the total losses generated due to splitting, OB switch traversals, and fiber attenuation on the last span of the ingress link and the first span of the egress link.

need to be coupled at the egress port. This is the case for, e.g., d_3 and d_6 incoming to node 3 via links 1–3 and 2–3, respectively. In the proposed RMSA approach, our goal is to perform connection routing such that the resulting need for splitting/coupling (in terms of the total degree of the deployed passive couplers) is minimized.

Connection routing and the resulting deployment of passive couplers affect the required size of the OB switch and the need for amplification inside nodes. The required OB switch size is a function of the sum of the ports of all components that need to be deployed at the node. The deployment of amplifiers at PFON nodes depends on the total loss experienced by connections that traverse the node between the last line amplifier on the ingress link and the first line amplifier on the egress link. This encompasses the loss due to splitting, coupling and OB traversals inside the node, as well as attenuation on the last span of the ingress link and the first span of the egress link. Conventional node architecture assumes the deployment of pre-amplifiers and boosters at each ingress and egress port, respectively. In our design approach, we leverage on node architecture programmability to bypass the unnecessary amplifiers inside nodes, i.e., amplifiers whose absence yields signal power losses that can be compensated by other existing amplifiers inside the node or at the links.

A more detailed view of the components traversed by connection d_1 is shown in Fig. 3. The figure shows the line amplifiers on links 1–3 and 3–4, with highlighted distances l_1 and l_4. Inside each node, a connection passes through the OB switch as many times as needed to traverse the necessary components.

Connections which undergo splitting and coupling at the node (e.g., d_1 in Fig. 2a) cross the OB three times, connecting *(i)* the input port of the node to the splitter, *(ii)* the splitter to the coupler, and *(iii)* the coupler to the output port of the node. These interconnections are denoted with red dashed lines in Fig. 3. Connections which bypass the node modules (e.g., d_8 in Fig. 2b) traverse the OB only once, to connect the input and the desired output port. If the loss experienced by a connection between the closest two line amplifiers at the ingress and egress link does not exceed an acceptable, predefined threshold that enables correct transmission, one or both amplifiers inside the node, depicted in gray color in Fig. 3, can be omitted.

To this end, for each connection, we calculate the total loss between the two closest amplification sites along the links incoming from and outgoing to the adjacent nodes. We assume the insertion loss of a passive 1:N coupler to be $L_{1:N}$=10log$N$, insertion loss per OB cross-connection of L_{OB}= 1 dB, amplifier input power threshold of -18 dBm, power at the amplifier output of 0 dBm per channel, and fiber attenuation coefficient of L_α=0.2 dB/km. For the example network from Fig. 2, distances l_i from node 3 to the first line amplifier along a link to/from the neighboring node i equal l_1=l_2=l_5=45 km, l_4=20 km, and l_7= 30 km.

For the solution in Fig. 2a, the total loss experienced by connection d_1 between the closest line amplifiers on the input fiber link from node 1 and on the output fiber link to node 4 equals $L_{d_1} = L_\alpha \cdot (l_1 + l_4) + L_{1:3} + L_{1:2} + 3 \cdot L_{OB} =$ 23.7 dB. This value is below the input power threshold of the first line amplifier on link 3–4, so the connection must be amplified at node 3, as depicted in Fig. 3. The figure shows two amplifiers (i.e., at the input and the output port), which are needed to accommodate for the losses of other connections that use the same input and/or output ports of node 3 but traverse different paths through the network and/or different components inside the node (as shown in Fig. 2a).

Analogous to the above considerations, losses experienced by other connections between the two line amplifiers closest to node 3 equal L_{d_2}= 22.4 dB, L_{d_3}= 23.7 dB, L_{d_4}= 20.7 dB, L_{d_5}= 20.4 dB, L_{d_6}= 21.7 dB, L_{d_7}= 9.7 dB, L_{d_8}= 15 dB. Hence, d_1–d_6 must be amplified at node 3, resulting in a total of 3 used EDFAs, as shown in Fig. 2a. The solution in Fig. 2b applies a slightly different routing scheme, which results in a lower number and total degree of splitters at node 3. In this case, losses for d_2, d_3, d_6 and d_8 equal L'_{d_2}= 21 dB, L'_{d_3}= 24 dB, L'_{d_6}= 16 dB, L'_{d_8}= 11 dB, and a single deployed EDFA is sufficient to support d_2 and d_3. As the example also illustrates, lower degree of used passive splitters/couplers also reduces the propagation of unfiltered signals to unwanted output ports, thus reducing the overall spectrum waste.

3.3 Single-step ILP Formulation of the RMSA Problem in PFONs

The single-step ILP formulation for PFON design relies on the model from [5]. For consistency, we use similar notation in our formulation, but we simplify and modify it to enable calculation of the splitter and coupler degrees.

Input parameters

- $\mathcal{G}(\mathcal{V}, \mathcal{E})$: a directed graph with a set of nodes $\mathcal{V}$, and a set of links $\mathcal{E}$;
- D: set of traffic demands, where each element d is associated to traffic volume q_d from source node $s_d \in \mathcal{V}$ to destination node $t_d \in \mathcal{V}$;
- P: set of physical routes, where each element P_d defines a set of K available candidate physical routes $p^d \in P_d$ for demand $d \in \mathsf{D}$, and each route is associated with a number of needed FSUs F_{p^d} according to the modulation format selection method in [3];
- $\tau_{(p^d, p^{\hat{d}})}$: indicator for disjoint routes, equal to 0 when $p^d \in P_d$ and $p^{\hat{d}} \in P_{\hat{d}}$ are link disjoint, and 1 otherwise;
- $\Gamma_{(p^d, p^{\hat{d}})}$: set of links $\in p^{\hat{d}}$ unintentionally traversed by the established optical channel for d over path p^d due to the broadcasting via optical splitters;
- α, β: objective function weighting coefficients;
- T: a large constant.

Variables

- $x_{p^d} \in \{0, 1\}$: equal to 1 if path $p^d \in P_d$ is used by $d \in \mathsf{D}$, and 0 otherwise;
- $f_d \in \mathbb{Z}^+$: the starting spectrum slot index for d;

- $S^{v}_{(\hat{u}v,vu)} \in \{0,1\}$: equal to 1 if any optical channel entering node $v \in \mathcal{V}$ via ingress link $(\hat{u}, v) \in \mathcal{E}$ is directed to the egress link (v, u), and 0 otherwise;
- $a^{v}_{(v,u)} \in \{0,1\}$: equal to 1 if there are demands added at node v and egressing towards node u, and 0 otherwise;
- $d^{v}_{(\hat{u},v)} \in \{0,1\}$: equal to 1 if there are demands ingressing from node $\hat{u}$ and dropped at node v, and 0 otherwise;
- $L^{v}_{\hat{u}v} \in \{0,1\}$: equal to 1 if a splitter is needed at the input port from node $\hat{u}$ of node v, and 0 otherwise.
- $L^{v}_{vu} \in \{0,1\}$: equal to 1 if a coupler is needed at the output port towards node u of node v, and 0 otherwise.
- $\Psi^{(d,\hat{d})}_{(p^d,p^{\hat{d}})} \in \{0,1\}$: equal to 1 if paths p^d and $p^{\hat{d}}$ are assigned to demands d and $\hat{d}$, respectively, and 0 otherwise;
- $\delta_{(d,\hat{d})} \in \{0,1\}$: equal to 0 if the starting slot number of d is greater than $\hat{d}$ (i.e., $f_d > f_{\hat{d}}$), and 1 otherwise;
- $\mathsf{Ci}^{v}_{(\hat{u},v)} \in \mathbb{Z}$: the degree of the splitter traversed by optical channels entering node v via ingress link $(\hat{u}, v)$;
- $\mathsf{Co}^{v}_{(v,u)} \in \mathbb{Z}$: the degree of the coupler traversed by optical channels exiting node v via egress link (v, u);
- $\mathsf{M_s}$: the maximum allocated frequency slot unit (FSU) among all network links.

Objective function

$$\text{Minimize: } \alpha \cdot \mathsf{M_s} + \beta \cdot \sum_{v \in \mathcal{V}} \Big(\sum_{(\hat{u},v) \in \mathcal{E}} \mathsf{Ci}^{v}_{(\hat{u},v)} + \sum_{(v,u) \in \mathcal{E}} \mathsf{Co}^{v}_{(v,u)} \Big) \tag{A.1}$$

Subject to

$$\sum_{p^d \in P_d} x_{p^d} = 1 \quad \forall d \in \mathsf{D} \tag{A.2}$$

$$\sum_{d \in \mathsf{D}} \sum_{p^d \in P_d : (\hat{u},v),(v,u) \in p^d} x_{p^d} \leq \mathsf{T} \cdot S^v_{(\hat{u}v,vu)} \quad \forall v \in \mathcal{V}, \forall (\hat{u},v),(v,u) \in \mathcal{E} \tag{A.3}$$

$$\sum_{d \in \mathsf{D}:s_d=v} \sum_{p^d \in P_d : (v,u) \in p^d} x_{p^d} \leq \mathsf{T} \cdot a^v_{(v,u)}, \forall (v,u) \in \mathcal{E} \tag{A.4}$$

$$\sum_{d \in \mathsf{D}:t_d=v} \sum_{p^d \in P_d : (\hat{u},v) \in p^d} x_{p^d} \leq \mathsf{T} \cdot d^v_{(\hat{u},v)}, \forall (\hat{u},v) \in \mathcal{E} \tag{A.5}$$

$$\mathsf{T} \cdot L^v_{\hat{u}v} \geq \sum_{(v,u) \in \mathcal{E}} S^v_{(\hat{u}v,vu)} + d^v_{(\hat{u},v)} - 1, \tag{A.6}$$

$$2 \cdot L^v_{\hat{u}v} \leq \sum_{(v,u) \in \mathcal{E}} S^v_{(\hat{u}v,vu)} + d^v_{(\hat{u},v)}, \quad \forall v \in \mathcal{V}, \forall (\hat{u},v) \in \mathcal{E}. \tag{A.7}$$

$$\mathsf{Ci}^v_{(\hat{u},v)} \geq \sum_{(v,u) \in \mathcal{E}} S^v_{(\hat{u}v,vu)} + d^v_{(\hat{u},v)} - \mathsf{T} \cdot (1 - L^v_{\hat{u}v}) \quad \forall v \in \mathcal{V}, \forall (\hat{u},v) \in \mathcal{E}. \tag{A.8}$$

$$x_{p^d} + x_{p^{\hat{d}}} - \Psi^{(d,\hat{d})}_{(p^d,p^{\hat{d}})} \leq 1 \quad \forall (d,\hat{d}) \in \mathsf{D}, \forall p^d \in P_d, \forall p^{\hat{d}} \in P_{\hat{d}} \tag{A.9}$$

$$x_{p^d} + x_{p^{\hat{d}}} - 2 \cdot \Psi^{(d,\hat{d})}_{(p^d,p^{\hat{d}})} \geq 0 \quad \forall (d,\hat{d}) \in \mathsf{D}, \forall p^d \in P_d, \forall p^{\hat{d}} \in P_{\hat{d}} \tag{A.10}$$

$$f_{\hat{d}} - f_d \leq \mathsf{T} \cdot \delta^{(d,\hat{d})} - 1, \forall d, \hat{d} \in \mathsf{D} \tag{A.11}$$

$$f_{\hat{d}} - f_d \geq \mathsf{T} \cdot \delta^{(d,\hat{d})} - \mathsf{T}, \forall d, \hat{d} \in \mathsf{D} \tag{A.12}$$

$$f_d + \sum_{p^d \in P_d} F_{p^d} \cdot x_{p^d} - 1 \leq \mathsf{M_s} \quad \forall d \in \mathsf{D} \tag{A.13}$$

$$\begin{aligned} &f_d - f_{\hat{d}} + \mathsf{T} \cdot (\delta^{(d,\hat{d})} + \Psi^{(d,\hat{d})}_{(p^d,p^{\hat{d}})}) \leq 2 \cdot \mathsf{T} - F_{p^d} \\ &\forall (d,\hat{d}) \in \mathsf{D}, \forall p^d \in P_d, \forall p^{\hat{d}} \in P_{\hat{d}}, \tau_{(p^d,p^{\hat{d}})} = 1 \end{aligned} \tag{A.14}$$

$$\begin{aligned} &f_d - f_{\tilde{d}} + \mathsf{T} \cdot (\delta^{(d,\tilde{d})} + \Psi^{(d,\hat{d})}_{(p^d,p^{\hat{d}})} + x_{p^{\tilde{d}}}) \leq 3 \cdot \mathsf{T} - F_{p^d} \\ &\forall (d,\hat{d},\tilde{d}) \in \mathsf{D}, \forall p^d \in P_d, \forall p^{\hat{d}} \in P_{\hat{d}}, \forall p^{\tilde{d}} \in P_{\tilde{d}} : \Gamma_{(p^d,p^{\hat{d}})} \cap p^{\tilde{d}} \neq \{\varnothing\} \end{aligned} \tag{A.15}$$

$$\begin{aligned} &f_{\tilde{d}} - f_d + \mathsf{T} \cdot (\delta^{(\tilde{d},d)} + \Psi^{(d,\hat{d})}_{(p^d,p^{\hat{d}})} + x_{p^{\tilde{d}}}) \leq 3 \cdot \mathsf{T} - F_{p^{\tilde{d}}} \\ &\forall (d,\hat{d},\tilde{d}) \in \mathsf{D}, \forall p^d \in P_d, \forall p^{\hat{d}} \in P_{\hat{d}}, \forall p^{\tilde{d}} \in P_{\tilde{d}} : \Gamma_{(p^d,p^{\hat{d}})} \cap p^{\tilde{d}} \neq \{\varnothing\}, \end{aligned} \tag{A.16}$$

The objective (A.1) is to minimize the index of the maximum FSU used in the network $\mathsf{M_s}$ and the total degree of passive couplers deployed at network nodes. The weighting coefficients α and β allow for prioritization between the two contributions of the objective function according to the network operator preferences. Constraint (A.2) guarantees that a single route is assigned to each demand d. The degrees of passive splitters and combiners needed to route the optical channels in node v are determined by (A.3)–(A.8). (A.3)–(A.5) model the internal routing at node v for pass through, added and dropped connections, respectively. Exact splitter degrees are then calculated in (A.6)–(A.8) by modelling an *if-then-else* relationship between $\sum_{(v,u)\in\mathcal{E}} S^v_{(\hat{u}v,vu)} + d^v_{(\hat{u},v)}$

and $\mathsf{C_i}^{v}_{(\hat{u},v)}$, using $L^{v}_{\hat{u}v}$ as an auxiliary variable. If $\sum_{(v,u)\in\mathcal{E}} S^{v}_{(\hat{u}v,vu)} + d^{v}_{(\hat{u},v)} = 1$, which means that all connections entering node v from $\hat{u}$ either pass through towards the same node u or get dropped at v, then $\mathsf{C_i}^{v}_{(\hat{u},v)}$ needs to be 0 as no splitter is needed. If $\sum_{(v,u)\in\mathcal{E}} S^{v}_{(\hat{u}v,vu)} + d^{v}_{(\hat{u},v)} > 1$, which means that connections entering node v from $\hat{u}$ are directed towards different nodes u and/or get dropped at v, then $\mathsf{C_i}^{v}_{(\hat{u},v)}$ needs to be equal to that sum. An analogous procedure is carried out for each egress port of every node v in order to model the need for deploying couplers at each port and use it as an auxiliary variable to determine the exact degrees of the couplers $\mathsf{C_o}^{v}_{(v,u)}$.

Constraints (A.9)–(A.10) and (A.11)–(A.12) determine the values of $\Psi^{(d,\hat{d})}_{(p^d,p^{\hat{d}})}$ and $\delta^{(d,\hat{d})}$, respectively, needed for spectrum assignment. Spectrum contiguity is enforced by (A.13). Spectrum continuity and non-overlapping of the spectrum assigned to different traffic demands that share common link(s) are enforced by (A.14). (A.15) and (A.16) ensure that the spectrum slots occupied by unfiltered optical channels are not assigned to any other demand $\tilde{d}$.

Note that the above formulation can be conveniently transformed into the variant which only aims at minimizing spectrum usage without considering the splitter degrees. This transformation is carried out by eliminating the $\mathsf{C_i}$ and $\mathsf{C_o}$ from the objective function, and by omitting constraints (A.3)–(A.8).

3.4 Two-Step ILP Formulation of the RMSA Problem in PFONs

To reduce complexity and obtain sub-optimal results for realistic problem instances, we formulate a two-step ILP model for RMSA in PFONs. In the first step, the model tries to find a lower bound on the highest used spectrum slot index in the network through routing, without considering spectrum allocation to individual requests. After solving this step, the values of the x_{p^d} variables are set, and used as input for spectrum allocation in the second step.

Step 1: Spectrum-aware routing

In the first step, the model aims at solving the routing sub-problem while avoiding the complexity associated with precise allocation of spectrum to individual requests. In addition to using the same variables related to connection routing as in the 1-step ILP model above, this phase introduces two additional variables:

- M_s^e: an estimate of the maximum used FSU index among all network links;
- $m_{(uv,p^d)} \in \{0,1\}$: an auxiliary variable whose value equals 1 if the unfiltered signal generated from p^d traverses link (u,v), and 0 otherwise.

Objective function

$$\text{Minimize: } \alpha \cdot \mathsf{M}_\mathsf{s}^\mathsf{e} + \beta \cdot \sum_{v\in\mathcal{V}} \Big(\sum_{(\hat{u},v)\in\mathcal{E}} \mathsf{C_i}_{(\hat{u},v)}^{v} + \sum_{(v,u)\in\mathcal{E}} \mathsf{C_o}_{(v,u)}^{v} \Big) \tag{A.17}$$

Subject to

$$\text{Constraints (A.2)–(A.10)}$$

$$K \cdot m_{(uv,p^d)} \geq \sum_{\hat{d}\in\hat{D}} \sum_{p\in p^{\hat{d}},\, \Gamma_{(p^d,p^{\hat{d}})} \cap p^{\tilde{d}} \neq \{\varnothing\}} \Psi_{(p^d,p^{\hat{d}})}, \quad \forall d\in D, \forall p \in p^d, \forall (u,v)\in\mathcal{E} \tag{A.18}$$

$$m_{(uv,p^d)} \leq \sum_{\hat{d}\in\hat{D}} \sum_{p\in p^{\hat{d}},\, \Gamma_{(p^d,p^{\hat{d}})} \cap p^{\tilde{d}} \neq \{\varnothing\}} \Psi_{(p^d,p^{\hat{d}})}, \quad \forall d\in D, \forall p \in p^d, \forall (u,v)\in\mathcal{E} \tag{A.19}$$

$$\sum_{d\in D} \sum_{p\in p^d, (u,v)\in p^d} x_{p^d} \cdot F_{p^d} + \sum_{d\in D} \sum_{p\in p^d} m_{(uv,p^d)} \cdot F_{p^d} \leq \mathsf{M}_\mathsf{s}^\mathsf{e}, \quad \forall (u,v)\in\mathcal{E} \tag{A.20}$$

The objective of the routing step, given in (A.17), is to minimize the sum of the estimated value of the maximum used FSU index M_s^e and the total degree of passive couplers deployed at network nodes. The value of $m_{(uv,p^d)}$ is determined from connection routing by (A.18) and (A.19), and used in (A.20) to approximate the maximum used FSU index on any link. The spectrum continuity and contiguity constraints are not considered in this phase, so an estimate on the maximum used FSU index is computed as the sum of the number of slots used to carry the traffic over any link and the slots used by unfiltered signals traversing that link. This represents a lower bound on the maximum FSU since the spectrum continuity and contiguity constraints lead to spectrum fragmentation.

Step 2: Spectrum assignment

After determining the routing and, consequently, the values of the x_{p^d} variables, the spectrum is allocated to the individual requests in the second step.

Objective function

$$\text{Minimize: } \mathsf{M_s} \tag{A.21}$$

Subject to

$$\text{Constraints (A.11)–(A.12)}$$

$$f_d + F_{p^d} - 1 \leq \mathsf{M_s}, \forall d \in D : x_{p^d} = 1 \tag{A.22}$$

$$\begin{gathered} f_d - f_{\hat{d}} + \mathsf{T} \cdot \delta^{(d,\hat{d})} \leq \mathsf{T} - F_{p^d}, \\ \forall (d,\hat{d}) \in \mathsf{D}, \forall p^d \in P_d, \forall p^{\hat{d}} \in P_{\hat{d}} : x_{p^d} = 1 \wedge x_{p^{\hat{d}}} = 1 \end{gathered} \tag{A.23}$$

$$\begin{gathered} f_d - f_{\tilde{d}} + \mathsf{T} \cdot \delta^{(d,\tilde{d})} \leq \mathsf{T} - F_{p^d}, \\ \forall (d,\hat{d},\tilde{d}) \in D, \forall p^d \in P_d, \forall p^{\hat{d}} \in P_{\hat{d}}, \forall p^{\tilde{d}} \in P_{\tilde{d}} : \\ \Gamma_{(p^d,p^{\hat{d}})} \cap p^{\tilde{d}} \neq \{\varnothing\} \wedge x_{p^d} = 1 \wedge x_{p^{\hat{d}}} = 1 \wedge x_{p^{\tilde{d}}} = 1 \end{gathered} \tag{A.24}$$

The objective of the spectrum assignment step, given by (A.21), is to minimize the maximum used FSU index in the network. A contiguous set of spectrum slots is allocated to each demand using (A.22). Constraint (A.23) avoids spectrum overlap among link-sharing demands and guarantee spectrum continuity. This constraint is analogous to (A.14) in the 1-step model. Constraint (A.24) avoids spectrum overlap of useful and unfiltered signals, replacing (A.15) and (A.16) from the 1-step model.

3.5 Complexity Analysis

The complexity of single-step ILP formulation in terms of the number of variables and constraints can be expressed as (A.25) and (A.26), respectively.

$$N_{var} = 4|\mathcal{V}|^2 + |\mathsf{D}|^2 \cdot (1 + \mathsf{K}^2) + |\mathsf{D}| \cdot (1 + \mathsf{K}) + |\mathcal{V}| \cdot |\mathcal{E}|^2 \tag{A.25}$$

$$\begin{aligned} N_{cnstr} = 2|\mathsf{D}| \cdot (1 + |\mathsf{D}|) + \mathsf{K}^2 \cdot |D|^2 \cdot (3 + 2\mathsf{K} \cdot |\mathsf{D}|) \\ + |\mathcal{V}| \cdot |\mathcal{E}| \cdot (\mathcal{E} + 3) \end{aligned} \tag{A.26}$$

To simplify the expressions, we can assume a fully-connected demand matrix where the number of demands and links grow linearly by $|\mathcal{V}|^2$. By considering the dominant factors, the number of variables and constraints can be approximated $N_{var} \approx |\mathcal{V}|^5 + K^2 \cdot |\mathcal{V}|^4$ and $N_{cnstr} \approx K^3 \cdot |\mathcal{V}|^6$, respectively.

The number of variables and constraints for the first step of the two-step ILP formulation are expressed in (A.27) and (A.28), respectively.

$$N_{var} = \mathsf{K}^2 \cdot |\mathsf{D}|^2 + |\mathcal{V}| \cdot |\mathcal{E}|^2 + 6|\mathcal{V}|^2 + \mathsf{K} \cdot |\mathsf{D}| \cdot (1 + |\mathcal{E}|) \tag{A.27}$$

$$N_{cnstr} = 2\mathsf{K}^2 \cdot |\mathsf{D}|^2 + |\mathcal{V}| \cdot |\mathcal{E}|^2 + 2\mathsf{K} \cdot |\mathsf{D}| \cdot |\mathcal{E}| + |\mathsf{D}| + 3|\mathcal{E}| \tag{A.28}$$

By following the same simplification assumptions as above, their complexity can be approximated by $N_{var} \approx |\mathcal{V}|^5 + K^2 \cdot |\mathcal{V}|^4$ and $N_{cnstr} \approx |\mathcal{V}|^5 + 2K^2 \cdot |\mathcal{V}|^4$, respectively. The main factor in reducing complexity is the lower number of constraints compared to the single-step ILP formulation.

Finally, the number of variables and constraints for the second step of ILP formulation can be expressed as (A.29) and (A.30), respectively.

$$N_{var} = 2|\mathsf{D}|^2 \tag{A.29}$$

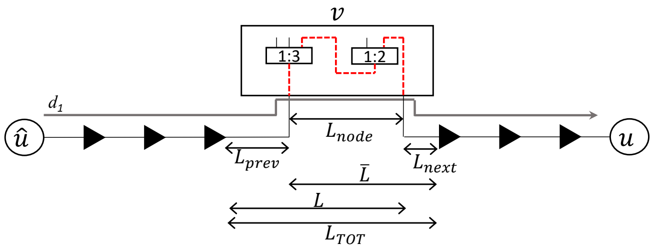

Figure 4: Loss contributions considered during amplifier placement.

$$N_{cnstr} = |\mathsf{D}|^3 + 3|\mathsf{D}|^2 + |\mathsf{D}| \tag{A.30}$$

After simplifying, they can be approximated as $N_{var} \approx 2|\mathcal{V}|^4$, and $N_{cnstr} \approx |\mathcal{V}|^6$. The strict conditions applied in (A.24) decrease the actual number of constraints which results in complexity reduction compared to the single-step ILP. In section 4.1, a comparison of the ILP execution times offers further insights into their run-time complexity.

3.6 Amplifier Placement

For the cost-minimizing RMSA solutions obtained by the ILP formulations, the placement of EDFAs is performed by computing the total loss experienced by each connection at each node, and deploying the EDFAs when necessary to compensate for these losses. Note that this work is concerned only by node architecture design, where our focus is on the placement of amplifiers inside nodes for node loss management purpose. We assume that the optical line system is already deployed and optimized for span loss management and that the launch channel power does not exceed the threshold for nonlinearities.

The pseudocode of the amplifier placement subroutine is shown in Algorithm 1. Fig. 4 shows the loss contributions considered during amplifier placement (we use the example of connection d_1 from Fig. 3). The amplifier placement algorithm takes as input the network topology $\mathcal{G}(\mathcal{V}, \mathcal{E})$, the routing solution R, the line amplifier output power P_{out} and input power threshold P_{in}, the insertion losses of the OB switch L_{OB} and the deployed 1:N couplers $L_{1:N}$, as well as the fiber attenuation L_{α}.

Algorithm 1: Amplifier placement procedure.

```
   Data: G(V,E), R, P_out, P_in, L_OB, L_1:N, L_α.
   Result: Placement of amplifiers at each node.
1  P_budget = P_out − P_in;
2  for v = 1 to |V| do
3  |  for p_d = 1 to |R| s.t. v ∈ p_d do
4  |  |  û ← predecessor of v in p_d;
5  |  |  u ← successor of v in p_d;
6  |  |  L ← loss of d between the last amplifier on link (û,v) and the
   |  |    used output port of v;
7  |  |  L̄ ← loss of d between the used input port of v and the first
   |  |    amplifier on link (v,u);
8  |  |  L_TOT ← total loss of d between last amplifier on (û,v) and first
   |  |    amplifier on (v,u);
9  |  |  if L_TOT > P_budget then
10 |  |  |  if L > P_budget and L̄ > P_budget then
11 |  |  |  |  Place amplifier at used input and output ports of v;
12 |  |  |  if L > P_budget and L̄ ≤ P_budget then
13 |  |  |  |  Place amplifier at used input port of v;
14 |  |  |  if L ≤ P_budget and L̄ > P_budget then
15 |  |  |  |  Place amplifier at used output port of v;
16 |  |  |  if L ≤ P_budget and L̄ ≤ P_budget then
17 |  |  |  |  Place amplifier at used input/output port with a higher
   |  |  |  |    degree coupler; or at input if both couplers are of same
   |  |  |  |    degree;
```

For each network node v, the algorithm processes the physical routes p_d of all demands d that traverse node v (lines 2-3). First, the predecessor and successor nodes in path p_d are identified, denoted as $\hat{u}$ and u, respectively (lines 4-5). Then, the loss contributions for each traversed components are calculated, as illustrated in Fig. 4 for connection d_1 and node $v = 3$.

L denotes the loss between the last amplification site on the ingress link $(\hat{u}, v)$ and the output of node v. It is calculated as the sum of fiber attenuation on link $(\hat{u}, v)$, denoted as L_{prev}, and the internal node loss L_{node}. Analogously, $\overline{L}$ refers to the losses between the input of node v and the first line amplifier on link (v, u). It is calculated as the sum of L_{node} and fiber attenuation on the first span of link (v, u), denoted as L_{next}. L_{TOT} measures the total loss between the two closest line amplifiers at the ingress and egress links of node v. If L_{TOT} exceeds the power budget P_{budget} between these two line amplifiers (line 9), the signal requires extra amplification at the node. In case both L and $\overline{L}$ exceed P_{budget}, an amplifier must be placed at the input and at the output port of node v associated to links $(\hat{u}, v)$ and (v, u) (lines 10-11). Otherwise, one amplifier is sufficient and its placement is determined as follows. If only the value of L exceeds P_{budget}, an amplifier is placed at the input port of node v connecting it to node $\hat{u}$ (lines 12-13). Conversely, if only $\overline{L}$ exceeds the threshold, an amplifier is placed at the output port of v connecting it to u (lines 14-15). In case both L and $\overline{L}$ are below the P_{budget} threshold, the necessary amplifier can be added at either of the two ports. In this case, the port that hosts a passive coupler of a higher degree is chosen, whereas the input port is selected if the two degrees are the same (lines 16-17).

4 Numerical Results

We evaluate the performance of the proposed single-step and two-step ILPs for the cost-efficient PFON design in terms of spectrum and component usage. Spectrum consumption considerations refer to the highest used FSU index in the network and the portion of spectrum wasted due to *drop-and-waste* transmission. Component usage considerations include the number and the degree of used passive couplers, the number of used EDFAs and the maximum size of the deployed OB switch matrix.

The results used in the analysis are obtained via simulations on the German and the Italian backbone networks, and a realistic regional network denoted as Reference network 1 [3]. The topologies are shown in Fig. 5 and their characteristics are summarised in Table 1. Each link is assumed to comprise one fiber per direction supporting 320 FSUs and additional fibers can be deployed in case capacity is exceeded [3]. Links are equipped with pre-deployed line amplifiers that compensate for the span losses. Adopting a similar approach as in [42], we assume even spacing of line amplifiers, whose value is varied in the analysis. We consider a multi-period scenario with 5 traffic periods of increasing traffic for the German and Italian networks, and 3 traffic periods for Reference network 1 [3]. At every period, the traffic volume is distributed among each node pair and direction in a non-uniform way as in [3]. We assume

Table 1: Characteristics of Network Topologies

Topology	Nodes	Links	Average nodal degree
German network	7	11	1.57
Italian network	10	15	1.5
Reference network 1	14	19	1.35

that each source-destination pair combines all the traffic volume in one direction into a single demand $d \in D$. Unless otherwise stated, we assume that reconfiguration is performed during the transition between traffic periods, i.e., the model is solved independently for each period. The weighting coefficients α and β are set to 1, which allows for balancing the two contributions of the same order of magnitude.

In Sec. 4.1, we first compare the results obtained by the single-step and two-step ILP formulations for smaller problem instances, i.e., the smallest, German topology and lighter network traffic load. All solutions are obtained using the Gurobi 7.5 solver[43] using 4 CPUs per problem instance, running on a server with 2.1 GHz Intel Xeon CPU and 128 GB of RAM. The results obtained by the single- and the two-step model for the PFON architecture are denoted as PF-RSA and PF-R+SA, respectively.

We then analyze the performance of the two-step ILP on larger problem instances in Sec. 4.2, comparing the proposed PFON solutions to FON and WSON benchmarks. The WSON solutions, denoted as WSON-RSA and WSON-R+SA for the equivalent single- and two-step approaches, were obtained by modifying the ILP from Sec. 3.3 to omit the PFON-related variables and constraints. For example, the modified single-step ILP formulation for WSON minimizes the maximum used spectrum slot (A.21) and uses constraints (A.2) and (A.13)–(A.14). The baseline FON solutions are obtained by the heuristic from [3] for scalability reasons. We also compare the proposed multi-criteria PFON solutions to those aimed only at spectrum minimization (i.e., setting α=1 and β=0 to disregard component usage), denoted as PF-SM-RSA and PF-SM-R+SA for the single-step and two-step approach, respectively.

Finally, we consider a scenario without reconfiguration between traffic periods to model the case where complete reprogramming of optical nodes is not

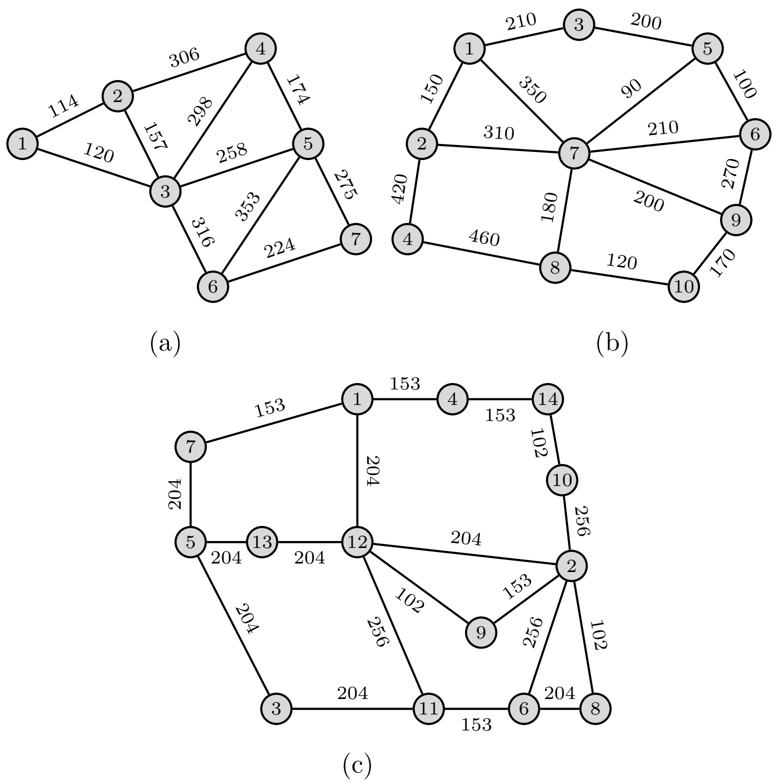

Figure 5: The German (a), the Italian (b) and the Reference network 1 topology (c) used in the simulations. The number next to each link indicates its length in km.

Table 2: Summary of Optimization Models

Abbreviation	Model
FON	Filterless optical networks solution
WSON-RSA	Single-step ILP solution for WSON
WSON-R+SA	Two-step ILP solution for WSON
PF-RSA	Single-step ILP solution for PFON
PF-R+SA	Two-step ILP solution for PFON
PF-SM-RSA	Spectrum minimizing single-step ILP solution for PFON
PF-SM-R+SA	Spectrum minimizing two-step ILP solution for PFON
PF-R+SA-TD	Two-step ILP solution for PFON with traffic domination

desirable by a network operator. Hence, an approach based on total traffic domination, inspired by [44] and denoted as PF-R+SA-TD, is introduced and tested on the German network topology. This approach optimizes connection routing (i.e., runs the first step of the two-step ILP) only once, for the traffic period with the largest total traffic demand. The resulting routing and node configuration are applied to serve the demands in earlier traffic periods, while allowing only for the optimization of the spectrum (obtained by solving the second step of the two-step ILP) in each period. All models and their abbreviations are summarized in Table 2.

4.1 Single-step and Two-step ILP Comparison

To assess the quality of the sub-optimal solutions obtained by the two-step ILP formulation, we compare them to the optimal solutions of the single-step ILP. Due to the prohibitively high complexity of the single-step ILP approach, optimal results could only be obtained for smaller-sized problem instances, i.e., those with a lower traffic load. To this end, we only use the German network topology serving half of the requests from the traffic matrices, i.e., 21 connection request serving 43.5 Tbit/s of total traffic for the highest load.

Fig. 6a shows the maximum FSU index used by the single- and two-step ILPs for PFON and WSON architectures. The optimal PF-RSA solution obtains, on average, only 1.6% lower maximum FSU than the sub-optimal two-step approach PF-R+SA. This advantage equals 1.7% for the variant where only spectrum usage is minimized (see PF-SM-RSA vs. PF-SM-R+SA) and 2.8% for the case of WSON (see WSON-RSA vs. WSON-R+SA), which indicates strong potential of the two-step approach to obtain solutions of very high quality. Depending on the traffic load, the PF-RSA solutions use between 10% and 18% more spectrum than WSON-RSA, and the trend is analogous for the two-step approach.

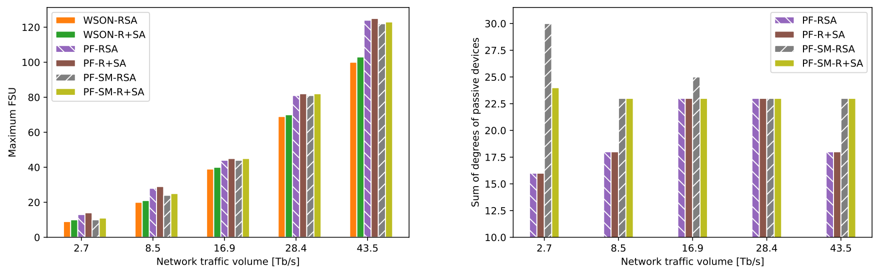

(a) Maximum used frequency slot unit (FSU)

(b) Sum of the degrees of passive devices

Figure 6: Single-step (RSA) and two-step (R+SA) ILP comparison for 21 traffic demands in the German network.

Fig. 6b shows the sum of the degrees of passive devices used for the single- and two-step ILPs solutions. Here, too, the two approaches have very close performance, with a $< 1\%$ gap on average over all traffic periods. However, differences are observable between the single- and multi-objective versions of the models. Since the single-objective variant does not consider the degree of the passive components, it tends to yield a higher total degree than the variant which considers it jointly with the spectrum. Overall, the spectrum-only minimizing ILP approaches tend to obtain on average 7% lower maximum FSU usage than those that consider the more complex objective, at the expense of 16% higher average degree of the used components.

Table 3 compares the execution times of the single-step and two-step ILP

Table 3: Solving Times of the ILP Formulations

Solution	Run time	
	21 demands	**42 demands**
WSON-RSA	16 minutes	13.87 days
WSON-R+SA	0.14 second	13.79 seconds
PF-RSA	4.2 days	28 days (non-optimal)
PF-R+SA	0.46 second	0.62 hours
PF-SM-RSA	3.6 hours	28 days (non-optimal)
PF-SM-R+SA	0.218 second	12.74 hours

formulation as an indicator of their run-time complexity. Apart from the instances with 21 request examined above, we test the approaches on a set of problem instances with full connectivity (i.e., 42 connection requests) to impose a greater strain on the ILPs. Results confirm the much lower complexity of the two-step model, which permits its applicability to problem instances of realistic sizes. In some cases, the execution of the single-step ILPs was terminated after 28 days without finding the optimal solution. In cases when both formulations were solved to the optimum, the two-step one was solved in 4 to 5 orders of magnitude shorter time than the single-step one. For example, the running time of PF-R+SA with 21 demand was $7.9 \cdot 10^5$ times shorter than that of PF-RSA. The above analysis shows that the two-step ILP formulation can find near-optimal solutions within a much shorter time than the single-step ILP.

4.2 Comparison of PFONs, FONs and WSONs

To evaluate the resource usage of PFONs, we compare the proposed two-step ILP with FON and WSON architectures under fully-connected traffic matrices for different network topologies. Figs. 7a, 7b, and 7c show the highest used FSU index for the different design strategies and a varying traffic load for the German, Italian network, and Reference network 1, respectively. The PFON architecture drastically reduces the spectrum usage compared to FONs. On average over all traffic scenarios for the German topology, PF-R+SA and PF-SM-R+SA use 43% and 45% less spectrum than the FON solution, respectively. The same trend is observed for the larger topologies.

For the Italian network, the PF-R+SA and PF-SM-R+SA schemes both use 38% less spectrum than FON on average. The analogous reduction over FON obtained by the two approaches for the Reference 1 network is 59% and 64%, respectively. The average overhead in spectrum usage compared to WSON solutions is 43% and 42% (German network), 66% and 65% (Italian network), and 66% and 61% for the PF-R+SA and PF-SM-R+SA schemes, respectively. The observed performance trends can be motivated as follows. In networks with lower connectivity, such as the Reference 1 topology, FON solutions have the highest spectrum usage for similar traffic loads compared to the more connected topologies, which can be explained with low flexibility in fiber tree design and connection routing. There, the PFON solutions obtain the most significant advantage over FON. Conversely, in topologies with higher connectivity, such as the German network, PFON again leverages greater flexibility in node configuration and route selection and achieves the lowest spectrum usage overhead over WSON architecture. This confirms the premise that the programmable filterless network represents a good compromise solution between passive filterless and filtered, wavelength-switched optical networks in terms of spectrum consumption.

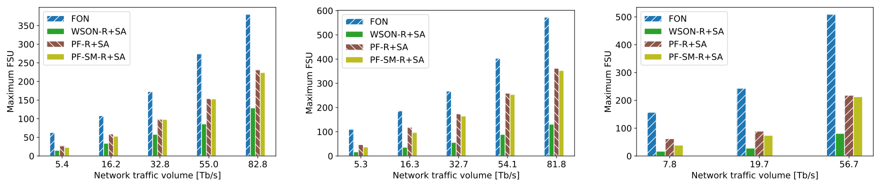

(a) German network **(b)** Italian network **(c)** Reference network 1

Figure 7: The maximum used frequency slot unit (FSU) for the three networks.

A deeper insight into the amount of spectrum wasted due to the *drop-and-waste* transmission is provided by Fig. 8. We express it as the ratio between the number of FSUs occupied by unfiltered channels and the total utilized number of FSUs. The PFON solutions waste significantly less spectrum than FON, where PF-R+SA and PF-SM-R+SA yield 44% and 36% lower spectrum dissipation on average over all network topologies, respectively. These results also reveal that the joint consideration of splitting and spectrum minimization leads to more efficient spectrum usage through the reduction of spectrum waste.

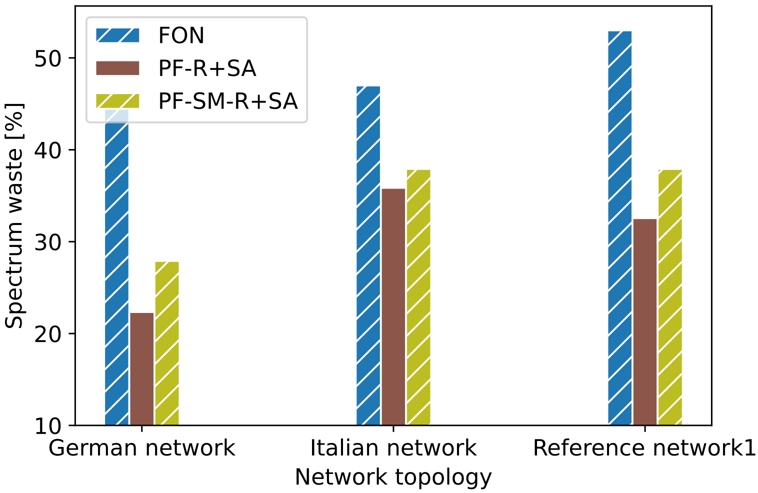

Figure 8: The average percentage of wasted spectrum for the three networks over all traffic periods.

The extent of unwanted distribution of signals to unintended destinations in PFONs and in FONs is compared in Fig. 9. We define a metric which we refer to as the unintended recipient metric, calculated as the ratio between the number of nodes that receive unwanted signals via unfiltered spectrum and the total number of demands. In a passive tree of N nodes, each demand will be unintentionally received by $(N-2)$ nodes (i.e., all nodes in the tree except the source and the intended destination), so this metric for the FON solutions based on fiber trees can be calculated as a constant. As can be seen in the figure, PFON reduces the average extent of unwanted broadcasting in the network by 21%, 39% and 50% compared to FON for the three considered networks, respectively. Further reduction of this metric could be achieved by incorporating it into the ILPs as an objective or a constraint, which is beyond the scope of this paper. Moreover, combining the programmable filterless architecture with SDM can in some cases completely eliminate unwanted signal broadcast, as shown in [7].

In the following, we analyse the component usage performance of the proposed approach. Fig. 10, shows the sum of the degrees of passive couplers

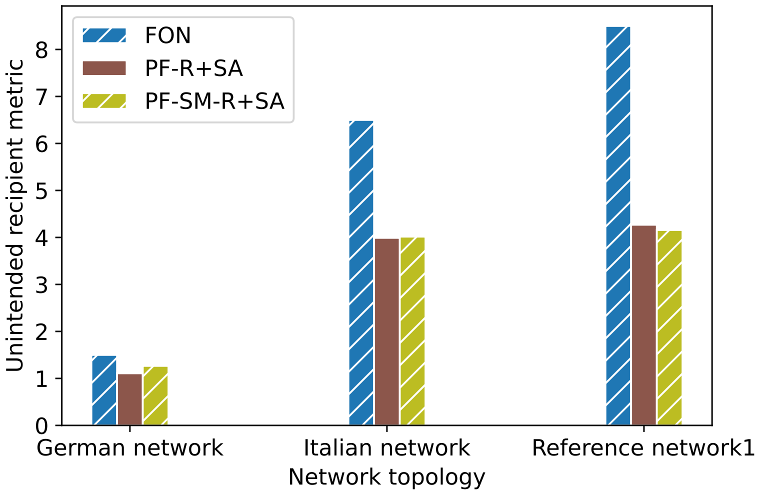

Figure 9: The average unintended recipient metric for the three networks.

deployed in the three networks on average over the traffic periods. In all cases, the multi-objective PF-R+SA outperforms PF-SM-R+SA. PF-R+SA decreases the value of this parameter by 16% compared to PF-SM-R+SA for the German topology, whereas the average value of the highest FSU index used by the two approaches over all traffic periods (shown in Fig. 7) are within 5% difference. The reduction in the sum of coupler degrees obtained by PF-R+SA is 14% for the Italian and 17% for the Reference network 1, at a spectrum usage overhead of 7% and 10%, respectively, compared to PF-SM-R+SA. These values indicate that jointly optimizing spectrum usage and splitter degree reduces spectrum waste without adversely affecting the maximum FSU usage.

Fig. 11 shows the total number of EDFAs deployed at network nodes by the considered approaches in the highest loaded traffic scenario for the three networks. To investigate the impact of line amplifier spacing and input power thresholds, we consider the scenarios with amplifier spacing values of 60, 75, and 100 km, and amplifier input power thresholds of -12, -15 and -18 dBm, as reported in the literature (e.g., [45]). The nodes in FONs and WSONs are hard-wired, with pre-amplifiers and boosters placed at each ingress and egress port, as shown in Fig. 1. Therefore, the number of deployed EDFAs in

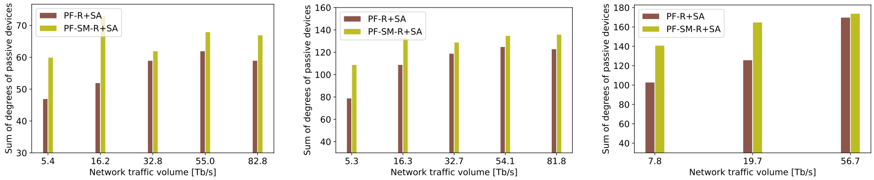

(a) German network **(b)** Italian network **(c)** Reference network 1

Figure 10: The average sum of the degrees of passive couplers deployed in the three networks over all traffic periods.

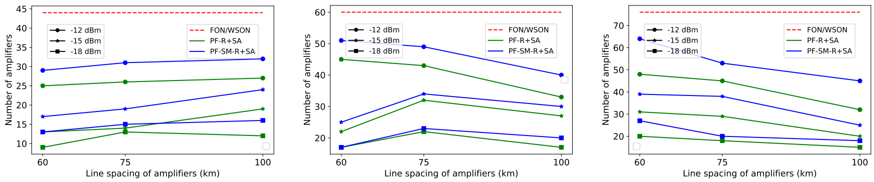

(a) German network **(b)** Italian network **(c)** Reference network 1

Figure 11: The total number of amplifiers used at the nodes for the three networks, for varied line amplifier spacing and input power threshold.

those architectures is fixed, and shown with a red dashed line in the figures. The PFON solutions require significantly fewer amplifiers than FON/WSON. The proposed PF-R+SA design approach performs the best in all considered settings. The advantages for the German topology are the greatest under amplifier spacing of 60 km and input power threshold of -18 dBm, where the PF-R+SA requires 80% fewer EDFAs at network nodes than FON/WSON. In Reference network 1, PF-R+SA obtains the greatest advantage for the 100 km amplifier spacing, where it decreases the number of amplifiers by 81% compared to both FON and WSON under the input power threshold of -18 dBm. This can be explained by the fact that there are 8 links with a length of 204 km and line amplifiers are installed close to the nodes of those links. The savings in nodal amplifier deployment are enabled by a reduction in the degree of passive splitters that lowers the insertion losses, combined with the relatively short distances between the last line amplifier on the incoming link and the first line amplifier on the outgoing link. As lower splitting degrees also create less unfiltered signals, the proposed PFON design brings considerable savings in terms of EDFA usage while maintaining low spectrum consumption.

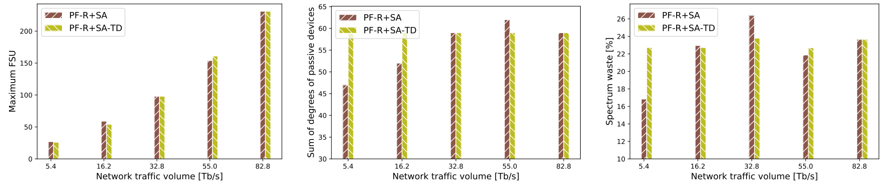

(a) Maximum frequency slot unit (FSU)

(b) Sum of the degrees of passive couplers

(c) Wasted spectrum

Figure 12: Comparison of period-independent and traffic domination approaches for the German topology.

On average over all amplifier threshold and placement scenarios, PF-R+SA reduces the number of amplifiers used at network nodes by 60%, 52%, and 62% compared to FON/WSON for the German, Italian, and Reference networks, respectively. It also uses 19%, 11% and 21% fewer amplifiers than PF-SM-R+SA on average, respectively.

The number and the size of switching components required to support the PFON and WSON solutions for different network topologies is reported in Table 4. The modest OB switch matrix dimensions indicate a strong advantage of the PFON architecture in terms of the cost of active switching components compared to the conventional WSON architecture. Namely, each ROADM node of degree d would require d SSSs in broadcast&select configuration, and $2d$ in route&select configuration. A PFON node, on the other hand, only requires one OB switch matrix to support the required functionalities. This results in an 84%, 83% and 82% reduction of the number of used optical switches for the three network topologies compared to a route&select WSON, respectively.

Finally, Figs. 12a, 12b, and 12c show the highest used FSU index, the sum of the degrees of passive couplers, and the spectrum waste for the period-independent planning scheme and the traffic domination approach in the German network, respectively. The sum of coupler degrees of PF-R+SA-TD for all traffic volumes is the same since connection routing and node configuration of the highest-loaded traffic period (traffic demand 5) are used in the other periods as well. The results reveal minor variations in the coupler degree sum (Fig. 12b) and spectrum waste (Fig. 12c) in the first traffic period, but

Table 4: Usage of Optical Switches for the Different Topologies

Network topology	Maximum OB switch size for PFON	Number of OB switches for PFON	Number of SSSs for WSON
German	20×20 (node 3)	7	44
Italian	34×34 (node 7)	10	60
Reference 1	32×32 (node 12)	14	76

no substantial difference between PF-R+SA and PF-R+SA-TD in terms of the highest used FSU. This indicates the potential of the proposed approach to maintain good performance while being attuned to an operator's needs, priorities and practical limitations.

5 Conclusion

The paper proposed a detailed design framework for programmable filterless optical network (PFON) architecture based on coherent elastic transmission and optical white box switches. The routing, modulation format and spectrum assignment problem in these networks was combined with the node architecture design problem and formulated as an integer linear program with the objective of minimizing spectrum usage and passive coupler degrees. To cope with the prohibitive complexity of the joint formulation, the problem was decomposed into two consecutive steps, allowing to obtain near-optimal solutions in drastically shorter time. Compared to passive filterless optical networks (FONs), the proposed PFON architecture decreases the highest used spectrum slot index by up to 64%, reduces the spectrum waste by up to 44%, and lowers the average extent of unwanted signal broadcasting in the network by up to 50%. Compared to conventional wavelength-switched optical networks (WSONs), PFON uses down to only 16% of the total number of optical switches at a trade-off with increased spectrum usage and reduces the number of optical amplifiers at network nodes by up to 81% compared to FON/WSON. This indicates the potential of the proposed programmable filterless architecture to obtain agile, flexible solutions at a fraction of WSON cost and FON spectrum usage.

References

[1] N. Amaya, G. Zervas, and D. Simeonidou, "Introducing node architecture flexibility for elastic optical networks," *IEEE/OSA J. Opt. Commun. Netw.*, vol. 5, no. 6, pp. 593–608, Jun. 2013.

[2] Polatis, *Series 6000n network optical switch*, 2022.

[3] É. Archambault, N. Alloune, M. Furdek, *et al.*, "Routing and spectrum assignment in elastic filterless optical networks," *IEEE/ACM Trans. Netw.*, vol. 24, no. 6, pp. 3578–3592, Dec. 2016.

[4] N. Sambo *et al.*, "Next generation sliceable bandwidth variable transponders," *IEEE Commun. Mag.*, vol. 52, no. 2, pp. 163–171, Feb. 2015.

[5] M. Furdek, A. Muhammad, G. Zervas, N. Alloune, C. Tremblay, and L. Wosinska, "Programmable filterless network architecture based on optical white boxes," in *ONDM*, 2016.

[6] K. Christodoulopoulos, I. Tomkos, and E. A. Varvarigos, "Elastic bandwidth allocation in flexible ofdm-based optical networks," *Journal of Lightwave Technology*, vol. 29, no. 9, pp. 1354–1366, 2011.

[7] A. Muhammad, M. Furdek, G. Zervas, and L. Wosinska, "Filterless networks based on optical white boxes and SDM," in *ECOC*, 2016.

[8] G. M. Saridis, B. J. Puttnam, R. S. Luis, *et al.*, "Experimental demonstration of a flexible filterless and bidirectional SDM optical metro/inter-DC network," in *ECOC*, 2016.

[9] L. Velasco, M. Klinkowski, M. Ruiz, and J. Comellas, "Modeling the routing and spectrum allocation problem for flexgrid optical networks," *Photonic Netw. Commun.*, vol. 24, no. 3, pp. 177–186, 2012.

[10] C. Tremblay, F. Gagnon, B. Châtelain, É. Bernier, and M. P. Bélanger, "Filterless optical networks: A unique and novel passive WAN network solution," in *OECC/IOOC*, 2007, pp. 466–467.

[11] É. Archambault, D. O'Brien, C. Tremblay, F. Gagnon, M. P. Bélanger, and É. Bernier, "Design and simulation of filterless optical networks: Problem definition and performance evaluation," *IEEE/OSA J. Opt. Commun. Netw.*, vol. 2, no. 8, pp. 496–501, Aug. 2010.

[12] J. P. Savoie, C. Tremblay, D. V. Plant, and M. P. Bélanger, "Physical layer validation of filterless optical networks," in *ECOC*, 2010, P5.08.

[13] B. Jaumard, Y. Wang, and D. Coudert, "Dantzig–wolfe decomposition for the design of filterless optical networks," *Journal of Optical Communications and Networking*, vol. 13, no. 12, pp. 312–321, 2021.

[14] Z. Xu, É. Archambault, C. Tremblay, *et al.*, "1+1 dedicated optical-layer protection strategy for filterless optical networks," *IEEE Commun. Lett.*, vol. 18, no. 1, pp. 98–101, Jan. 2014.

[15] Z. Xu, C. Tremblay, É. Archambault, *et al.*, "Flexible wavelength assignment in filterless optical networks," *IEEE Commun. Lett.*, vol. 18, no. 14, pp. 565–568, Apr. 2015.

[16] P. Littlewood, M. P. Belanger, C. Tremblay, M. Nooruzzaman, and N. Alloune, "Network resource optimization based on time-varying traffic in optical networks," 10623126B2, 2020.

[17] M. Nooruzzaman, N. Alloune, C. Tremblay, P. Littlewood, and M. P. Bélanger, "Resource savings in submarine networks using agility of filterless architectures," *IEEE Communications Letters*, vol. 21, no. 3, pp. 512–515, 2017.

[18] G. Mantelet, C. Tremblay, D. V. Plant, P. Littlewood, and M. P. Bélanger, "PCE-based centralized control plane for filterless networks," *IEEE Commun. Mag.*, vol. 51, no. 1, pp. 44–51, Jan. 2014.

[19] A. Clauberg, *IPv6 deployment in Germany and Croatia*, [Online], 2012.

[20] M. Gunkel, A. Mattheus, F. Wissel, *et al.*, "Vendor-interoperable elastic optical interfaces: Standards, experiments, and challenges [invited]," *IEEE/OSA J. Opt. Commun. Netw.*, vol. 7, no. 12, B184–B193, Dec. 2015.

[21] D. Uzunidis, E. Kosmatos, C. Matrakidis, A. Stavdas, and A. Lord, "DuFiNet: Architectural considerations and physical layer studies of an agile and cost-effective metropolitan area network," *IEEE/OSA J. Opt. Commun. Netw.*, vol. 99, no. PP, pp. 1–7, Dec. 2018.

[22] D. Uzunidis, M. Presi, A. Sgambelluri, F. Paolucci, A. Stavdas, and F. Cugini, "Bidirectional single-fiber filterless optical networks: Modeling and experimental assessment," *Journal of Optical Communications and Networking*, vol. 13, no. 6, pp. C1–C9, 2021.

[23] F. Paolucci, R. Emmerich, A. Eira, *et al.*, "Disaggregated edge-enabled c+ l-band filterless metro networks," *Journal of Optical Communications and Networking*, vol. 12, no. 3, pp. 2–12, 2019.

[24] O. Karandin, O. Ayoub, F. Musumeci, M. Tornatore, *et al.*, "A techno-economic comparison of filterless and wavelength-switched optical metro networks," in *Proceedings of International Conference of Transparent Optical Networks*, 2020, pp. 1–4.

[25] P. Pavon-Marino, F.-J. Moreno-Muro, M. Garrich, *et al.*, "Techno-economic impact of filterless data plane and agile control plane in the 5g optical metro," *Journal of Lightwave Technology*, vol. 38, no. 15, pp. 3801–3814, 2020.

[26] L. Askari, O. Ayoub, F. Musumeci, and M. Tornatore, "On dynamic service chaining in filterless optical metro-aggregation networks," *IEEE Access*, vol. 8, pp. 222 233–222 241, 2020.

[27] O. Ayoub, A. Bovio, F. Musumeci, and M. Tornatore, "Survivable virtual network mapping in filterless optical networks," in *2020 International Conference on Optical Network Design and Modeling (ONDM)*, IEEE, 2020, pp. 1–6.

[28] O. Ayoub, L. Askari, A. Bovio, F. Musumeci, and M. Tornatore, "Virtual network mapping vs embedding with link protection in filterless optical networks," in *GLOBECOM 2020-2020 IEEE Global Communications Conference*, IEEE, 2020, pp. 1–6.

[29] M. Ibrahimi, O. Ayoub, O. Karandin, *et al.*, "Qot-aware optical amplifier placement in filterless metro networks," *IEEE Communications Letters*, vol. 25, no. 3, pp. 931–935, 2020.

[30] P. Pavon-Marino, M. Garrich, F. J. Moreno-Muro, *et al.*, "Hands-on demonstration of open-source filterless-aware offline planning and analysis tool for WDM networks," in *2020 Optical Fiber Communications Conference and Exhibition (OFC)*, 2020, pp. 1–3.

[31] O. Ayoub, O. Karandin, M. Ibrahimi, A. Castoldi, F. Musumeci, and M. Tornatore, “Tutorial on filterless optical networks [invited],” *J. Opt. Commun. Netw.*, vol. 14, no. 3, pp. 1–15, Mar. 2022.

[32] O. Ayoub, F. Fatima, A. Bovio, F. Musumeci, and M. Tornatore, “Traffic-adaptive re-configuration of programmable filterless optical networks,” in *ICC 2020-2020 IEEE International Conference on Communications (ICC)*, IEEE, 2020, pp. 1–6.

[33] V. Abedifar and M. Eshghi, “Routing, modulation format, spectrum and core allocation in space-division-multiplexed programmable filterless networks,” *Optical fiber technology*, vol. 49, pp. 37–49, 2019.

[34] M. Garrich, N. Amaya, G. S. Zervas, *et al.*, “Architecture on demand design for high-capacity optical SDM/TDM/FDM switching,” *IEEE/OSA J. Opt. Commun. Netw.*, vol. 7, no. 1, pp. 21–35, Jan. 2015.

[35] M. Džanko, M. Furdek, B. Mikac, G. Zervas, E. Hugues-Salas, and D. Simeonidou, “Synthesis, resiliency and power efficiency of function programmable optical nodes,” in *ConTEL*, 2015.

[36] A. Muhammad, G. Zervas, N. Amaya, D. Simeonidou, and R. Forchheimer, “Introducing flexible and synthetic optical networking: Planning and operation based on network function programmable ROADMs,” *IEEE/OSA J. Opt. Commun. Netw.*, vol. 6, no. 7, pp. 635–648, Jul. 2014.

[37] M. Džanko, M. Furdek, G. Zervas, and D. Simeonidou, “Evaluating availability of optical networks based on self-healing network function programmable ROADMs,” *IEEE/OSA J. Opt. Commun. Netw.*, vol. 6, no. 11, pp. 974–987, Nov. 2014.

[38] M. Furdek, M. Džanko, N. Skorin-Kapov, and L. Wosinska, “Planning of optical networks based on programmable ROADMs,” in *ACP*, 2015.

[39] M. Furdek, M. Džanko, M. Matanic, I. Boric, L. Wosinska, and B. Mikac, “Multi-hour network provisioning utilizing function programmable ROADMs,” in *ICTON*, 2015.

[40] H. Liu, A. Peters, M. Garrich, and G. Zervas, “OSNR-aware composition of an open and disaggregated optical node and network,” *IEEE/OSA J. Opt. Commun. Netw.*, vol. 9, no. 10, pp. 844–854, Oct. 2017.

[41] M. Džanko, B. Mikac, and M. Furdek, "Dedicated path protection for optical networks based on function programmable nodes," *Opt. Switch. Netw.*, vol. 27, pp. 79–87, Jan. 2018.

[42] M. Ibrahimi, O. Ayoub, F. Musumeci, *et al.*, "Minimum-cost optical amplifier placement in metro networks," *Journal of Lightwave Technology*, vol. 38, no. 12, pp. 3221–3228, 2020.

[43] Gurobi Optimization, LLC, *Gurobi Optimizer Reference Manual*, 2021.

[44] R. Aparicio-Pardo, N. Skorin-Kapov, P. Pavon-Marino, and B. Garcia-Manrubia, "(Non-)reconfigurable virtual topology design under multi-hour traffic in optical networks," *IEEE/ACM Transactions on Networking*, vol. 20, no. 5, pp. 1567–1580, 2012.

[45] O. Karandin, O. Ayoub, M. Ibrahimi, *et al.*, "Optical metro network design with low cost of equipment," in *2021 International Conference on Optical Network Design and Modeling (ONDM)*, 2021, pp. 1–4.

PAPER B

DeepDefrag: A deep reinforcement learning framework for spectrum defragmentation

Ehsan Etezadi, Carlos Natalino, Renzo Diaz, Anders Lindgren, Stefan Melin, Lena Wosinska, Paolo Monti, Marija Furdek

2022 IEEE Global Communications Conference, GLOBECOM 2022 - Proceedings, p. 3694-3699,
Rio de Janeiro, Brazil, Dec. 2022

The layout has been revised.

Abstract

Exponential growth of bandwidth demand, spurred by emerging network services with diverse characteristics and stringent performance requirements, drives the need for dynamic operation of optical networks, efficient use of spectral resources, and automation. One of the main challenges of dynamic, resource-efficient EONs is spectrum fragmentation. Fragmented, stranded spectrum slots lead to poor resource utilization and increase the blocking probability of incoming service requests. Conventional approaches for SD apply various criteria to decide when, and which portion of the spectrum to defragment. However, these polices often address only a subset of tasks related to defragmentation, are not adaptable, and have limited automation potential. To address these issues, we propose *DeepDefrag*, a novel framework based on reinforcement learning that addresses the main aspects of the SD process: determining when to perform defragmentation, which connections to reconfigure, and which part of the spectrum to reallocate them to. DeepDefrag outperforms the well-known OF-FF defragmentation heuristic, achieving lower blocking probability under smaller defragmentation overhead.

1 Introduction

The ongoing drastic growth in bandwidth-intensive applications with dynamic behaviour and high-performance requirements, including high-resolution video on demand, cloud computing, Internet of Things applications, and content delivery networks, strains the optical backbone networks. To satisfy these requirements in a cost-efficient manner, the network must support dynamic, automated, and resource-efficient operations. elastic optical networks (EONs)[1] are considered a future-proof solution to satisfy these needs due to their ability to allocate spectrum at a fine granularity that matches the spectrum requirements of various service requests served by lightpaths. However, spectrum fragmentation is a major challenge for the resource efficiency of dynamic EONs [2] where service requests can arrive and depart at any point in time.

spectrum fragmentation (SF) is generated by the dynamic departures of optical connections that leave relatively small, isolated, unused spectrum chunks scattered across the available fiber bandwidth [3]. Accommodating newly arriving service requests requires the availability of contiguous and continuous spectrum slots, which is not possible under fragmented spectrum conditions with a detrimental effect to service blocking ratio (SBR).

Various spectrum defragmentation (SD) strategies have been proposed to help solve this issue. SD plays a crucial role in consolidating the spectrum usage, improving the utilization of the spectrum grid and reducing the SBR [4]. SD aims at reorganizing the spectrum allocation of different connections such that more (incoming) services can be accommodated, maximizing the spectrum use. The main tasks of SD in dynamic network scenarios entail:

1. deciding on the best time to perform SD, amidst arbitrary arrival and departures of service requests;

2. deciding on the number and the order of distinct network connections to be reconfigured, and

3. finding the alternative spectral resources and reallocating the reconfigured connections.

Spectrum reallocation aimed at minimizing spectrum fragmentation by reconfiguring a minimum number of connections has been proven to be NP-complete already in the static scenario, where the set of connections does not change over time [5]. Traffic dynamicity further exacerbates the problem complexity since the set of connections present in the network constantly changes.

SD schemes can in general be classified as proactive or reactive [2]. Proactive schemes are executed regardless of whether the network is experiencing spectrum blocking, and are run either periodically or based on some threshold. Reactive schemes, on the other hand, are triggered by the blocking of service requests. SD can be performed by reallocating the spectrum only, or by combining it with connection rerouting. SD approaches that do not interrupt the running services are known as hitless [6]. Examples of hitless SD techniques include push-pull retuning [7], where the spectrum occupied by a connection to be re-allocated is first expanded to include the target spectrum as well, and then shrunk; and make-before-break [4], where a new connection is established over the target spectrum before the original one is torn down.

The main objective of SD is to decrease the SBR. However, frequent reallocation of a large number of connections is undesirable because of the extra reconfiguration overhead. Hence, SBR, the number of connection reallocations, and the number of SD cycles should be considered jointly in order to balance the benefits and drawbacks of SD. Moreover, SD methods should adapt to the changing network conditions to ensure the most appropriate set of actions at a given time. Existing SD approaches rely on, e.g., integer linear program (ILP) models [8] or heuristic algorithms [9] that, guided by deterministic thresholds and policies, address a subset of the listed tasks. However, none of the prior solutions is able to address all of the aforementioned SD tasks simultaneously, and they require precise parametrization to achieve acceptable performance.

Driven by the need to automate complex networking problems, reinforcement learning (RL) has recently been demonstrated as a promising technique for, e.g., optical network slicing [10] and resource assignment [11], [12]. The key advantage of RL is that it leverages knowledge obtained by observing the environment to independently guide its decisions and maximize a long-term reward without being explicitly programmed to do so. deep reinforcement learning (DRL) combines RL with deep neural networks, allowing to parameterize action policies and analyze complex systems for high-dimensional input data, such as traffic matrices.

In this paper, we propose *DeepDefrag*, a novel DRL-based framework that jointly addresses all of the aforementioned tasks associated with the SD process. DeepDefrag decides on the timing and composition of the SD actions, i.e., the number, order, and target spectrum for reconfigured connections. The proposed framework adapts to the network state to select the appropriate course of actions, and can also consider the priorities of the network operator such as minimizing the number of connection reallocations. We assess the performance of the framework through extensive simulations, demonstrating that DeepDefrag outperforms a state-of-the-art heuristic, i.e., older-first first-fit (OF-FF), algorithm in several aspects.

2 Related Work

A variety of approaches have been investigated in the literature to mitigate the impact of SF, including an ILP formulation to address proactive parallel SD in EONs [8], and heuristic algorithms for hitless bandwidth defragmentation

[13]. ILP models and heuristic algorithms for three defragmentation techniques, denoted as Push-Pull, Hop-Tuning, and Replanning were proposed in [9]. Heuristic approaches from [14] use different service attributes to select the best connection to reallocate. The older-first (OF), bigger-first (BF), longer-lasting-first (LLF), and longer-path-first (LPF) algorithms use service age, size, remaining holding time, and path length to guide their proactive defragmentation decisions, respectively. A first-fit (FF) spectrum assignment policy is then applied to reallocate the spectrum slots. In [15], the authors analyzed the performance of different SD algorithms such as lowest-slot-index-first, holding-time-aware, and proactive-reactive defragmentation in terms of blocking probability, entropy, and SF ratio. A trade-off between SD gain and the degree of lightpath disruptions was further investigated in [16], and a mathematical model is developed to optimize the fragmentation ratios over all links while taking into account both spectrum continuity and contiguity constraints.

Machine learning techniques have recently found a useful application in SD as well. An unsupervised machine learning technique for rearranging the fragmented spectrum based on lightpath clustering was presented in [17]. In [18], Elman neural networks were used to forecast traffic demands, and the spectrum was allocated using a two-dimensional rectangular packing model that reduces unnecessary fragmentation.

In [11], the authors proposed a DRL-based routing, modulation and spectrum assignment (RMSA) algorithm that decides on both routing and spectrum assignment concurrently, resulting in reduced blocking probability. The work in [19] modeled the connection admission control and routing and spectrum assignment (RSA) problems as a Markov decision process (MDP), and defined the concept of deterministic policy for RSA problem in the policy iteration algorithm. The study in [20] highlighted DRL as a competitive alternative to established and well-known solutions when it comes to optimization problems in optical networks, e.g., routing and wavelength assignment (RWA). A recent study in [21] applied DRL to solve the on-demand, reactive hitless SD problem. Upon an unsuccessful RMSA attempt, a DRL agent selects one of the pre-defined stretch schemes that extends the size of the fragmented spectrum to accommodate for blocked services. In spite of the strong potential of DRL in solving complex optical networking problems, benefits of this technique in addressing the SD problem remain to be assessed. To this end, we propose a novel, DRL-based framework for proactive SD and investigate the related challenges and network performance improvements.

3 Problem Formulation

We consider a scenario where an EON serves dynamic traffic. The network topology is represented by a graph $G(V, E)$, comprising a set of nodes V and a set of links E. The network receives service requests defined by $D_i(s_i, d_i, b_i, a_i, h_i)$, where s_i and d_i are the source and the destination nodes, b_i is the requested bit rate, while a_i and h_i are the arrival and the holding times. The network serves the service requests by assigning a physical route, a modulation format and spectral resources, i.e., by solving the RMSA problem. The required number of spectrum slots, denoted as n_i, is determined by the spectrum efficiency of the modulation format, which is related to the length of the selected path [21]. If a path with $n_i + 1$ continuous and contiguous spectrum slots is found (the extra slot accounts for the guardband), the connection is established and the request is served. Otherwise, the request is blocked.

To mitigate the impact of spectrum fragmentation on the SBR, we perform periodic defragmentation. Solving the SD problem means reallocating the spectrum used by the existing connections with the ultimate goal of consolidating the free spectrum available for future use. We consider a proactive defragmentation scenario where only spectrum reallocation is possible, i.e., no rerouting is performed. When reallocating the spectrum of a connection, spectrum jump is allowed, i.e., the target and the original spectrum can be separated by slots occupied by other connections. We consider a hitless, make-before-break scenario.

The first challenge in the considered SD problem is to determine the best time to perform a defragmentation operation. At any point in time, the network snapshot consists of spectrum slots either occupied by existing connections, or free, possibly stranded due to fragmentation. The second challenge is to determine the set of connections to be reconfigured and the order of doing so, as well as to identify and allocate alternative spectrum slots to the connections. During SD, the standard spectrum continuity and contiguity constraints must hold.

4 The DeepDefrag Scheme

4.1 System Model

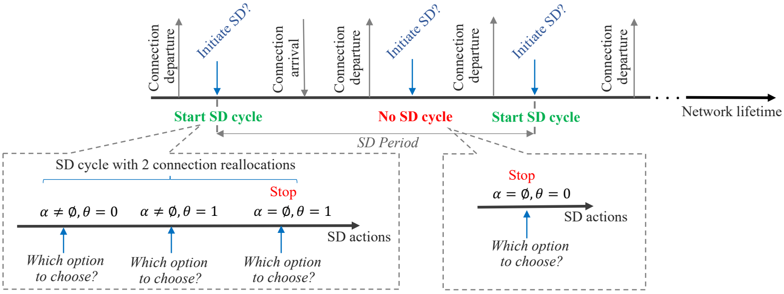

Figure 1: The DeepDefrag scheme decisions taken and implemented during network operation.

Figure 1 illustrates the DeepDefrag scheme under dynamic traffic, highlighting the SD cycles triggered amidst service arrivals and departures. Upon each connection departure, DeepDefrag decides whether to initiate a defragmentation cycle or not. If a new SD cycle is initiated, DeepDefrag iteratively chooses a connection to reconfigure and the target spectrum to reallocate it to until the cycle ends. An example with SD cycle comprising two connection reallocations is shown in the left-hand inset in the bottom of the figure. The figure also shows two variables used by DeepDefrag. θ is a network control flag with value 0 when the network is not undergoing an SD cycle, and 1 when an SD cycle is in progress. The selected action α equals the index of the connection selected for re-allocation, while $\alpha = \varnothing$ represents the *stop* action.

For the example shown in the figure, $\theta = 0$ and $\alpha \neq \varnothing$ when the SD cycle starts and the first connection is reallocated. DeepDefrag can then choose to continue the current defragmentation cycle by reallocating another connection, or to stop by returning $\alpha = \varnothing$. In the example, DeepDefrag chooses to reallocate another connection, after which the SD cycle stops. The time between two successive SD cycles is referred to as SD period. The scheme can also choose not to initiate an SD cycle upon a connection departure. This is depicted in Fig. 1 upon the departure of the second connection, and the detailed actions and values of the decision variables are shown in the inset on the right hand side. Here, the algorithm decides not to take any action ($\alpha = \varnothing$), while a defragmentation cycle is not in progress ($\theta = 0$).

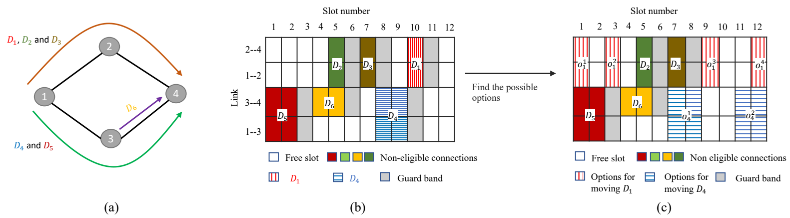

Figure 2: A simple network example (a) with two connections eligible for defragmentation (b) and the different options for their spectrum reallocation (c).

At each SD cycle, the DeepDefrag scheme considers a set of options, as illustrated in Fig. 2, with the snapshot of a small network example. The considered network state comprises six services established in the network, denoted as D_1 to D_6. Their routing is depicted in Fig. 2 a), while the spectrum assignment across the 12 available spectrum slots on each link is shown in Fig. 2 b). Connections considered eligible for reallocation are those using fragmented spectrum slots, which means that there is at least one free spectrum slot between them and their neighboring connections both at the lower and at the higher end of their used spectrum (considering that one guardband slot is a part of the spectrum allocated to each connection). In the example, only services D_1 and D_4 are eligible for reallocation.

DeepDefrag then considers several options for reallocating the spectrum of the eligible connections, as illustrated in Fig. 2 c). Each option represents reallocating one connection to the beginning or to the end of the existing free blocks along the path of that connection. For service D_1, two free blocks along links 1–2 and 2–4 can be considered for its allocation: slots 1–4 and 9–12. Therefore, service D_1 has four alternative spectrum options, which are at the beginning (denoted as o_1^1 and o_1^3) and at the end (o_1^2 and o_1^4) of the two candidate blocks. Alternatives for service D_4 are at the beginning and at the end of the only free block on links 1–3 and 3–4, i.e., slots 7–12, denoted as o_4^1 and o_4^2 in the figure. We use the event model from Fig. 1 and the intuition introduced in Fig. 2 to design a DRL agent that solves the SD problem.

4.2 Markov Decision Process Model

The DeepDefrag scheme proposed in this paper uses DRL to solve the SD problem introduced in the previous section. DRL is an area of machine learning concerned with intelligent agents that leverage deep learning to take actions in an observation environment with the goal of maximizing a cumulative reward. In the following, we present the MDP model of DeepDefrag, including the definitions of observation and action space, and reward function.

Observation Space

in DeepDefrag, the observation space exposes the current state of the network and the reallocation options to the agent. The agent observes the state of the environment and makes decisions based on the observations. Hence, the observation should reflect the critical aspects of the problem. The observation space of DeepDefrag has several components. $State_{ij} = (s_i, d_i, a_i, n_i, r_i, l_i, f_i, t_i, f_{ij}, t_{ij}, z_{ij})$ represents the set of attributes for reallocation option j of service D_i. Apart from the service attributes defined in Sec. 3, the environment is characterized by the remaining time of the service r_i, the number of links l_i along the path allocated to the service, the currently assigned starting spectrum slot f_i, and the total number of available slots along path t_i. f_{ij} and t_{ij} represent the new candidate starting slot and the size of the free spectrum block used by option j for reallocating connection D_i, respectively. $z_{ij} \in \{0, 1\}$ indicates whether option j is at the beginning $(= 0)$ or at the end $(= 1)$ of the free block.

Action Space

the actions that can be selected by the agent are defined by the action space. In DeepDefrag, at each decision step, the agent selects one of the existing options. After processing the eligible connections (see Fig. 2 for details), each possible action in the action space is defined as a vector of elements (D_i, f_{ij}) for different eligible connections and reallocation options, plus $\varnothing$ that represents the *stop* action. When an SD cycle is not in progress, *stop* action means that there is no need to reallocate more connections.

Reward function

the reward function, defined by (1), measures the immediate gain achieved by each action taken by DeepDefrag.

$$Reward = \begin{cases} 1 - SBR & \theta = 0,1 \wedge \alpha = \varnothing \\ 1 - SBR - Ps - Pe & \theta = 0 \wedge \alpha \neq \varnothing \\ 1 - SBR - Pe & \theta = 1 \wedge \alpha \neq \varnothing \end{cases}, \tag{B.1}$$

We encourage the agent to minimize SBR by adopting it as the main term of the function. The value of SBR refers to the ratio between the blocked and the total number of processed service requests. When no connection reallocation takes place ($\alpha = \varnothing$), the reward is equal to 1 − SBR to capture the objective of minimizing the blocking (the top term in (1)). To limit the number of SD cycles and reallocated connections, each new SD cycle and each connection reallocation is associated with a penalty, denoted with Ps and Pe, respectively. When the agent initiates the cycle by reallocating a connection, both penalties are applied (the middle term in (1)). When an SD cycle is in progress, each connection reallocation is penalized (the bottom term in (1)). Note that these penalty values can be set based on the cost incurred by the network operator at each reallocation instance.

5 Simulation Settings

To evaluate the performance of DeepDefrag, we carry out simulations of a dynamic traffic scenario and assess the value of SBR, as well as the reconfiguration actions' frequency and volume. We use the NSFNET topology with 14 nodes and 22 links, each supporting 320 spectrum slots. Service requests are generated based on a Poisson process. We set the traffic load to 170 Erlang to achieve approximately 10% SBR for the scenario without defragmentation. 80% of service requests is long-lived with an average holding time of 25 time units and exponential distribution, while the remaining 20% of requests have an average holding time of 12.5 time units. The considered bit rate is 100 Gbit/s for 50%, 200 Gbit/s for 30%, and 400 Gbit/s for the remaining 20% of the requests. BPSK, QPSK, 8-QAM, and 16-QAM modulation formats are utilized with a maximum reach length of 10000 km, 2000 km, 1250 km, and

625 km, and with slot capacity of 12.5 Gbit/s, 25 Gbit/s, 37.5 Gbit/s, and 50 Gbit/s, respectively [12]. The transmission reach of the signal determines the candidate modulation formats, and the one with the highest spectral efficiency is selected. Shortest available route (among 5 pre-computed shortest paths) and first-fit spectrum assignment are used to obtain the RMSA solutions for all considered scenarios.

The performance of DeepDefrag is evaluated through comparison with three heuristic algorithms denoted as OF-FF, RND, and *No-SD*. In the OF-FF strategy, the set of eligible connections is defined according to their age, such that the longest-running connections are reconfigured first. First-fit spectrum allocation is then used to find new spectrum slots for the reconfigured connections. This strategy is used for benchmarking purposes since studies show that it performs very well in terms of SBR [14]. OF-FF has two parameters: the SD period, i.e., the number of request arrivals between two defragmentation periods, and the number of connections to be reallocated at each cycle. The values of both parameters are fixed throughout the network lifetime. We analyze the performance of OF-FF under different configurations and report on two most representative settings that enable a fair comparison with DeepDefrag. Configuration where both the SD period and the number of reallocations are set to 10, denoted as OF-FF(10,10), obtains the same SBR as DeepDefrag, allowing us to compare their defragmentation overheads. Configuration with the SD period length of 20 and the number of reallocations equal to 4, denoted as OF-FF(20,4), has the same defragmentation overhead as DeepDefrag, allowing us to examine their SBR. The random heuristic RND randomly selects one of the options from the action space (including *stop*). Finally, the *No-SD* approach reveals the network performance when defragmentation is not undertaken.

We implement the DeepDefrag scheme and environment extending the Optical RL-Gym [22], a framework for creating RL environments that model optical network problems such as resource management and reconfiguration. Stable-Baselines3 [23], an open-source implementation of DRL algorithms in Python, is applied to train the RL agent. We use the Deep Q-Networks algorithm (DQN)[24] with a learning rate of $5 * 10^{-6}$ and a discount factor of 0.95. The adopted neural network has 5 layers with 256 neurons each. The penalty factors Ps and Pe are set to 0.3 and 0.05, respectively, to model a higher cost of an SD cycle initiation than a connection reallocation. The episode length

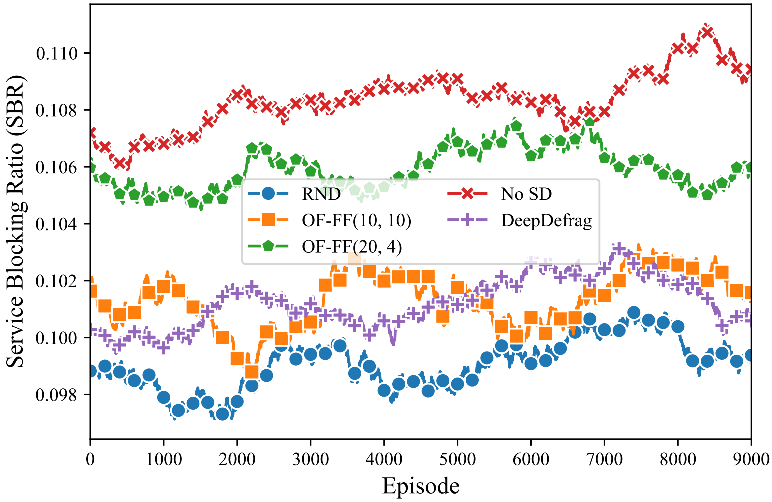

Figure 3: service blocking ratio (SBR) obtained by the different spectrum defragmentation (SD) schemes

is set to 200 decision steps, and the training is performed over 9000 episodes. Results presented in the next section are obtained by assessing the performance of the agent as it is trained. For statistical purposes, in the following comparison comments, we average the results over the last 500 episodes.

6 Numerical Results

Figure 3 shows the SBR values for the different schemes, indicating advantages of DeepDefrag. Considering the rolling 500-episode average, DeepDefrag lowers the blocking rate by 10% compared to the *No-SD* scenario with no defragmentation. The OF-FF(10,10) and OF-FF(20,4) schemes yield on average 10.8 % and 3% lower SBR than *No-SD*, which is aligned with the result reported by [14]. Compared to OF-FF(20,4), which has the same defragmentation overhead, DeepDefrag reduces the SBR by 6.2%. This confirms the efficiency of defragmentation actions performed by DeepDefrag in reducing the SBR.

Figure 4 depicts the number of connection reallocations per 100 arrivals for

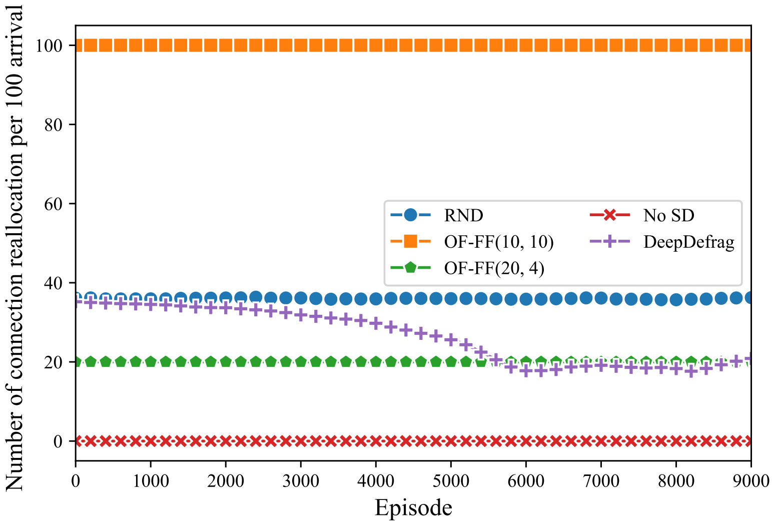

Figure 4: Number of connections reallocated by the different SD schemes per 100 arrivals

the different strategies. On average, upon convergence, DeepDefrag reallocates only 20.2 connections per 100 request arrivals, closely matching OF-FF(20,4). Moreover, DeepDefrag reallocates 80% connection fewer than OF-FF(10,10), which is the OF-FF configuration with the same SBR as DeepDefrag.

Figure 5 shows the number of SD cycles. Also in this case, DeepDefrag outperforms all the benchmark SD heuristics, triggering only 4.9 SD cycles per 100 request arrivals on average. This is a 51% reduction compared to OF-FF(10,10). After analyzing the learning aspects in Figs. 4 and 5, we can see that DeepDefrag learns how to reduce the SD overhead in terms of connection reallocations and defragmentation cycles in 5500 training episodes, as indicated by the decline in the reconfiguration frequency and volume. As the above analysis shows, DeepDefrag outperforms the considered SD heuristics in all examined metrics.

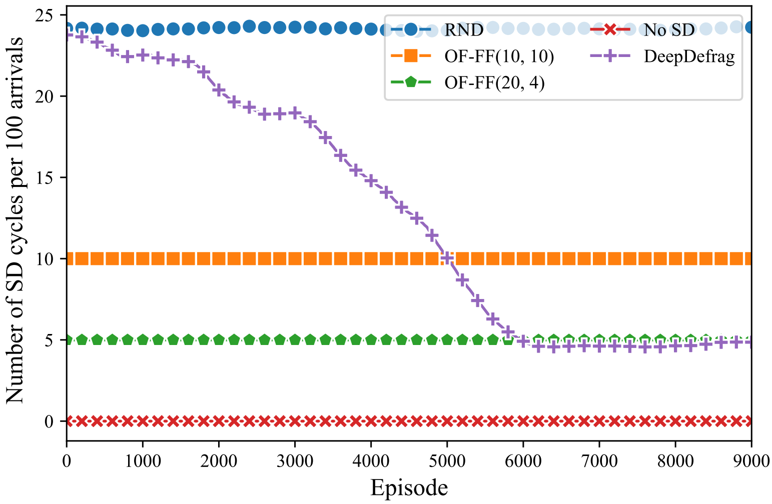

Figure 5: Number of SD cycles for different SD schemes per 100 arrivals

7 Conclusions

This paper proposes DeepDefrag, a novel framework based on the deep reinforcement learning (DRL) that addresses several aspects of the spectrum defragmentation (SD) problem in an integrated manner. It determines whether and when to perform SD, which connections to reallocate and in which order, and finds new spectrum to be used by the connection. Simulation results indicate the ability of DeepDefrag to efficiently reduce the blocking rate while using fewer SD cycles and reallocating a lower number of connections than the state-of-the-art heuristic approaches, demonstrating its applicability to dynamic network conditions and strong potential for automating SD.

References

[1] M. Jinno, H. Takara, B. Kozicki, Y. Tsukishima, Y. Sone, and S. Matsuoka, "Spectrum-efficient and scalable elastic optical path network: Architecture, benefits, and enabling technologies," *IEEE Communications Magazine*, vol. 47, no. 11, pp. 66–73, 2009.

[2] R. Wang and B. Mukherjee, "Provisioning in elastic optical networks with non-disruptive defragmentation," *Journal of Lightwave Technology*, vol. 31, no. 15, pp. 2491–2500, 2013.

[3] Y. Yin, H. Zhang, M. Zhang, *et al.*, "Spectral and spatial 2d fragmentation-aware routing and spectrum assignment algorithms in elastic optical networks," *Journal of Optical Communications and Networking*, vol. 5, no. 10, A100–A106, 2013.

[4] B. C. Chatterjee, S. Ba, and E. Oki, "Fragmentation problems and management approaches in elastic optical networks: A survey," *IEEE Communications Surveys & Tutorials*, vol. 20, no. 1, pp. 183–210, 2017.

[5] S. Ba, B. C. Chatterjee, and E. Oki, "Defragmentation scheme based on exchanging primary and backup paths in 1+1 path protected elastic optical networks," *IEEE/ACM Transactions on Networking*, vol. 25, no. 3, pp. 1717–1731, 2017.

[6] M. Zhang, Y. Yin, R. Proietti, Z. Zhu, and S. J. B. Yoo, "Spectrum defragmentation algorithms for elastic optical networks using hitless spectrum retuning techniques," in *2013 Optical Fiber Communication Conference and Exposition and the National Fiber Optic Engineers Conference (OFC/NFOEC)*, 2013, pp. 1–3.

[7] Y. Aoki, X. Wang, P. Palacharla, *et al.*, "Dynamic and flexible photonic node architecture with shared universal transceivers supporting hitless defragmentation," in *2012 38th European Conference and Exhibition on Optical Communications*, 2012, pp. 1–3.

[8] M. Zhang, C. You, and Z. Zhu, "On the parallelization of spectrum defragmentation reconfigurations in elastic optical networks," *IEEE/ACM Transactions on Networking*, vol. 24, no. 5, pp. 2819–2833, 2016.

[9] D. A. Moniz, "Replanning of optical networks based on defragmentation techniques," 2015.

[10] M. R. Raza, C. Natalino, P. Öhlen, L. Wosinska, and P. Monti, "Reinforcement learning for slicing in a 5G flexible RAN," *Journal of Lightwave Technology*, vol. 37, no. 20, pp. 5161–5169, 2019.

[11] M. Shimoda and T. Tanaka, "Mask RSA: End-to-end reinforcement learning-based routing and spectrum assignment in elastic optical networks," in *2021 European Conference on Optical Communication (ECOC)*, 2021, pp. 1–4.

[12] X. Chen, B. Li, R. Proietti, H. Lu, Z. Zhu, and S. J. B. Yoo, "Deep-RMSA: A deep reinforcement learning framework for routing, modulation and spectrum assignment in elastic optical networks," *Journal of Lightwave Technology*, vol. 37, no. 16, pp. 4155–4163, 2019.

[13] M. Zhang, Y. Yin, R. Proietti, Z. Zhu, and S. B. Yoo, "Spectrum defragmentation algorithms for elastic optical networks using hitless spectrum retuning techniques," in *2013 Optical Fiber Communication Conference and Exposition and the National Fiber Optic Engineers Conference (OFC/NFOEC)*, IEEE, 2013, pp. 1–3.

[14] J. Comellas, L. Vicario, and G. Junyent, "Proactive defragmentation in elastic optical networks under dynamic load conditions," *Photonic Network Communications*, vol. 36, no. 1, pp. 26–34, 2018.

[15] S. Fernández-Martínez, B. Baran, and D. P. Pinto-Roa, "Spectrum defragmentation algorithms in elastic optical networks," *Optical Switching and Networking*, vol. 34, pp. 10–22, 2019.

[16] N. T. Khai, R. Romero Reyes, and T. Bauschert, "Spectrum defragmentation with improved lightpath migration scheme in flex-grid networks," in *2021 International Conference on Optical Network Design and Modeling (ONDM)*, 2021, pp. 1–6.

[17] S. Trindade and N. L. da Fonseca, "Machine learning for spectrum defragmentation in space-division multiplexing elastic optical networks," *IEEE Network*, vol. 35, no. 1, pp. 326–332, 2021.

[18] Y. Xiong, Y. Yang, Y. Ye, and G. N. Rouskas, "A machine learning approach to mitigating fragmentation and crosstalk in space division multiplexing elastic optical networks," *Optical Fiber Technology*, 2019.

[19] R. Romero Reyes and T. Bauschert, "Towards DRL-based routing and spectrum assignment in optical networks: Lessons to be learned from Markov decision processes," in *IEEE Latin-American Conference on Communications (LATINCOM)*, 2021, pp. 1–6.

[20] N. D. Cicco, E. F. Mercan, O. Karandin, *et al.*, "On deep reinforcement learning for static routing and wavelength assignment," *IEEE Journal of Selected Topics in Quantum Electronics*, vol. 28, no. 4, pp. 1–12, 2022.

[21] R. Li, R. Gu, W. Jin, and Y. Ji, "Learning-based cognitive hitless spectrum defragmentation for dynamic provisioning in elastic optical networks," *IEEE Communications Letters*, vol. 25, no. 5, pp. 1600–1604, 2021.

[22] C. Natalino and P. Monti, "The Optical RL-Gym: An open-source toolkit for applying reinforcement learning in optical networks," in *22nd International Conference on Transparent Optical Networks (ICTON)*, 2020.

[23] A. Raffin, A. Hill, A. Gleave, A. Kanervisto, M. Ernestus, and N. Dormann, "Stable-Baselines3: Reliable reinforcement learning implementations," *Journal of Machine Learning Research*, vol. 22, no. 268, pp. 1–8, 2021.

[24] V. Mnih, K. Kavukcuoglu, D. Silver, *et al.*, *Playing atari with deep reinforcement learning*, 2013.

PAPER C

Deep reinforcement learning for proactive spectrum defragmentation in elastic optical networks [Invited]

Ehsan Etezadi, Carlos Natalino, Renzo Diaz, Anders Lindgren, Stefan Melin, Lena Wosinska, Paolo Monti, Marija Furdek

Published in IEEE/Optica Journal of Optical Communications and Networking (JOCN),
vol. 15, no. 10, pp. 86-96.

The layout has been revised.

Abstract

The immense growth of Internet traffic calls for advanced techniques to enable the dynamic operation of optical networks, efficient use of spectral resources, and automation. In this paper, we investigate the proactive SD problem in elastic optical networks and propose a novel deep reinforcement learning-based framework *DeepDefrag* to increase spectral usage efficiency. Unlike the conventional, often threshold-based heuristic algorithms that address a subset of the defragmentation-related tasks and have limited automation capabilities, DeepDefrag jointly addresses the three main aspects of the SD process: determining when to perform defragmentation, which connections to reconfigure, and which part of the spectrum to reallocate them to. By considering services attributes, spectrum occupancy state expressed by several different fragmentation metrics, as well as reconfiguration cost, DeepDefrag is able to consistently select appropriate reconfiguration actions over the network lifetime and adapt to changing conditions. Extensive simulation results reveal superior performance of the proposed scheme over a scenario with exhaustive defragmentation and a well-known benchmark heuristic from the literature, achieving lower blocking probability at a smaller defragmentation overhead.

1 Introduction

The tremendous growth of bandwidth-intensive applications that have dynamic behavior and high performance requirements (e.g., high-definition video on demand, cloud computing, Internet of Things, content delivery networks) puts a significant strain on the optical backbone networks. Dynamic, automated, and resource-efficient network operation is essential to fulfilling these requirements. Elastic optical networks (EONs) [1] enable both fine-grained spectrum slicing and high-capacity super-channels that match the spectrum requirements of service requests. However, EONs are prone to spectrum fragmentation (SF), where the requested service bandwidth exceeds the number of continuous and contiguous free spectrum slots. In dynamic traffic scenarios, the establishment and tear-down of optical connections often exacerbates SF by scattering relatively small unoccupied spectral gaps across the available fiber bandwidth [2], [3]. When these spectral gaps are insufficient to support incoming service requests, SF has a direct, detrimental impact on the blocking probability of service demands [4].

To alleviate the impact of fragmentation, spectrum allocation should be consolidated to leave as few unusable spectral gaps as possible. This process is called spectrum defragmentation (SD), and is known to improve spectrum grid utilization and reduce service blocking ratio (SBR) [5]. The goal of SD is to make the spectral gaps larger and better aligned across the network links. This enables for accommodating more services, thus maximizing the use of the spectrum.

1. *When to reconfigure?* Deciding on the best time to perform SD among arbitrary service arrivals and departures.

2. *What to reconfigure?* Determining the number and the order of connections to be reallocated.

3. *Where to reallocate the connections to?* Finding new spectral resources for the reconfigured connections.

The problem of minimizing spectrum fragmentation by reconfiguring a minimum number of connections has been shown to be NP-complete in static traffic scenarios [6]. Traffic dynamicity further increases the problem complexity due to the constantly changing set of connections in the network. Hence, tractable optimization approaches are needed to solve the highly complex problem of dynamic SD.

SD approaches can be classified into two main schemes: reactive and proactive [2]. Reactive approaches are triggered by service blocking. Proactive approaches are executed without waiting for the blocking to occur. They typically monitor network performance metrics to find the best time for SD or perform it periodically. These schemes are further classified into two types, namely with or without rerouting of connections [5]. The latter approaches only reallocate the spectrum of the connections, while the former may modify their routes as well. SD approaches that interrupt running services are referred to as non-hitless, while those that do not cause any traffic disruption are known as hitless [7]. Push-pull retuning is a hitless approach where the spectrum occupied by a connection is first expanded until it includes both the original and the targeted spectrum slots and then shrunk to include only the targeted slots [8]. Another hitless SD approach is make-before-break, where an additional connection is established over the target route and spectrum before tearing down the original one, allowing for a spectrum jump [5]. It should be noted that make-before-break is considered non-disruptive specifically for the optical layer, while interruptions may occur at the higher layers depending on the employed protocol and/or rerouting strategy.

While SD has been shown to decrease the SBR, it also imposes a reconfiguration overhead that is not desirable by network operators. Depending on the SD approach, the overhead may entail terminating, reallocating, and reestablishing selected connections. Consequently, performing SD too frequently or on an excessive number of connections may drastically increase the complexity of network control and management. In fact, the frequency of SD cycles and the number of connection reallocations within each cycle are used to measure the SD overhead [9]. This indicates that the potential SBR improvement and the corresponding overhead should be considered jointly and flexibly in the design and evaluation of SD approaches. Existing SD strategies (e.g., [10], [11]) handle only a subset of the aforementioned SD tasks and they do so by utilizing deterministic thresholds and policies, which makes them inapplicable to dynamic settings with changing network conditions.

Different from the deterministic, threshold-based policies, in reinforcement learning (RL), the algorithm makes decisions by learning from the environment, aiming at maximizing the long-term reward without being explicitly programmed. RL has recently been demonstrated as a promising technique for solving large-scale online control tasks, e.g., routing and resource assignment in EON [12], [13] and 5G network slicing [14]. The DRL method combines RL with deep neural networks (DNNs), allowing complex systems to be analyzed for high-dimensional input data, including traffic matrices and images. One of the valuable capabilities of some DRL agents is to learn online and adapt to changing network conditions. Through the online learning process, the DRL agent continuously interacts with the environment, receives feedback, and updates its policy accordingly.

To utilize the merit of DRL in automating SD, we proposed DeepDefrag, a novel DRL-based framework that jointly addresses all of the tasks involved in the SD process: determining when to perform defragmentation, which connections to reconfigure, and which part of the spectrum to reallocate them to [15]. DeepDefrag considers the network state to select the most appropriate course of action and can take into account the priorities of a network operator, such as minimizing the number of SD cycles and connection reallocations. Our preliminary study in [15], considered only a subset of connections as eligible for reconfiguration and did not examine the spectrum occupancy state in the decision-making process. This paper extends and improves DeepDefrag by

1. considering all connections in the network as candidates for reconfiguration,
2. considering full information about the spectrum occupancy, including different fragmentation metrics, and
3. revising the reward function to allow for a more comprehensive evaluation of the impact of actions.

An evaluation of the impact of different penalties modeling the SD overhead, and of changes in the traffic load is also included. The performance of the proposed DeepDefrag framework is evaluated through comparison with several heuristic algorithms from the literature. The simulation results reveal that DeepDefrag outperforms the well-known existing older-first first-fit (OF-FF) algorithm in different aspects. Moreover, it yields SBR values close to an approximated (heuristic) lower bound obtained through exhaustive spectrum defragmentation. We demonstrate that, unlike preconfigured algorithms like OF-FF, DeepDefrag can effectively handle changes in the traffic load by considering the new situation and learning the policy for the updated circumstances. This adaptability allows DeepDefrag to continuously optimize its actions and make informed decisions that align with the current network conditions, resulting in improved performance and spectrum resource utilization.

2 Related work and background

2.1 Spectrum fragmentation metrics

In general, spectrum fragmentation metrics in EONs measure the efficiency of spectral utilization. A better fragmentation metric value indicates that the occupied frequency slots are used more efficiently, with fewer unusable gaps between occupied slots. These metrics help network operators monitor and optimize the utilization of optical spectrum resources, ensuring high performance and efficient use of available resources. The SF issue in EONs has been widely analyzed in the literature and several fragmentation metrics have been introduced. Wang et al. [16] present the concept of utilization entropy to measure the level of optical spectrum fragmentation. Authors in [17] define an external fragmentation metric as a ratio of the largest free contiguous fragment of the spectrum and the sum of the size of all free spectral fragments. The spectrum compactness metric from [18] indicates the occupation of spectrum on a link or in the network by calculating the difference between the maximum and the minimum indices of occupied slots. Takita et al. [19] define the high slot mask metric as an indicator of the maximum number of occupied spectrum slots in the network.

In this paper, we incorporate the spectrum occupancy state into the DRL agent to enhance its understanding of the network state. However, considering a large number of SF metrics is impractical due to the increased complexity of computing the metrics at every step, and the potential increase in the training time of the DRL agent. As highlighted in [20], different metrics capture various aspects of SF, and the selection of metrics depends on the specific requirements and context. Therefore, we carefully chose three metrics to measure the fragmentation state of the network: the number of cuts [21], the Shannon entropy (SE) [17], and the root of sum of squares (RSS) [20]. In support of our choices, previous studies such as [12] have demonstrated the suitability of incorporating RSS into the reward function of DRL agents for routing and spectrum assignment in EONs. Furthermore, the effectiveness of the number of cuts and SE in enhancing network utilization has been highlighted in [21] and [22], respectively.

In Fig. 1, we exemplify the parameters and calculation of these metrics with a snapshot of a simple network example with five nodes and four links, each with 12 spectrum slots. The considered network state comprises six connections established in the network, denoted by D_1 to D_6. The connection routes are depicted in Fig. 1(a), while the spectrum assignment state for each link is shown in Fig. 1(b). We assume one spectrum slot is used as guardband between adjacent connections on a link. The notation includes the following parameters: e is the index of a link, E is the total number of links, s is the

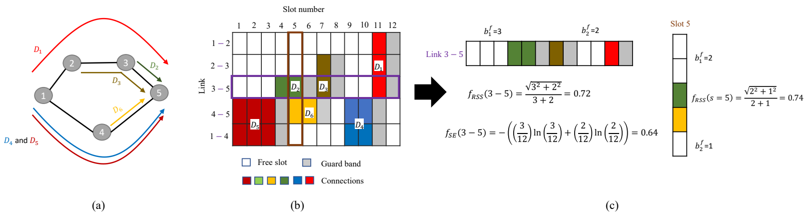

Figure 1: A simple network example serving six connections (a). The spectrum occupancy state (b). Shannon entropy and root of sum of squares metrics (c).

index identifying a spectrum slot on a link, S is the total number of slots of a link, b_i^f is the size of free spectrum block i, and N is the number of free spectrum blocks.

The number of cuts denotes the number of links with free adjacent spectrum slots on the path selected for a connection. The SE values for a link and the entire network are formulated by (C.1) and (C.2), respectively. Equation (C.3) defines the RSS metric for a link e, while it can be calculated for a slot s analogously. The two metrics are referred to as spectral and spatial fragmentation, respectively [12]. Finally, the RSS metric for the network is calculated as the average of spectral and spatial RSS metrics over all the links and slots in (C.4). A higher SE value implies higher fragmentation, while a higher RSS value implies lower fragmentation.

$$f_{SE}(e) = -\sum_{i=1}^{N} \frac{b_i^f}{S} \ln \frac{b_i^f}{S} \tag{C.1}$$

$$F_{SE} = \frac{\sum_e^E f_{SE}(e)}{E} \tag{C.2}$$

$$f_{RSS}(e) = \frac{\sqrt{\sum_i^N (b_i^f)^2}}{\sum_i^N b_i^f} \tag{C.3}$$

$$F_{RSS} = \frac{\sum_s^S f_{RSS}(s)}{S} + \frac{\sum_e^E f_{RSS}(e)}{E} \tag{C.4}$$

Figure 1(c) shows how the values of the SE and RSS metrics for link $(3-5)$

and slot number (5) (highlighted with frames) are calculated. In the example, connection D_1 occupies slot 11, so slot 10 is checked to calculate the number of cuts. Slot 10 is free on all three links included in the path of D_1, so the number of cuts is equal to 3 for this connection. The number of cuts for D_3 is equal to 1 since slot 6 is occupied on link $(3-5)$ and free on link $(2-3)$.

2.2 Spectrum defragmentation techniques

In recent years, extensive research has examined spectrum fragmentation and its mitigation, relying on integer linear program (ILP) formulations, (meta)heuristics and machine learning techniques. The work in [10] models the proactive parallel connection reconfiguration in EONs mathematically as an ILP formulation and studies the complexity of the problem. ILP models for three defragmentation techniques denoted as Push-Pull, Hop-Tuning, and Replanning are proposed in [11]. The authors in [23] delve deeper into the trade-off between SD gain in terms of fragmentation ratio and the extent of connection disruptions in terms of reconfiguration delays. They create a mathematical model to optimize high-slot marks as the fragmentation metric across all links.

Heuristic and metaheuristic algorithms are also widely used to tackle the fragmentation problem and decrease the SBR. The authors in [24] investigate heuristic algorithms for hitless bandwidth defragmentation, including spectrum sweeping and hop tuning. In [9], SD is performed periodically, and connections are selected for reallocation based on service attributes. Older-first (OF) selects the longest-lasting connections, longer-lasting-first (LLF) selects those with the longest remaining holding time, bigger-first (BF) selects the connections with the biggest size, and longer-path-first (LPF) selects those with the longest path for reconfiguration. A first-fit (FF) spectrum assignment policy is employed to reallocate spectrum slots. Simulation results indicate that the algorithms exhibit similar performance, with the OF algorithm demonstrating the best performance within a marginal difference of one percent.

In [25], different SD heuristic algorithms, including lowest-slot-index-first, holding-time-aware, and proactive-reactive defragmentation, are compared based on their blocking probability, entropy, and bandwidth fragmentation ratio. The authors in [26] propose a reactive disruptive scheme and a proactive non-disruptive scheme. Both schemes utilize the holding time information of existing connections to minimize the SBR. The authors in [27] use a meta-heuristic nature-inspired optimization technique called jellyfish search optimization to solve spectrum defragmentation and show performance improvement compared to the state-of-the-art heuristic algorithms.

SD has recently benefited from adopting machine learning techniques. An application from [28] uses unsupervised machine learning to rearrange the fragmented spectrum based on connection clustering. In [29], Elman neural networks (NNs) are employed to predict traffic demands, and a two-dimensional rectangular packing model is used to allocate spectrum in a way that minimizes fragmentation. A machine learning-assisted signal-quality-aware proactive defragmentation scheme for the C + L band system is proposed in [30]. The scheme prioritizes minimizing the fragmentation index and quality of transmission (QoT) maintenance for the defragmentation algorithms.

2.3 Reinforcement learning in optical networks

Multiple studies have explored the efficacy of RL for solving resource allocation problems in EONs, such as the DRL-based routing, modulation and spectrum assignment (RMSA) algorithm in [31], which performs joint routing and spectrum assignment by masking infeasible options to improve the blocking probability performance. In [31], the connection admission control and routing and spectrum assignment (RSA) problems are modeled as a Markov decision process (MDP), and the concept of deterministic policy for the RSA problem in the policy iteration algorithm is introduced. The work in [32] demonstrates that DRL is an effective alternative to established and well-known solutions for optical network optimization problems, including routing and wavelength assignment (RWA). A DRL approach for resource provisioning in a dynamic multi-band EON is studied in [33] and compared to a heuristic algorithm. The authors in [34] investigate the problem of global optimization of network performance in a survivable EON use case and propose a DRL-based algorithm with the objective of improving the overall network performance in terms of cost value and survivability, where two RL agents are utilized to provide working and protection paths. In [35], DRL is used to tackle the on-demand, reactive hitless SD problem. Upon a failure of an incoming service request, the DRL agent selects one of the pre-defined schemes that increase the size of the fragmented spectrum to accommodate blocked services. To the best of our knowledge, the merit of DRL in solving proactive SD has not been evaluated yet in spite of its strong potential to solve complex problems. Therefore, in the next sections, we propose a DRL-based framework for proactive SD and evaluate its performance against heuristic algorithms.

3 Problem formulation

We consider a network topology represented by a graph $G(\mathcal{V}, \mathcal{E})$, where $\mathcal{V}$ and $\mathcal{E}$ represent the set of nodes and fiber links, respectively. We model a service request from node s to d ($s, d \in \mathcal{V}$) as $D_i(s_i, d_i, b_i, a_i)$, with b_i and a_i denoting the requested bit rate, arrival time, respectively. To provision service requests, the network must solve the RMSA problem of finding an end-to-end physical route, determining the modulation format, and allocating the required spectral resources. We adopt the model from [13] to decide on the modulation format limited by the length of the selected path. The number of required spectrum slots, denoted by n_i, is determined by $\lceil b_i/(12.5 \times m) \rceil$, where 12.5 Gbit/s is the data rate that a spectrum slot of BPSK signal can support, and m is spectral efficiency of the selected modulation format. A connection is established if a path with $n_i + 1$ continuous and contiguous spectrum slots is found, where the extra slot accounts for the guardband. If these spectrum resources are not found, the service request is blocked.

We consider a dynamic EON scenario in which service requests arrive and depart throughout the network operation. At any given time, the spectrum grid state information about the existing connections is known. In the considered proactive SD scenario, only spectrum reallocation is performed, without connection rerouting. The goal is to reallocate the spectrum of a subset of connections to consolidate the free available spectrum for future use. We consider a hitless, make-before-break scenario. The first challenge of proactive SD is to find the best time to perform a defragmentation operation. The second challenge is to determine the set of connections and the order in which they should be reconfigured. Finally, the new spectrum slots must be identified for the services.

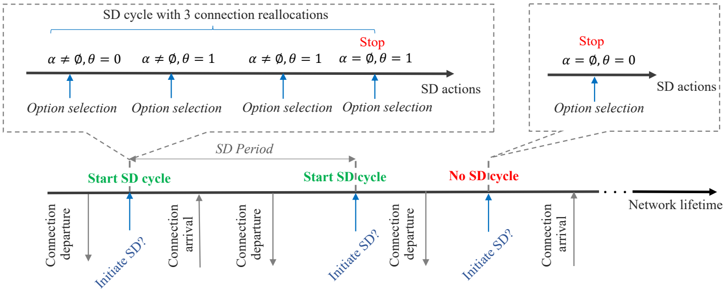

Figure 2: The DeepDefrag scheme decisions taken and implemented during network operation.

4 The DeepDefrag scheme

4.1 System model

Figure 2 illustrates the DeepDefrag scheme under dynamic traffic, where SD cycles are triggered in response to connection departures. When a connection departs, DeepDefrag assesses whether to initiate a defragmentation cycle or not. If the decision is to start a new SD cycle, DeepDefrag selects a connection to reconfigure and identifies the target spectrum. This process is repeated until DeepDefrag decides to conclude the cycle. The left-hand inset at the top of the figure provides an example of an SD cycle that includes three connection reallocations. The DeepDefrag scheme uses two variables to model the SD process. $\theta \in \{0, 1\}$ is a network control flag with a value of 1 when an SD cycle is in progress, and 0 otherwise. The selected action is denoted as α, with value equal to the index of the connection selected for reconfiguration, or α=$\varnothing$ to represent the *stop* action.

As shown in Fig. 2, θ=0 and $\alpha \neq \varnothing$ when DeepDefrag starts an SD cycle and reallocates the first connection. At this point, DeepDefrag has the option to either continue the ongoing SD cycle by reallocating another connection or to terminate it by returning $\alpha = \varnothing$. In this particular example, DeepDefrag decides to reallocate two other connections (θ=1, $\alpha \neq \varnothing$), and then stops the SD cycle (θ=1, α=$\varnothing$). Note that only sequential reconfiguration of individual connections is considered (i.e., two or more connections are not reconfigured

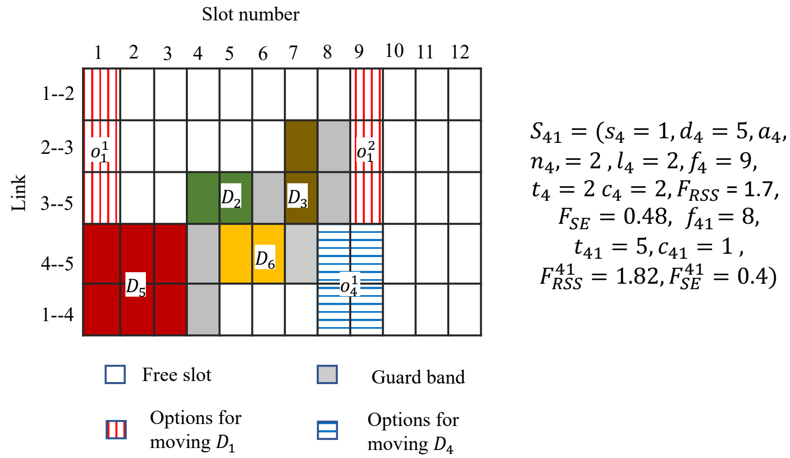

Figure 3: Different options for spectrum reallocation of the connections, and the state representation

jointly). The time between two sequential SD cycles is referred to as the SD period. DeepDefrag can also decide not to trigger an SD cycle upon a connection departure. Fig. 2 illustrates this scenario after the departure of the third connection, where the actions and variables involved in the decision-making process are presented in the inset on the right hand side. Here, the SD cycle is not currently in progress (θ=0), and the scheme chooses to take no action (α=$\varnothing$).

DeepDefrag considers all connections as candidates for reallocation and examines several options to reassign the spectrum. All available spectrum blocks that can accommodate the connection are enumerated, and each option represents reallocating a connection to the beginning of every available free block along its path. Let us consider the same example as in Fig. 1 and analyze the reallocation options for connections D_1 and D_4, shown in Fig. 3. For connection D_1, which is currently using slot 11, two free blocks along links 1–2, 2–3, and 3–5 can be considered as alternatives: slots 1–3 and 9–12. Therefore, connection D_1 has two alternative spectrum options, which are at the beginning of the two candidate blocks, denoted as o_1^1 and o_1^2. The alternative for connection D_4 is at the beginning of the only free block on links 1–4 and 4–5, i.e., slots 8–12, denoted as o_4^1 in the figure. It should be noted that one option is available for connection D_2 and one for connection D_3, which are not shown in the figure. By combining the event model from Fig. 2 and the intuition developed in Fig. 3, a DRL agent can be designed to solve the SD problem.modeling

4.2 Markov decision process modeling

The DeepDefrag scheme uses DRL to solve the proactive SD problem discussed in the previous section. DRL is a machine learning technique focused on solving control problems, where a DRL agent interacts with the environment and has the objective of maximizing a notion of cumulative reward. Such control problems are commonly modeled as MDPs. The following section outlines the MDP model of DeepDefrag, which covers the definitions of the observation space, action spaces, and reward function.

Observation space

The observation space should provide the DRL agent with enough information to characterize the current state of the environment (i.e., the optical network in our case). The observation space of DeepDefrag consists of several components. The state representation for reallocation option j of connection D_i is denoted as S_{ij}, and defined as follows:

$$S_{ij} =< s_i, d_i, a_i, n_i, l_i, f_i, t_i, c_i, F_{RSS}, F_{SE}, f_{ij}, t_{ij}, c_{ij}, F_{RSS}^{ij}, F_{SE}^{ij} > ,$$

where l_i is the number of links along the path allocated to the connection, f_i is the currently assigned starting spectrum slot, t_i is the total number of available slots along path, and c_i is the number of cuts (as defined in Sec. 2.2.1) along the current path. The RSS and SE metrics for the current state of the network are represented by F_{RSS} and F_{SE}, respectively. f_{ij}, c_{ij}, and t_{ij} represent the new candidate starting slot, the number of cuts, and the size of the free spectrum block used by option j for reallocating connection D_i, respectively. Finally, F_{RSS}^{ij}, F_{SE}^{ij} are the RSS and SE metrics of the network if D_i is chosen to be reallocated to option j. The example of the state representation for option o_4^1 is represented in Fig 3.

Action space

The action space represents the set of all actions the agent can perform in a specific environment. As shown in Fig 2, for our environment, the agent can select one of the available options in each decision step. In the DeepDefrag environment, we denote the set of possible actions as $\mathbb{J}$. Each action is characterized by the tuple $<D_i, f_{ij}>$, which represent the connection and the new starting slot of the selected option, respectively. The set $\mathbb{J}$ also contains the $\varnothing$ action, which denotes termination of an SD cycle in progress, or the absence of initiating a new one.

Reward function

The reward function is a function that provides a numerical score based on the state of the environment and the action taken by the agent. The critical challenge of using RL is to find the appropriate reward function that reflects the behavior of the environment and steers the agent towards the most suitable policy. The reward value r_i for DeepDefrag is defined by (C.5).

$$r_i = \begin{cases} -\frac{\log_{10} SBR}{3} & \theta \in \{0,1\} \wedge \alpha{=}\varnothing \\ -\frac{\log_{10} SBR}{3} - Ps - Pe & \theta = 0 \wedge \alpha \neq \varnothing \\ 1 + \frac{\log_{10}(F_{RSS}^{ij} - F_{RSS})}{3} - Pe & \theta = 1 \wedge \alpha \neq \varnothing \end{cases}, \tag{C.5}$$

The SBR is the main term of the reward function due to its direct representation of the objective of performing SD. The value of SBR is defined as the ratio between the blocked and the total number of processed service requests. The design of the reward function aims to strongly penalize even a slight increase of the SBR. Therefore, the logarithm of the SBR is used in the reward function to amplify the small changes of SBR when the agent chooses not to start an SD cycle ($\alpha{=}\varnothing$, i.e., the first term of (C.5)). To limit the SD overhead, each new SD cycle and each connection reallocation are associated with a penalty, denoted by Ps and Pe, respectively. Both penalties are considered in the reward function whenever the agent initiates a new SD cycle by reallocating a connection, i.e., the second term in (C.5). The third term in (C.5) refers to the reward for connection reallocation within an SD cycle in progress. As mentioned in Sec. 2.2.1, a higher value of the RSS metric implies lower fragmentation. Hence, the agent uses the difference between the RSS metric before and after reconfiguration to evaluate the benefit of the connection reallocation. The logarithmic function is employed to guarantee that a small increment of the RSS metric yields a significant increase of the reward value. The penalty for connection reallocation is also considered. The logarithm addends in the reward function are normalized using a factor of 3 to conform to the range between zero and one. This normalization process facilitates setting the values of the penalties relative to the other components of the reward. It also helps the DRL agent to learn more efficiently by balancing the magnitudes of the reward values and preventing them from becoming too large or too small.

The penalty values in the reward function (i.e., P_s and P_e) are determined by the network operator based on the costs associated with each proactive SD cycle and reallocation, respectively. In this work, the values of the penalties are selected based on the target resulting SD overhead.

4.3 Learning Process using Deep Q-Networks

We utilize the deep Q-Networks (DQN) algorithm [36] to determine the policy for the proposed SD approach. The objective of the DQN algorithm is to learn a policy that maximizes the long-term reward by estimating the state-action values, also known as Q-values, using a DNN. These Q-values represent the expected long-term reward for each state-action pair. To approximate the Q-values, we employ an NN, which takes the network state S_t as input. The output of the NN provides the predicted state-action values for all possible actions given the input state. For training, we utilized two NNs with the same architecture. One network, called the Q-Value-Network, uses the parameter θ to estimate the state-action values $Q(S_t, A_t, \theta)$ for a given state-action pair (S_t, A_t), where S_t represents the network state at time t, and A_t represents the action taken by the agent at time t. The other network, called the Q-Target-Network, employs the parameter θ^- to determine the target Q-value. Algorithm 2 illustrates the DeepDefrag training and operation, which combines DQN training with proactive SD. In this algorithm, M represents the number of episodes, T denotes the length of each episode, γ represents the discount factor, ϵ represents the exploration rate, and C signifies the frequency of updating the target network. A detailed description of all the hyperparameters can be found in the original DQN paper [36].

Algorithm 2: DeepDefrag Algorithm: Combination of DQN algorithm and proactive spectrum defragmentation

Input: Replay memory size N, episodes M, time steps T, target update frequency C, discount factor γ

Output: Trained Deep Q-Network for spectrum defragmentation

1 Initialize replay memory D with size N;
2 Create action-value function Q with random weights θ;
3 Create target action-value function $\hat{Q}$ with weights $\theta^- = \theta$;
4 **for** *episode* $= 1$ *to* M **do**
5   Reset environment to initial state s_0;
6   **for** *time step* $t = 1$ *to* T **do**
7   Choose action a_t using ϵ-greedy policy based on Q;
8   **if** a_t *is* $< D_i, f_{ij} >$ **then**
9   Reallocate D_i to slot f_{ij}, observe reward r_t and next state s_{t+1};
10   **else**
11   Serve the next incoming service request, observe reward r_t and next state s_{t+1};
12   Store transition (s_t, a_t, r_t, s_{t+1}) in D;
13   Randomly sample a minibatch of transitions (s_i, a_i, r_i, s_{i+1}) from D;
14   Compute target values y_i:;
15   **foreach** *sample in minibatch* **do**
16   **if** $t = T - 1$ **then**
17       $y_i \leftarrow r_i$;
18   **else**
19       $y_i \leftarrow r_i + \gamma \max_{a'} \hat{Q}(s_{i+1}, a', \theta^-)$;
20   Perform gradient descent on loss:
21   $\mathcal{L}(\theta) = \frac{1}{B}\sum_i (y_i - Q(s_i, a_i, \theta))^2$;
22   **if** *step* mod $C = 0$ **then**
23   Update target network weights: $\theta^- = \theta$;

The algorithm begins with the initialization step (lines 1-3). Then, for each episode of the training process, the environment is reset, and the loop for time steps begins (lines 4-6). During the training process, the agent adopts the ϵ-greedy policy to balance exploration and exploitation. This means that the agent selects the action with the maximum Q-value with a probability of 1-ϵ, and chooses a random action with a probability of ϵ (line 7). If the agent decides to perform a reallocation, it moves the connection D_i to the starting slot related to the selected action f_{ij} (lines 8-9). Otherwise, it continues the network operation while observing the reward and the next state (lines 10-11). The agent stores the transition samples in the replay memory for training purposes (line 12). The training step takes place at the end of each episode. Samples are randomly selected from the replay memory to train the NN (line 13). The target values for each transition in the mini-batch are calculated (line 14). If the next state is terminal, the target value is set to the immediate reward r_i. Otherwise, it is calculated as the sum of the immediate reward r_i and the discounted maximum expected reward. The NN parameter θ is updated using Mini-batch Gradient Descent (line 15), while the Q-Target-Network parameter θ^- is updated with the current Q-Value-Network parameter θ every C iterations.

The training phase of the agent (lines 13–16 of Alg. 2) can be executed offline, meaning that it will not interfere with the network operation. In the predicting phase of the DQN (line 7 of Alg. 2), the trained model is utilized to predict the action for a given state. This phase is composed only of a simple DNN inference. Consequently, the time required for performing an inference becomes negligible compared to other events taking place in the network. Ideally, new experiences collected during operation are included in the memory and used to further improve the agent.

5 Simulation settings

We conduct simulations on a dynamic traffic scenario to evaluate the performance of DeepDefrag. We use the value of SBR, frequency, and volume of reconfiguration actions as performance metrics. Two network topologies are used to evaluate the DeepDefrag model: the NSFNET topology [13] with 14 nodes and 22 links, and the German topology [37] with 50 nodes and 88 links. In both topologies, we assume that each link supports 320 spectrum slots. To generate service requests, we use a Poisson process and tune the traffic load to 80 and 340 Erlang for the NSFNET and German topology, respectively. These values ensure a SBR of approximately 2% for the scenario without SD. 80% of service requests are long-lived with an average holding time of 25 time units, while the remaining 20% have an average holding time of 12.5 time units. The holding time of the connections follows an exponential distribution. The considered bit rate is 100 Gbit/s for 50%, 200 Gbit/s for 30%, and

400 Gbit/s for the remaining 20% of the service requests.

The choice of having an 80-20 split between long short-lived traffic aims at recreating a realistic traffic scenario experienced by a network operator in the Nordic countries where, within the optical layer, there exist connections that support the packet network and carry the majority of the traffic load. These connections are typically bound by long-term contracts and demonstrate consistent and stable behavior at the optical layer within the network.

We adopt BPSK, QPSK, 8-QAM, and 16-QAM modulation formats, with a spectral efficiency m of 1, 2, 3, and 4 b/Hz/s, respectively, as described in [13]. Modulation formats with higher spectrum efficiency are preferred, as long as the distance of the path is supported by the chosen modulation format. Specifically, the reach for the different modulation formats are as follows: 625 km for 16-QAM, 1250 km for 8-QAM, and 2000 km for QPSK. BPSK can be used for any path length in the adopted topologies [38]. For each request for all considered scenarios, the RMSA solution is obtained by choosing the shortest available path among five pre-computed shortest paths, and assigning the first available slots (first fit).

The performance of DeepDefrag is assessed through comparison with three heuristic algorithms denoted as older-first first-fit (OF-FF), exhaustive spectrum defragmentation (X-SD), and no spectrum defragmentation (No-SD). In the OF-FF strategy, the connections are selected according to their age, where the longest-running connections are reconfigured first, and the new spectrum is decided using the first-fit spectrum allocation scheme. This strategy is used for benchmarking purposes as it has shown excellent performance in terms of SBR [9]. OF-FF has two parameters: the SD period, which defines the number of request arrivals between two defragmentation cycles, and the number of connection reallocations per SD cycle. We evaluate the performance of OF-FF under different configurations and report on two representative settings to enable a fair comparison with DeepDefrag. The first setting has the same defragmentation overhead as DeepDefrag, enabling us to compare their performance in terms of SBR. In the second configuration, we ensure that the OF-FF has comparable levels of SBR as DeepDefrag. This enables a direct comparison of their performance in terms of SD overhead, namely the number of connection reallocations and SD cycles.

We also simulate the X-SD approach to find a (heuristic) lower bound on the SBR by reallocating an unlimited number of connections upon each connection departure and applying FF spectrum assignment to find the new slots. Note that the service blocking in this strategy occurs due to lack of resources, which cannot be avoided by any proactive defragmentation scheme. Moreover, achieving the absolute minimum SBR would require the use of optimal techniques (e.g., ILP). However, these techniques are not practical for this problem due to their complexity and scalability issues. Finally, the *No-SD* approach represents the network performance without defragmentation.

To implement the DeepDefrag scheme, we extended the Optical RL-Gym framework, which models optical networking problems related to resource management and reconfiguration as RL environments [39]. The DRL agent was trained using Stable-Baselines3 [40], an open-source implementation of DRL algorithms in Python. We trained the DRL agent using the DQN algorithm with a learning rate of $5 * 10^{-6}$, exploration rate 0.2, and a discount factor of 0.96. The NN has 5 layers with 384 neurons each. The values of DRL hyperparameters were defined through a hyperparameter analysis performed offline. Ten possible options for the oldest connections are introduced to the DRL agent.

To assess the impact of defragmentation penalties on the performance of DeepDefrag, we conduct experiments using two sets of penalty factors. The first one consists of Ps=0.8 and Pe=0.1, while the second set has Ps=0.3 and Pe=0.05. In both sets, the value of Ps is higher than Pe, reflecting the higher cost associated with initiating an SD cycle compared to a connection reallocation. The use of these two penalty sets allows us to understand the impact of SD penalties on the behavior of DeepDefrag, showing that network operators can fine-tune the penalty values based on their specific requirements, costs, and priorities.

Finally, we assess the performance of the proposed DeepDefrag approach under varying traffic load. To this end, we initiate the network operation with a load of 80 Erlang for the NSFNET topology. Subsequently, we change the load to new values: a higher load of 90 Erlang, and a lower load of 70 Erlang. This allows us to assess the agent's ability to adjust and converge to effective solutions under changing load conditions.

To train the agent, we set the episode length to 400 decision steps and perform training over 8000 episodes, which includes approximately 2 million service arrivals. It is important to note that fluctuations in the results are expected due to the inherent stochastic nature of the Poisson process. Hence,

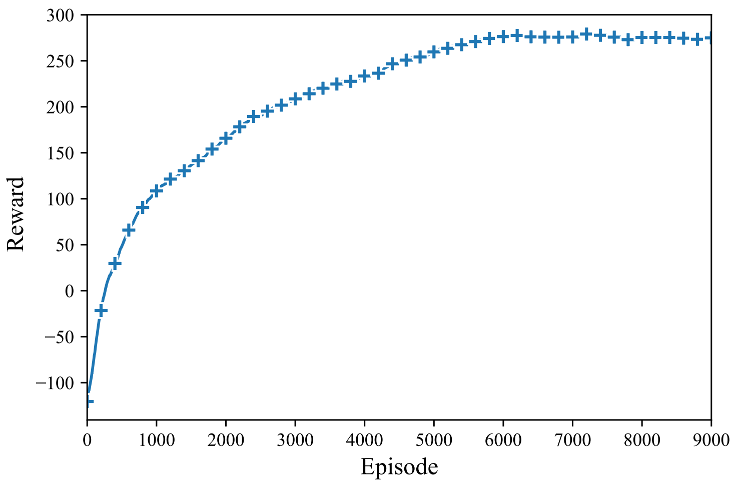

Figure 4: Episodic sum of reward values for NSFNET.

we conduct simulations of the DeepDefrag agent using 10 different seeds for the random number generator of the network environment to ensure robustness of the numerical results. We assess the performance of the DeepDefrag agent as it is trained and average the results over the last 1000 episodes for statistical purposes, followed by a calculation of the confidence interval to quantify the level of uncertainty in the results.

6 Numerical results

Figure 4 depicts the progression of the episodic sum of reward values for DeepDefrag with the penalty set (0.8, 0.1) in the NSFNET topology. The plot shows the sum of the rewards of all actions taken within an episode. The result demonstrates how DeepDefrag optimizes its policy over time, leading to higher reward values. Eventually, around episode 6,000, the agent converges to a stable value. Naturally, as discussed later in this section, in normal operating conditions, the agent will continue to be trained in order to reflect the latest network conditions.

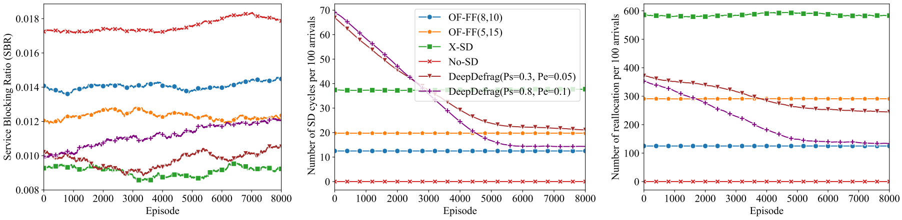

(a) Service blocking ratio (SBR) **(b)** Number of SD cycles per 100 arrivals **(c)** Number of reallocations per 100 arrivals

Figure 5: Performance of the considered spectrum defragmentation schemes for the NSFNET network topology.

Figure 5 shows the performance of the considered schemes for the NSFNET topology, indicating the advantages of DeepDefrag. As shown in Fig. 5a, the two approaches performing the best and the worst in terms of the SBR are *X-SD* and *No-SD*, respectively. *X-SD* achieves 49% lower SBR than *No-SD*, which indicates the potential gain that can be achieved by sequential proactive SD algorithms. Figures 5b and 5c depict the number of SD cycles and connection reallocations per 100 arrivals for the different strategies.

Upon convergence of the DRL agent, DeepDefrag leads to a notable SBR reduction compared to the *No-SD* scenario. With the penalty set (0.8, 0.1), DeepDefrag achieves a 32% lower SBR than *No-SD*. For the penalty set (0.3, 0.05), DeepDefrag reduces the SBR by 38.6%. The confidence interval of the results for DeepDefrag is 1.6% with a 95% confidence level. For the sake of simplicity, we select penalty configuration (0.8, 0.1) for the rest of the paper. Two different configurations are evaluated for OF-FF. The first configuration is denoted by OF-FF (5, 15), with the SD period equal to 5 connection departures, and allowing up to 15 connection reallocations per SD cycle. OF-FF (5, 15) achieves approximately the same SBR as DeepDefrag in the NSFNET topology, allowing for a comparison of their defragmentation overheads. The second configuration is denoted by OF-FF (8, 10), with the SD period equal to 8 request departures and 10 reallocations per cycle. This results in almost the same defragmentation overhead as DeepDefrag, enabling an examination of their SBR. On average, the OF-FF (8, 10) and OF-FF (5, 15) schemes yield a 20.2% and 29.4% lower SBR than *No-SD*, respectively, which aligns with the result reported by [9]. As shown in these figures, DeepDefrag has almost the same defragmentation overhead as OF-FF (8, 10), while it reduces SBR by 15.8%. The X-SD achieves 23.3% lower SBR than and DeepDefrag, but at the cost of a higher defragmentation overhead. This confirms the effectiveness of DeepDefrag in reducing the SBR by selecting appropriate actions. Next, we move our attention to the configuration when DeepDefrag and OF-FF have close SBR performance, i.e., OF-FF (5, 15). DeepDefrag triggers 14.1 SD cycles per 100 arrivals on average as depicted in Fig. 5b. This is 29.5% lower than the number of SD cycles triggered by OF-FF. As shown in Fig. 5c, DeepDefrag reallocates 132 connections per 100 request arrivals on average, which is a 56% reduction compared to OF-FF (5, 15).

The observed results illustrate how, during the training phase, the lower SBR values can be attributed to the agent's frequent execution of SD cycles and reallocation of a significant number of connections. As the agent progresses and learns to make better decisions, it finds a beneficial trade-off between the SBR and extensive reallocation, i.e., reduces the number of SD cycles and connection reallocations, while slightly increasing the SBR.

When comparing the two penalty sets, DeepDefrag with the (0.3, 0.05) configuration achieves a 10.2% lower SBR than the (0.8, 0.1) configuration. This advantage comes at the expense of a 44.2% higher number of connection reallocations and a 30% higher number of SD cycles. These results highlight the trade-offs involved in selecting penalty values for DeepDefrag. By adjusting the penalties, operators can effectively balance the reduction in SBR with the associated costs of connection reallocations and SD cycles.

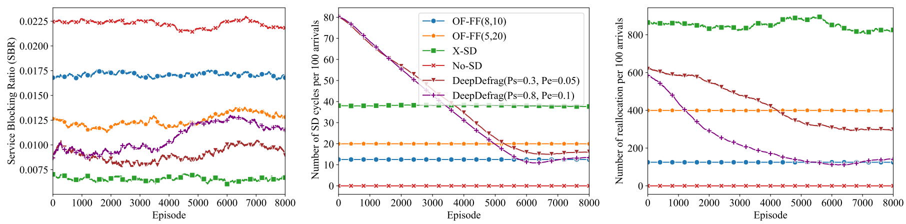

(a) Service blocking ratio (SBR) **(b)** Number of SD cycles per 100 arrivals **(c)** Number of reallocations per 100 arrivals

Figure 6: Performance of the considered spectrum defragmentation schemes for the German network topology.

Figure 6 depicts the SD performance when the considered schemes are applied in the German topology. Also for this topology, DeepDefrag, after convergence, outperforms all the benchmark SD heuristics. In this case, X-SD reduces the SBR by 69.5% compared to *No-SD* (Fig. 6a). DeepDefrag with the penalty set (0.8, 0.1) achieves 50% lower SBR than *No-SD*. Moreover, it decreases the SBR by 34.8% in comparison with OF-FF (8, 10), which has an equivalent defragmentation overhead to DeepDefrag. In addition, DeepDefrag has comparable SBR as OF-FF (5, 20), while reducing the number of SD cycles and connection reallocations by 34.1% and 75%, respectively (Figs. 6b and 6c). Similar trends for the different sets of DeepDefrag penalties are observed as in the case of the NSFNET topology, trading-off the frequency and volume of reallocations for the SBR. Examining the learning aspects depicted in the figures indicates the ability of DeepDefrag to reduce the SD overhead in terms of connection reallocations and defragmentation cycles upon 5,500 and 6000 training episodes for the NSFNET and the German topology, respectively.

The gap between *X-SD* and *No-SD* in terms of SBR is 49% and 69.5% for the German and the NSFNET topology, respectively, indicating a more prominent effect of SF in the German network under the considered traffic scenario. Hence, the ability of DeepDefrag to select appropriate actions becomes more substantial, resulting in a better overall performance in the German topology compared to the NSFNET. In summary, DeepDefrag outperforms the considered SD heuristic algorithms evaluated across all of the examined metrics. It also achieves an acceptable performance in terms of SBR compared to X-SD.

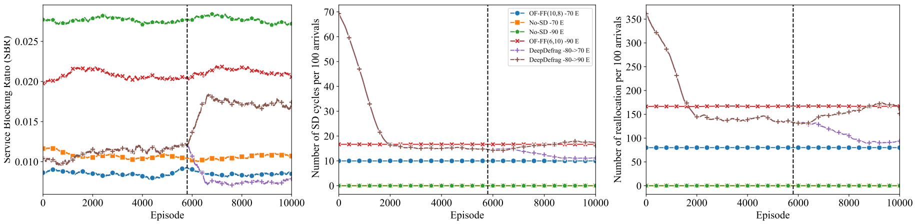

(a) Service blocking ratio (SBR) **(b)** Number of SD cycles per 100 arrivals **(c)** Number of reallocations per 100 arrivals

Figure 7: Performance of DeepDefrag for the NSFNET network topology with changing load conditions. The black dashed vertical line indicates the moment when the load changes.

Figure 7 illustrates the results for the scenario with changing load conditions in the NSFNET topology. The agent is initially trained when the network is experiencing a load of 80 Erlang. Around episode number 5,800, indicated by the black dashed vertical line, the load changes to 90 Erlang and 70 Erlang, respectively. The results demonstrate that the agent successfully adapts to both an increase and a decrease of the traffic load. To ensure a fair comparison, in this case we report the results for the configurations of the OF-FF scheme that have equivalent SD overhead as DeepDefrag. For the load of 90 Erlang, DeepDefrag outperforms the No-SD scheme by 36.7% in terms of SBR. Additionally, it exhibits an 18.2% improvement over the OF-FF (6,10) configuration. Similarly, for the load of 70 Erlang, DeepDefrag demonstrates a 28.9% performance advantage over the No-SD scheme, and a 9.5% improvement compared to the OF-FF (10,8) configuration. These findings highlight DeepDefrag's ability to adapt to acceptable solutions across varying load levels, demonstrating its effectiveness in managing spectrum resources throughout the network lifetime under different operating conditions.

7 Conclusion

In this paper, we propose a deep reinforcement learning (DRL)-based framework called DeepDefrag. The framework jointly addresses different aspects of the spectrum defragmentation (SD) problem. DeepDefrag determines when to perform SD, which connections to reallocate and in what order, and which target spectrum slots to be utilized by the reconfigured connections. DeepDefrag considers spectrum occupancy information, including three fragmentation metrics (i.e., number of cuts, Shannon entropy (SE), and root of sum of squaress (RSSs)), as input to the decision process. Simulation results show that DeepDefrag can effectively reduce the service blocking ratio (SBR) while requiring fewer SD cycles and connection reallocations compared to heuristic methods from the literature. In some cases, the SBR achieved by DeepDefrag approaches that of an exhaustive method, while incurring substantially lower overhead. Finally, simulations with varying load conditions demonstrate that DeepDefrag is able to effectively adjust to changing network conditions.

Funding

Work partially supported by Sweden's innovation agency VINNOVA, within the framework of the EUREKA cluster CELTIC-NEXT project AI-NET-PROTECT (2020-03506).

References

[1] M. Jinno, H. Takara, B. Kozicki, Y. Tsukishima, Y. Sone, and S. Matsuoka, "Spectrum-efficient and scalable elastic optical path network: Architecture, benefits, and enabling technologies," *IEEE Communications Magazine*, vol. 47, no. 11, pp. 66–73, 2009.

[2] R. Wang and B. Mukherjee, "Provisioning in elastic optical networks with non-disruptive defragmentation," *Journal of Lightwave Technology*, vol. 31, no. 15, pp. 2491–2500, 2013.

[3] Y. Yin, H. Zhang, M. Zhang, *et al.*, "Spectral and spatial 2d fragmentation-aware routing and spectrum assignment algorithms in elastic optical networks," *Journal of Optical Communications and Networking*, vol. 5, no. 10, A100–A106, 2013.

[4] W. Shi, Z. Zhu, M. Zhang, and N. Ansari, "On the effect of bandwidth fragmentation on blocking probability in elastic optical networks," *IEEE Transactions on Communications*, vol. 61, no. 7, pp. 2970–2978, 2013.

[5] B. C. Chatterjee, S. Ba, and E. Oki, "Fragmentation problems and management approaches in elastic optical networks: A survey," *IEEE Communications Surveys & Tutorials*, vol. 20, no. 1, pp. 183–210, 2017.

[6] S. Ba, B. C. Chatterjee, and E. Oki, "Defragmentation scheme based on exchanging primary and backup paths in 1+1 path protected elastic optical networks," *IEEE/ACM Transactions on Networking*, vol. 25, no. 3, pp. 1717–1731, 2017.

[7] M. Zhang, Y. Yin, R. Proietti, Z. Zhu, and S. J. B. Yoo, "Spectrum defragmentation algorithms for elastic optical networks using hitless spectrum retuning techniques," in *2013 Optical Fiber Communication Conference and Exposition and the National Fiber Optic Engineers Conference (OFC/NFOEC)*, 2013, pp. 1–3.

[8] Y. Aoki, X. Wang, P. Palacharla, *et al.*, "Dynamic and flexible photonic node architecture with shared universal transceivers supporting hitless defragmentation," in *2012 38th European Conference and Exhibition on Optical Communications*, 2012, pp. 1–3.

[9] J. Comellas, L. Vicario, and G. Junyent, "Proactive defragmentation in elastic optical networks under dynamic load conditions," *Photonic Network Communications*, vol. 36, no. 1, pp. 26–34, 2018.

[10] M. Zhang, C. You, and Z. Zhu, "On the parallelization of spectrum defragmentation reconfigurations in elastic optical networks," *IEEE/ACM Transactions on Networking*, vol. 24, no. 5, pp. 2819–2833, 2016.

[11] D. Moniz, A. Eira, A. de Sousa, and J. Pires, "On the comparative efficiency of non-disruptive defragmentation techniques in flexible-grid optical networks," *Optical Switching and Networking*, vol. 25, pp. 149–159, 2017.

[12] M. Shimoda and T. Tanaka, "Mask RSA: End-to-end reinforcement learning-based routing and spectrum assignment in elastic optical networks," in *2021 European Conference on Optical Communication (ECOC)*, 2021, pp. 1–4.

[13] X. Chen, B. Li, R. Proietti, H. Lu, Z. Zhu, and S. J. B. Yoo, "DeepRMSA: A deep reinforcement learning framework for routing, modulation and spectrum assignment in elastic optical networks," *Journal of Lightwave Technology*, vol. 37, no. 16, pp. 4155–4163, 2019.

[14] M. R. Raza, C. Natalino, P. Öhlen, L. Wosinska, and P. Monti, "Reinforcement learning for slicing in a 5G flexible RAN," *Journal of Lightwave Technology*, vol. 37, no. 20, pp. 5161–5169, 2019.

[15] E. Etezadi *et al.*, "DeepDefrag: A deep reinforcement learning framework for spectrum defragmentation," in *Proc. of GLOBECOM*, 2022, pp. 3694–3699.

[16] X. Wang, Q. Zhang, I. Kim, P. Palacharla, and M. Sekiya, "Utilization entropy for assessing resource fragmentation in optical networks," in *Optical Fiber Communication Conference*, Optica Publishing Group, 2012, OTh1A–2.

[17] D. Amar, E. Le Rouzic, N. Brochier, J.-L. Auge, C. Lepers, and N. Perrot, "Spectrum fragmentation issue in flexible optical networks: Analysis and good practices," *Photonic Network Communications*, vol. 29, pp. 230–243, 2015.

[18] X. Yu, J. Zhang, Y. Zhao, *et al.*, "Spectrum compactness based defragmentation in flexible bandwidth optical networks," in *OFC/NFOEC*, IEEE, 2012, pp. 1–3.

[19] Y. Takita, K. Tajima, T. Hashiguchi, and T. Katagiri, "Wavelength defragmentation with minimum optical path disruptions for seamless service migration," in *2016 Optical Fiber Communications Conference and Exhibition (OFC)*, IEEE, 2016, pp. 1–3.

[20] P. Lechowicz, M. Tornatore, A. Włodarczyk, and K. Walkowiak, "Fragmentation metrics and fragmentation-aware algorithm for spectrally/spatially flexible optical networks," *Journal of Optical Communications and Networking*, vol. 12, no. 5, pp. 133–145, 2020.

[21] Y. Yin, M. Zhang, Z. Zhu, and S. B. Yoo, "Fragmentation-aware routing, modulation and spectrum assignment algorithms in elastic optical networks," in *2013 Optical Fiber Communication Conference and Exposition and the National Fiber Optic Engineers Conference (OFC/NFOEC)*, IEEE, 2013, pp. 1–3.

[22] P. Wright, M. C. Parker, and A. Lord, "Minimum- and maximum-entropy routing and spectrum assignment for flexgrid elastic optical networking [invited]," *Journal of Optical Communications and Networking*, vol. 7, no. 1, A66–A72, 2015.

[23] N. T. Khai, R. Romero Reyes, and T. Bauschert, "Spectrum defragmentation with improved lightpath migration scheme in flex-grid networks," in *2021 International Conference on Optical Network Design and Modeling (ONDM)*, 2021, pp. 1–6.

[24] M. Zhang, Y. Yin, R. Proietti, Z. Zhu, and S. B. Yoo, "Spectrum defragmentation algorithms for elastic optical networks using hitless spectrum retuning techniques," in *2013 Optical Fiber Communication Conference and Exposition and the National Fiber Optic Engineers Conference (OFC/NFOEC)*, IEEE, 2013, pp. 1–3.

[25] S. Fernández-Martínez, B. Baran, and D. P. Pinto-Roa, "Spectrum defragmentation algorithms in elastic optical networks," *Optical Switching and Networking*, vol. 34, pp. 10–22, 2019.

[26] S. K. Singh and A. Jukan, "Efficient spectrum defragmentation with holding-time awareness in elastic optical networks," *Journal of Optical Communications and Networking*, vol. 9, no. 3, B78–B89, 2017.

[27] S. Selvakumar and S. Manivannan, "A spectrum defragmentation algorithm using jellyfish optimization technique in elastic optical network (eon)," *Wireless Personal Communications*, pp. 1–19, 2021.

[28] S. Trindade and N. L. da Fonseca, "Machine learning for spectrum defragmentation in space-division multiplexing elastic optical networks," *IEEE Network*, vol. 35, no. 1, pp. 326–332, 2021.

[29] Y. Xiong, Y. Yang, Y. Ye, and G. N. Rouskas, "A machine learning approach to mitigating fragmentation and crosstalk in space division multiplexing elastic optical networks," *Optical Fiber Technology*, 2019.

[30] R. K. Jana, B. C. Chatterjee, A. P. Singh, *et al.*, "Machine learning-assisted nonlinear-impairment-aware proactive defragmentation for c+l band elastic optical networks," *Journal of Optical Communications and Networking*, vol. 14, no. 3, pp. 56–68, 2022.

[31] R. Romero Reyes and T. Bauschert, "Towards DRL-based routing and spectrum assignment in optical networks: Lessons to be learned from Markov decision processes," in *IEEE Latin-American Conference on Communications (LATINCOM)*, 2021, pp. 1–6.

[32] N. D. Cicco, E. F. Mercan, O. Karandin, *et al.*, "On deep reinforcement learning for static routing and wavelength assignment," *IEEE Journal of Selected Topics in Quantum Electronics*, vol. 28, no. 4, pp. 1–12, 2022.

[33] N. E. D. El Sheikh, E. Paz, J. Pinto, and A. Beghelli, "Multi-band provisioning in dynamic elastic optical networks: A comparative study of a heuristic and a deep reinforcement learning approach," in *2021 International Conference on Optical Network Design and Modeling (ONDM)*, IEEE, 2021, pp. 1–3.

[34] X. Luo, C. Shi, L. Wang, X. Chen, Y. Li, and T. Yang, "Leveraging double-agent-based deep reinforcement learning to global optimization of elastic optical networks with enhanced survivability," *Optics express*, vol. 27, no. 6, pp. 7896–7911, 2019.

[35] R. Li, R. Gu, W. Jin, and Y. Ji, "Learning-based cognitive hitless spectrum defragmentation for dynamic provisioning in elastic optical networks," *IEEE Communications Letters*, vol. 25, no. 5, pp. 1600–1604, 2021.

[36] V. Mnih, K. Kavukcuoglu, D. Silver, *et al.*, *Playing atari with deep reinforcement learning*, 2013.

[37] R. Carpa, M. D. de ASSUNÇÃO, O. Glück, L. Lefèvre, and J.-C. Mignot, "Responsive algorithms for handling load surges and switching links on in green networks," in *IEEE International Conference on Communications (ICC)*, 2016, pp. 1–7.

[38] B. Kozicki, H. Takara, Y. Sone, A. Watanabe, and M. Jinno, "Distance-adaptive spectrum allocation in elastic optical path network (slice) with bit per symbol adjustment," in *Conference on Optical Fiber Communication (OFC/NFOEC), collocated National Fiber Optic Engineers Conference*, 2010, pp. 1–3.

[39] C. Natalino and P. Monti, "The Optical RL-Gym: An open-source toolkit for applying reinforcement learning in optical networks," in *22nd International Conference on Transparent Optical Networks (ICTON)*, 2020.

[40] A. Raffin, A. Hill, A. Gleave, A. Kanervisto, M. Ernestus, and N. Dormann, "Stable-Baselines3: Reliable reinforcement learning implementations," *Journal of Machine Learning Research*, vol. 22, no. 268, pp. 1–8, 2021.

PAPER D

Demonstration of DRL-based intelligent spectrum management over a T-API-enabled optical network digital twin

Ehsan Etezadi, Carlos Natalino, Vignesh Karunakaran, Renzo Diaz, Anders Lindgren, Stefan Melin, Achim Autenrieth, Lena Wosinska, Paolo Monti, Marija Furdek

49th European Conference on Optical Communications (ECOC), Glasgow, Scotland, Oct. 2023

The layout has been revised.

Abstract

This demonstration showcases the applicability and benefits of a deep reinforcement learning (DRL) agent for spectrum defragmentation in a realistic deployment. This is achieved by integrating the DRL agent with the operations of a carrier-grade optical network digital twin via standard T-API messages. © 2023 The Author(s)

1 Introduction

One of the main challenges in dynamic elastic optical networks (EONs) is spectrum fragmentation (SF) which stems from the discrepancy between the incoming connection requests and the available spectral gaps. SF leads to inefficient use of the spectrum, degrading the performance of EON in terms of SBR[1]. SD is a way to consolidate the spectrum usage by reconfiguring a subset of connections, thus reducing gaps unsuitable for incoming connectivity services. Numerous SD approaches rely on, e.g., threshold-based heuristic algorithms[2] or integer linear programming models[3], typically aimed at SBR minimisation. Such methods may require bespoke threshold configuration or take long to find a solution, which limits their flexibility and applicability in dynamic service provisioning scenarios.

Intelligent and adaptable techniques, such as those based on machine learning (ML), are needed to meet the network operators' quest for efficient and automated network management. DeepDefrag[4], a recently proposed SD framework based on DRL, has been shown to outperform existing deterministic algorithms in SBR minimisation. DeepDefrag performs proactive SD by deciding on the reconfiguration timing, the concerned subset of connections, and their target spectrum.

Integrating ML-based techniques in real-world optical network deployments is challenging due to, among other, potential mismatch between the data these techniques require and information made available by vendor-specific management tools. Optical network disaggregation addresses this issue by defining, among other elements, a set of standard application programming interfaces (APIs) that allow operators to interact with network elements[5]. Transport API (T-API), an example of such standards, supports a hierarchical software-defined networking (SDN) architecture that fits multi-vendor/multi-domain scenarios. T-API is regarded as a promising standard for different use cases, including connectivity service creation over dense wavelength-division multiplexing (DWDM) networks[6] and enabling quantum encryption of optical end-to-end services[7]. However, so far, the potential benefits of SD techniques have not been validated in T-API systems, especially those using carrier-grade T-API implementations. Such implementations can be provided by, e.g., a digital twin[8], which mirrors the behaviour of real devices, allowing a realistic and real-time system performance evaluation without the prohibitive overhead of testing on real devices.

In this demonstration, we develop a new defragmentation module that uses standard T-API messages to realise SD decisions taken by a DRL agent, i.e., DeepDefrag. We demonstrate the module's capabilities through a dashboard that enables the audience to parameterise network operation settings, view the fragmented network state, observe the DRL-based SD decisions, and inspect their realisation over a carrier-grade digital twin. The DRL agent intelligently decides when to trigger defragmentation, selects the connections and the order of their reallocation, and finds the target spectrum slots.

2 Workflow

Figure 1 illustrates the workflow of the proposed demonstration, including the message exchange between the SD module and the T-API-enabled digital twin. In the following, we describe each message, highlighting the associated T-API use case[9].

In phase *1*, the SD module periodically requests information about existing connectivity services (including their unique identifiers) and topology from the digital twin (use cases 0a and 0b). The defragmentation module uses this information as input to the DRL agent, which, based on the current network state, decides whether to initiate an SD cycle or not.

Phase *2* starts when the DRL agent initiates an SD cycle. The DRL agent iteratively selects a connectivity service for reallocation and the target spectrum. Note that the path does not change during defragmentation. This process is repeated until the DRL agent stops the SD cycle.

Connectivity services are reallocated following a *break-before-make* approach. The service selected for reallocation is removed (use case 10), after which it is

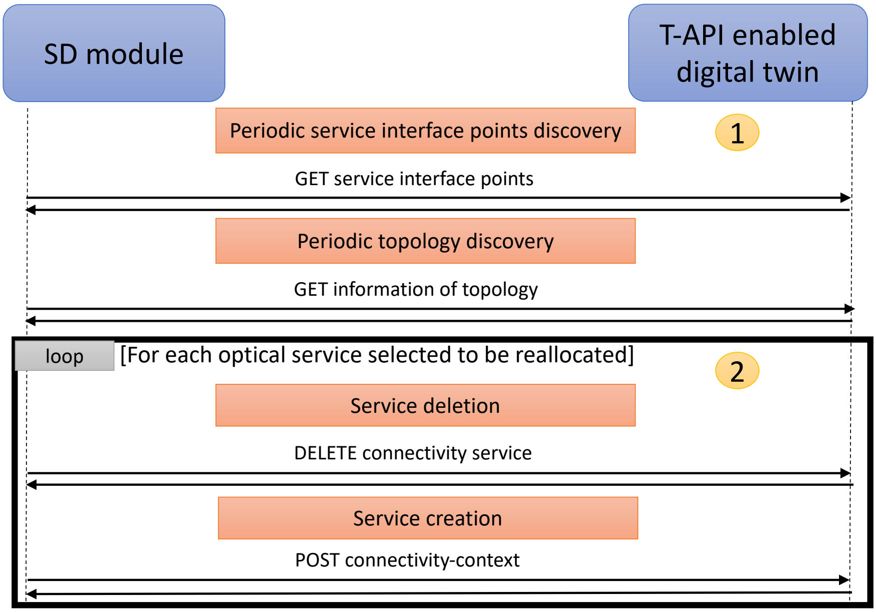

Figure 1: Communication between the spectrum defragmentation (SD) module and the digital twin.

re-established by specifying the nodes, links and target spectrum slots. The process of establishing a connectivity service, which traverses specific nodes or links and occupies specific spectrum slots, is defined in use cases 2c, 3a, and 3b, respectively. The *break-before-make* approach allows our defragmentation module to take advantage of defragmentation solutions that overlap with the spectrum currently used by the service under reconfiguration.

3 Demonstration implementation

Figure 2 illustrates the deployment adopted in this demonstration. The defragmentation module is implemented specifically for this demonstration using Python. It uses the Optical RL-Gym[10] to generate connectivity service requests following a Poisson process. The aim is to obtain a representation of the network state resulting from long-term operation (i.e., steady state represen-

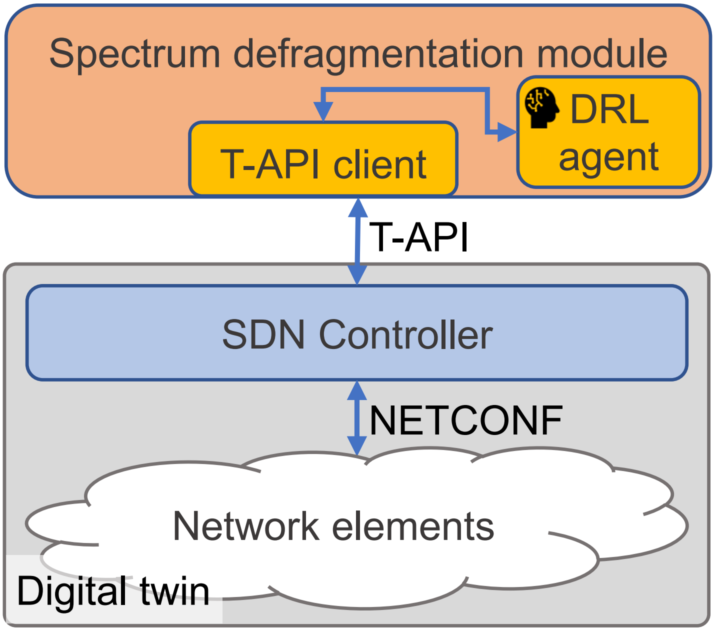

Figure 2: Demonstrator architecture.

tation). The DeepDefrag[4] DRL agent making the defragmentation decisions during the demonstration is trained separately beforehand for practical purposes.

The digital twin of the optical network is implemented by mirroring each optical network element instance in its digital form, i.e., using the same operating system running over virtual machines. The deployed digital twin is controlled by a production-grade SDN domain controller, supporting T-API in the northbound and NETCONF in the southbound interface. The interaction between the defragmentation module and the digital twin uses the T-API specification version 2.1[9]. The defragmentation module and dashboard run on the demonstrator computer connected to the digital twin located at a remote lab through a secure channel.

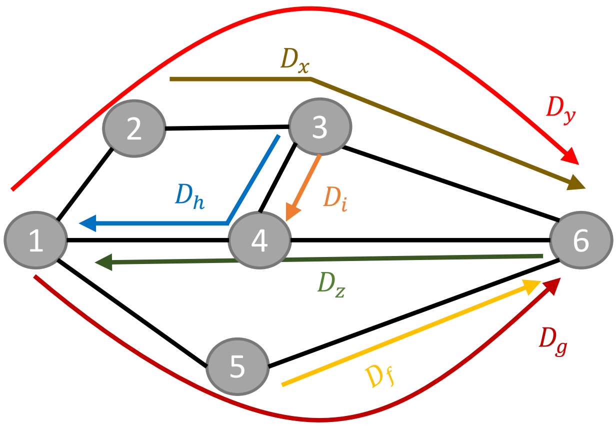

Figure 3: Simple network example with 7 connectivity services.

4 Demonstration storyline

The demonstration begins with an empty network and fully unassigned spectrum. In the first part, the demo focuses on simulating a fragmented network state. The audience can select the parameters for generating the connectivity service requests (e.g., inter-arrival time, holding time, bandwidth) in addition to the simulation run time. The fragmented network state at the end of the simulation is consolidated into the digital twin. Fig. 3 illustrates a simple network topology and a snapshot of active connectivity services. Fig. 4(a) shows the fragmented spectrum resulting from the simulated arrivals and departures consolidated into the digital twin.

The second part of the demo consists in invoking the DeepDefrag agent and graphically showing its decisions about services selected for reallocation and their target spectrum. Fig. 4(b) illustrates a hypothetical decision where the agent, based on the spectrum state from Fig. 4(a), decides to reallocate connectivity service D_y from slot 12 to 6.

The audience can inspect the execution of individual decisions within a defragmentation cycle or advance to the end of the cycle. Fig. 4(c) illustrates the spectrum state at the end of a hypothetical defragmentation cycle that

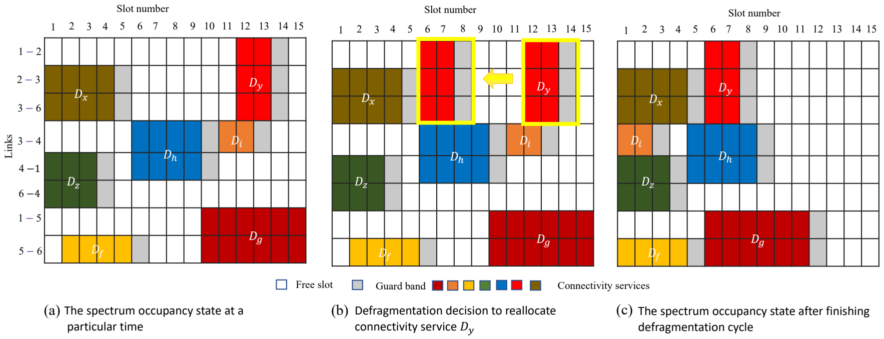

Figure 4: The spectrum grid shown on the dashboard at different stages.

started with the state in Fig. 4(a). Note that 5 out of 7 connectivity services were reconfigured, representing an aggressive defragmentation cycle. For the demo, a more realistic number of slots is set up, and the number of active services will depend on the parameters set by the audience (e.g., inter-arrival time, holding time, and simulation time).

In addition to the spectrum visualisation illustrated in Fig. 4, various spectrum fragmentation metrics (e.g., number of cut [11], and root of sum of squares [12]) that vary with time are displayed to the audience, not included here due to space constraints. The impact of provisioning, departures, and defragmentation of connectivity services on the variations of these metrics is presented to the audience. The audience can also inspect the messages exchanged by the module and the digital twin, revealing how T-API can be leveraged to implement the proposed approach.

5 Innovation

This demonstration is the first to take advantage of DRL to perform intelligent spectrum management over a T-API-enabled carrier-grade optical network deployment, exemplified here by a digital twin. The demonstration serves not only as a proof-of-concept of defragmentation operations over T-API, but also showcases a dashboard where the audience configures connectivity service parameters, and observes how the DRL agent intelligently defragments the spectrum. This work can foster discussions and spark interest in the ECOC community regarding the real-world implementation of intelligent spectrum management strategies in optical networks and their realisation using currently available interfaces.

6 Conclusions

This paper presents the first experimental and interactive demonstration of a proactive spectrum defragmentation module for elastic optical networks using the **ONF!** (**ONF!**) Transport API standard over a digital twin. The algorithm uses the merits of deep reinforcement learning to find the best set of actions based on the network condition.

7 Acknowledgements

Work partially supported by Sweden's innovation agency VINNOVA, within the framework of the EUREKA cluster CELTIC-NEXT project AI-NET-PROTECT (2020-03506), and Vetenskapsrådet (2019-05008).

References

[1] W. Shi, Z. Zhu, M. Zhang, and N. Ansari, "On the effect of bandwidth fragmentation on blocking probability in elastic optical networks," *IEEE Transactions on Communications*, vol. 61, no. 7, pp. 2970–2978, 2013.

[2] J. Comellas, L. Vicario, and G. Junyent, "Proactive defragmentation in elastic optical networks under dynamic load conditions," *Photonic Network Communications*, vol. 36, no. 1, pp. 26–34, 2018.

[3] M. Zhang, C. You, and Z. Zhu, "On the parallelization of spectrum defragmentation reconfigurations in elastic optical networks," *IEEE/ACM Transactions on Networking*, vol. 24, no. 5, pp. 2819–2833, 2016.

[4] E. Etezadi *et al.*, "DeepDefrag: A deep reinforcement learning framework for spectrum defragmentation," in *Proc. of GLOBECOM*, 2022, pp. 3694–3699.

[5] F. Paolucci and A. Sgambelluri, "Telemetry in disaggregated optical networks," in *International Conference on Optical Network Design and Modeling (ONDM)*, 2020, pp. 1–3.

[6] V. Lopez, R. Vilalta, V. Uceda, *et al.*, "Transport API: A solution for SDN in carriers networks," in *European Conference on Optical Communication (ECOC)*, 2016, pp. 1–3.

[7] V. López, A. Gomez, A. Aguado, *et al.*, "Extension of the ONF transport API to enable quantum encryption in end-to-end services," in *European Conference on Optical Communication (ECOC)*, 2019.

[8] D. Jones, C. Snider, A. Nassehi, J. Yon, and B. Hicks, "Characterising the digital twin: A systematic literature review," *CIRP Journal of Manufacturing Science and Technology*, vol. 29, pp. 36–52, 2020.

[9] ONF, *Tr-547, functional requirements for transport api*, https://opennetworking.org, Jul. 2020.

[10] C. Natalino and P. Monti, "The Optical RL-Gym: An open-source toolkit for applying reinforcement learning in optical networks," in *International Conference on Transparent Optical Networks (ICTON)*, 2020.

[11] Y. Yin, M. Zhang, Z. Zhu, and S. B. Yoo, "Fragmentation-aware routing, modulation and spectrum assignment algorithms in elastic optical networks," in *2013 Optical Fiber Communication Conference and Exposition and the National Fiber Optic Engineers Conference (OFC/NFOEC)*, IEEE, 2013, pp. 1–3.

[12] P. Lechowicz, M. Tornatore, A. Włodarczyk, and K. Walkowiak, "Fragmentation metrics and fragmentation-aware algorithm for spectrally/spatially flexible optical networks," *Journal of Optical Communications and Networking*, vol. 12, no. 5, pp. 133–145, 2020.

PAPER E

Joint Fragmentation- and QoT-Aware RBMSA in Dynamic Multi-Band Elastic Optical Networks

Ehsan Etezadi, Farhad Arpanaei, Carlos Natalino, Lena Wosinska, Erik Agrell, Paolo Monti, David Larrabeiti, Marija Furdek

24th International Conference on Transparent Optical Networks (ICTON), Bari, Italy, Jul. 2024

The layout has been revised.

Abstract

Efficient utilization of fiber bandwidth is essential for reducing the total cost of ownership associated with deploying new fiber plants. One of the challenges in dynamic multi-band elastic optical networks (DMB-EONs) is spectrum fragmentation. It stems from the wavelength continuity constraint, the dynamic arrival and departure of service requests, and variations in quality of transmission (QoT) across the wavelength division multiplexing (WDM) channels. This study introduces a QoT-aware algorithm for routing, band, modulation format and spectrum assignment (RBMSA) that considers the spectrum fragmentation along each channel to reduce SBR in DMB-EONs. Simulation results indicate that the proposed algorithm reduces SBR by up to 33.2% compared to a reference RBMSA algorithm that considers only QoT at the cost of increasing the average path length by 4.4%.

1 Introduction

Traditional C-band elastic optical networks (EONs) face challenges in keeping pace with the data traffic surge triggered by the proliferation of high-bit-rate applications like video streaming, cloud computing, and internet of thing (IoT) devices [1]. Dynamic multi-band elastic optical network (DMB-EON) provide a cost-effective solution to enhance data transmission capacity by efficiently utilizing multiple wavelength bands across the optical spectrum, i.e., the L, S, E, O, and U bands [2].

One of the crucial challenges in EON is spectrum fragmentation (SF), where spectrum resources become divided into small, non-continuous, and non-contiguous idle chunks over the links due to the dynamic nature of service demands and wavelength availability [3]. SF can lead to inefficient use of network capacity and increased blocking probability for incoming service requests. SF-aware algorithms proactively utilize information on how spectrum resources are used to reduce the number of blocked service requests [4].

Moreover, the quality of transmission (QoT) of an optical connection (i.e., a lightpath (LP)) varies across different channels due to the inter-channel stimulated Raman scattering (ISRS) phenomenon, which results in power depletion from shorter to longer wavelengths in wavelength division multiplexing (WDM) systems using resources outside the C-band [5]. ISRS, together with the dynamic behavior of service requests with varying capacity requirements and the wavelength continuity constraint increases the SF in the network. Hence, the joint SF- and QoT-aware routing, band, modulation format and spectrum assignment (RBMSA) algorithm is crucial for DMB-EONs. The [6] uses Q-learning to address fragmentation and impairment-aware routing, modulation and spectrum assignment (RMSA) in C+L band elastic optical networks. In this paper, for the first time, we propose a heuristic algorithm for the spectrum fragmentation- and QoT-aware (SFQA) RBMSA for C+L+S-band DMB-EONs. The proposed heuristic algorithm considers two different SF metrics and the generalized signal to noise ratio (GSNR) level of the channels available along different candidate paths. We conduct a comprehensive performance evaluation of the proposed algorithm and compare it to other heuristic algorithms from the literature, demonstrating that the SFQA algorithm outperforms the ones that consider only the QoT of the channels in the terms of service blocking ratio (SBR).

2 System Model and Physical Layer Assumptions

We consider a DMB-EON scenario in which service requests arrive and depart throughout the network's lifetime. Transmission is possible in multiple bands, utilizing pre-defined channels, each comprising six spectrum slots. For each service request, we must determine a path from the source to the destination node and a set of channels along that path that collectively meet the requested bit rate. Different channels may be allocated for the same service request, but they must all follow the same path. Additionally, the continuity constraint dictates that the channels assigned to a particular path must be the same across all links along the chosen path.

We assume that nodes are equipped with C+L+S-band bit-rate variable transponders (BVTs) and reconfigurable optical add-drop multiplexers (ROADMs). A BVTs utilizes flexible modulation formats, soft decision forward error correction, and variable bit rates [7]. The in-line amplifier sites are equipped with C-band erbium-doped fiber amplifiers (EDFA) for the C-band channels, L-band EDFAs for the L-band channels, and thulium doped fiber amplifier (TDFA) for the S-band. The amplified spontaneous emission (ASE)-shaped noise is considered for the idle channels to guarantee the power profile consistency [8], [9]. Moreover, the in-line amplifier sites are equipped with the digital gain equalizers (DGEs) to have the optimal launch power for each span based on the hyper-accelerated power optimization strategy proposed in [10].

Regarding the GSNR estimation, we apply a Gaussian noise (GN)/enhanced GN semi-closed form model to estimate the non-linear interference (NLI) noise power, including the Kerr effects and ISRS [11], [12]. This model was validated through field trials experiments [13]. According to the incoherent GN model for uncompensated optical transmission links [14], the end-to-end GSNR for a LP on channel i can be derived as follows:

$$GSNR^i_{\text{LP}}|_{\text{dB}} = 10\log_{10}\left[\left(OSNR^{-1}_{\text{ASE}}+SNR^{-1}_{\text{NLI}}+SNR^{-1}_{\text{TRx}}\right)^{-1}\right]-\sigma_{\text{Flt}}|_{\text{dB}}-\sigma_{\text{Ag}}|_{\text{dB}}, \tag{E.1}$$

where $OSNR_{\text{ASE}} = \Sigma_{s\in S} P^{s+1,i}_{\text{tx}}/P^{s,i}_{\text{ASE}}$ and $SNR_{\text{NLI}} = \Sigma_{s\in S} P^{s+1,i}_{\text{tx}}/P^{s,i}_{\text{NLI}}$. Moreover, $P^{s+1,i}_{\text{tx}}$ is the launch power at the beginning of span $s+1$, $P^{s,i}_{\text{ASE}} = n_{\text{F}} h f^i (G^{s,i}-1) R_{\text{ch}}$ is noise power caused by the doped fiber amplifier (DFA) equipped with the DGE, and the NLI noise power ($P^{s,i}_{\text{NLI}}$) is calculated from (2) in [11]. Moreover, n_{F}, h, f^i, $G^{s,i} = P^{s+1,i}_{\text{tx}}/P^{s,i}_{\text{rx}}$, S, and R_{ch} are the noise figure of DFA, the Planck constant, channel frequency, center frequency of the spectrum, DFA gain, set of spans, and channel symbol rate, respectively. $P^{s,i}_{\text{rx}}$ is the received power at the end of span s. SNR_{TRx}, σ_{Flt}, σ_{Ag} are the transceiver signal-to-noise ratio (SNR), SNR penalty due to wavelength selective switches filtering, and SNR margin due to the ageing. Hence, the GSNR for all potential connections from arbitrary sources to destinations in the network can be computed. Subsequently, the modulation format profiles of the K shortest path-channel pairs are pre-calculated, employing GSNR thresholds for each modulation format as defined in the literature [15].

3 Proposed Spectrum Fragmentation- and QoT-Aware (SFQA) RBMSA

Various metrics have been introduced in the literature to measure SF in EONs, aiding network operators in monitoring and optimizing the utilization of optical spectrum resources [16]. Our proposed fragmentation-aware method uti-

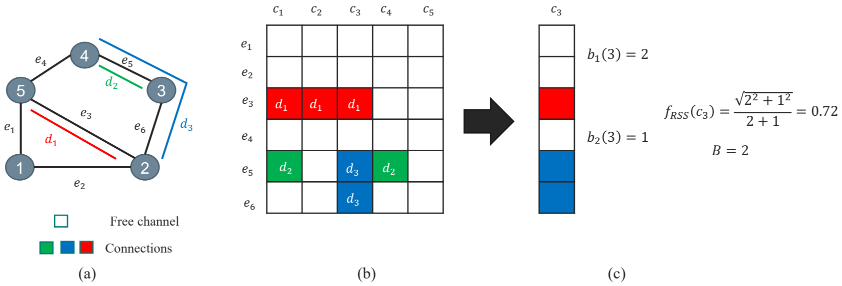

Figure 1: An example with a subset of six network links supporting three services (a). The spectrum occupancy state (b). Calculation of the RSS metric value for channel 3 (c).

lizes two SF metrics that specifically consider fragmentation in the channels, i.e., number of cuts (NoC) and root of sum of squares (RSS). To illustrate how these metrics are calculated, Fig. 1 presents a snapshot of a simple network example with five nodes and six links, with each link having a capacity of 5 channels. The figure illustrates the current state of the network with three established services, denoted as d_1 to d_3. The spectrum allocation of each link is shown in Fig. 1b. The notation includes the following parameters: e is the index of a link, c is the index of a channel, b_i is the size of the i^{th} free block, and B is the number of free blocks.

$$f_{RSS}(c) = \frac{\sqrt{\sum_{i=1}^{B} (b_i(c))^2}}{\sum_{i=1}^{B} b_i(c)} \tag{E.2}$$

Figure 1c illustrates the value for the RSS metric for the channel c_3 as defined in (E.2). To determine the value of NoC for each channel, an assessment of the state of all links within the designated channel is conducted. The NoC for a link with respect to a given channel corresponds to the instances where the state of the link is different from the state of its adjacent links within the same channel. The state of a link refers to whether it is occupied or unoccupied. In the example in Fig. 1b, link e_5 uses channel c_3. Looking at its neighbors we see that links e_4 is not using c_3 while e_6 does. So, there is a cut between links e_4 and e_5, and the NoC for link e_5 with respect to channel c_3 is 1. The NoC value for all the links with respect to c_3 can be calculated analogously. The value of NoC across the network for a given channel is equal to the summation of the NoC value of all the links, i.e., 10 with respect to c_3 in the example.

Algorithm 3: The SFQA algorithm

Input: d, P, C, MFT, COM, $T \in [RSS, NoC]$,
Output: C_s
$C_s \leftarrow \varnothing$; `// channels selected for each service request`
for *each* p *in* P **do**
  for *each* c *in* C **do**
    if c *is free on* p *by checking* COM **then**
      $M(p,c) \leftarrow$ get modulation level using MFT
      if T *is* RSS **then**
        $FS(p,c) \leftarrow F_{established}(p,c) - F_{current}(p,c)$
      else if T *is* NoC **then**
        $FS(p,c) \leftarrow F_{current}(p,c) - F_{established}(p,c)$
$P_{sorted} \leftarrow$ sort the paths P based on best $M(p,c)$ of their channels, and if two paths have the same best modulation format of their channels, sort based on the best $FS(p,c)$ of their channels
$br \leftarrow$ the bit rate of d
for *each* p *in* P_{sorted} **do**
  $C_{sorted} \leftarrow$ sort the channels on path p based on best $M(p,c)$, and if two channels have the same best modulation format, sort based on the best $FS(p,c)$
  $r \leftarrow br$
  for *each* c *in* C_{sorted} **do**
    C_s appends the channel c
    $r \leftarrow r - 100 * M(p,c)$
    if $r < 0$ **then**
      return C_s
  $C_s \leftarrow \varnothing$
return C_s

The pseudo-code of the SFQA algorithm for RBMSA of a service request is given in Algorithm 3. The basic intuition of this approach is to optimize the selection of paths and channels for service requests based on the available modulation format options and the fragmentation metric targets. The algorithm receives as input the service request d, the set of candidate paths between the source and the destination of d as P, the complete set of channels that can be used across all frequency bands C, pre-computed modulation format tables for all paths and channels MFT, the channel occupancy matrix COM, and the desired fragmentation metric, denoted as T. The algorithm outputs a list of selected channels whose combined bit rate satisfies the requested bit rate; an empty list signifies that the service request is blocked.

The algorithm comprises two parts. The first part involves computing the fragmentation score (FS) for all potential paths and channels available for the service request. Meanwhile, the second part focuses on selecting the path and corresponding channels based on the calculated FS. Upon the arrival of the service request d, the algorithm is triggered and evaluates all candidate paths between the source and destination nodes. For each path, it assesses the free channels and retrieves their respective modulation formats, storing them in $M(p, c)$ (lines 2–5). Subsequently, it calculates the FS for each channel, considering a hypothetical scenario where the channel is selected to establish the service. This involves computing the difference between the SF value in the current spectrum state ($F_{current}$) and the hypothetical SF value ($F_{established}$) assuming the service is hypothetically established on the channel (line 6–9). If the metric of interest is RSS, the $F_{current}$ and $F_{established}$ are computed using (E.2). If NoC is considered, the $F_{current}$ and $F_{established}$ refer to the two corresponding values of NoC for channel c.

The second part of the algorithm aims to find the best path for the service request. The paths are sorted based on the best modulation format of their channels. If two paths have the same best modulation format, the FS is used to sort them (line 10). The algorithm proceeds by iteratively examining each path in P_{sorted} (line 12) and sorting its available channels according to their modulation format. If multiple channels exhibit identical modulation formats, the algorithm prioritizes them based on their FSs (line 13). Finally, the algorithm iterates through the sorted channels, appending each channel to the list of selected channels, and evaluating the residual bit rate r by considering the channel modulation format and the service request bit rate (line 16–17).

However, there is a chance that the selected path does not have sufficient channels to support the full bit rate requested. In such cases, the selected channels are reset, and the algorithm proceeds to examine another path (line 20). If none of the paths contain enough channels to accommodate the request, the algorithm returns C_s with an empty value, indicating that the service d is blocked.

4 Simulation Settings and Results

This paper focuses on C+L+S-band EONs, where an aggregate bandwidth of 20 THz (6+6+8) is divided into 268 channels, each one with 75 GHz (6 * 12.5 GHz), considering a 400 GHz gap between adjacent bands. The simulations are conducted on the Japanese network topology with 14 nodes, 22 links [17], and a maximum span length of 80 km. Six modulation formats are evaluated, ranging from PM-BPSK to PM-64QAM at 64 Gbaud. Each channel can support bit rates spanning from 100 to 600 Gb/s when employing PM-BPSK and PM-64QAM, respectively. EDFAs with noise figures of 4.5 dB and 5 dB are employed for the C- and L-bands, respectively. A TDFA with a noise figure of 6 dB is utilized for the S-band. Standard single mode fiber with a zero-water peak is assumed, and spectrum continuity is enforced for channel assignment along a given path. A dynamic scenario is considered where the service requests are generated using a Poisson process, and an exponential distribution is assumed for the holding time of the services, with an average of 25 time units. The offered traffic load values are adjusted to achieve approximately 0.01% to 1% SBR for the proposed algorithms. The bit rate for service requests is selected randomly between 50 Gb/s and 600 Gb/s with a granularity of 50 Gb/s. Two million service requests are simulated, with the *SFQA* algorithm executed for each service request. The value of K is set to 5. The proposed algorithm is developed in the Optical RL-Gym framework [18].

Two versions of the proposed heuristic algorithm are analyzed depending on the SF metric used: the one that uses the NoC metric is referred to as *SFQA-Cut*, and the one that uses the RSS metric is called *SFQA-RSS*. To evaluate the performance of the proposed algorithm, a comparison is made with two heuristic algorithms, namely *BM-SP*, and *SP-BM*. *BM-SP* selects a path with the best modulation format across its channels, favoring shorter paths in case of a tie in terms of best modulation format. Conversely, *SP-BM* favors path length minimization over modulation format efficiency. It always selects the shortest path first and then identifies the channel with the best modulation that is possible along the chosen path. Note that in all approaches, when confronted with identical modulation formats or fragmentation metrics for the channels along the same path, preference is given to the channel with the lowest frequency.

Figure 2 depicts the performance of the considered strategies as a function of

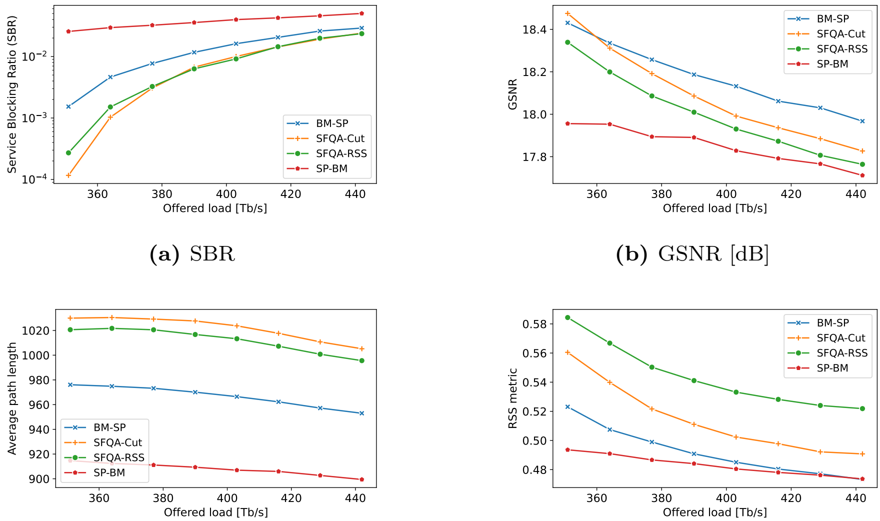

(a) SBR

(b) GSNR [dB]

(c) Average path length [km]

(d) RSS metric

Figure 2: Performance of the RBMSA schemes for Japanese topology.

the offered load. The *SFQA* algorithm demonstrates superior performance in terms of SBR as shown in Fig. 2a. More specifically, *SFQA-RSS* slightly outperforms *SFQA-Cut* and surpasses *BM-SP* and *SP-BM* algorithms by 33.2% and 74% on average across all loads, respectively. This highlights the advantages of incorporating occupancy state information into the path and the channel selection processes. This observation is further supported by Fig. 2b, illustrating the in GSNR levels across different scenarios. While the GSNR level of *BM-SP* surpasses the one of *SFQA*, its SBR performance suffers due to its lack of consideration for SF metrics. However, as can be seen in Fig. 2c, the benefit of *SFQA* in terms of SBR come at a cost of longer paths. More specifically, the *SFQA-RSS* algorithm exhibits (on average) paths 4.4% and 10.2 % longer than the ones from obtained with the *BM-SP* and *SP-BM* algorithms. To obtain a deeper insight into the network performance, Fig. 2d presents the network RSS metric values for different algorithms, The analysis shows that the network with greater fragmentation (lower RSS values) tend to experience higher SBR. Furthermore, Fig. 2d illustrates that the RSS metric decreases as load increases, indicating stronger fragmentation under higher loads.

5 Conclusion

This paper presents a heuristic algorithm for routing, band, modulation format and spectrum assignment (RBMSA) in dynamic multi-band elastic optical network (DMB-EON) that utilizes the QoT of the channels, and the spectrum occupancy information, measured by the number of cuts (NoC) and root of sum of squares (RSS) metrics. Simulation results demonstrate the effectiveness of the proposed algorithm in reducing SBR compared to benchmark algorithm by up to 33.2%, at the cost of increasing the average path length by 4.4%

Acknowledgements: This work has been supported by Sweden's innovation agency VINNOVA within the framework of the EUREKA cluster CELTIC-NEXT project AI-NET-PROTECT (2020-03506), and Vetenskapsrådet (2019-05008). Authors from UC3M acknowledge support from the CONEX-PLUS project under the Marie Sklodowska-Curie Action program (grant no. 801538) and EU-funded SEASON project (grant no.101096120).

References

[1] W. Klaus et al., "The role of parallelism in the evolution of optical fiber communication systems," *Proceedings of the IEEE*, vol. 110, no. 11, pp. 1619–1654, 2022.

[2] T. Hoshida et al., "Ultrawideband systems and networks: Beyond C + L -band," *Proceedings of the IEEE*, vol. 110, no. 11, pp. 1725–1741, 2022.

[3] B. C. Chatterjee et al., "Fragmentation problems and management approaches in elastic optical networks: A survey," *IEEE Communications Surveys & Tutorials*, vol. 20, no. 1, pp. 183–210, 2018.

[4] B. Bao et al., "SDFA: A service-driven fragmentation-aware resource allocation in elastic optical networks," *IEEE Transactions on Network and Service Management*, vol. 19, no. 1, pp. 353–365, 2022.

[5] P. Poggiolini, "A generalized gn-model closed-form formula," *arXiv preprint arXiv:1810.06545*, 2018.

[6] J. L. Ravipudi and M. Brandt-Pearce, "Impairment-and fragmentation-aware dynamic routing, modulation and spectrum allocation in c+ l band elastic optical networks using q-learning," *Optical Switching and Networking*, vol. 47, p. 100 717, 2023.

[7] Infinera Blog, *What the heck are modem SNR and holistic co-design?* `https://www.infinera.com/blog/what-the-heck-are-modem-snr-and-holistic-co-design/tag/optical/`, Accessed April 2024.

[8] F. Arpanaei et al., "Launch power optimization for dynamic elastic optical networks over C+L bands," in *International Conference on Optical Network Design and Modelling (ONDM)*, Coimbra, Portugal, 2023, ISBN: 978-3-903176-54-6.

[9] V. Curri, "Multiband optical transport: A cost-effective and seamless increase of network capacity," in *OSA Advanced Photonics Congress 2021*, Optica Publishing Group, 2021, NeTu2C.3.

[10] F. Arpanaei et al., "Hyperaccelerated power optimization in multi-band elastic optical networks," in *Optical Fiber Communications Conference and Exhibition (OFC)*, 2024, Th1I.6.

[11] P. Poggiolini et al., "Closed form expressions of the nonlinear interference for UWB systems," in *European Conference on Optical Communications (ECOC)*, 2022, Tu1D.1.

[12] M. R. Zefreh et al., "A GN-model closed-form formula supporting ultra-low fiber loss and short fiber spans," *ArXiv*, vol. /abs/2111.04584. 2021.

[13] Y. Jiang et al., "Experimental test of closed-form EGN model over C+L bands," in *European Conference on Optical Communications (ECOC)*, 2023, pp. 254–257.

[14] P. Poggiolini et al., "The GN-model of fiber non-linear propagation and its applications," *Journal of Lightwave Technology*, vol. 32, no. 4, pp. 694–721, Feb. 2014, ISSN: 1558-2213.

[15] F. Arpanaei et al., "Enabling seamless migration of optical metro-urban networks to the multi-band: Unveiling a cutting-edge 6D planning tool for the 6G era," *Journal of Optical Communications and Networking*, vol. 16, no. 4, pp. 463–480, 2024.

[16] M. Quagliotti et al., "Spectrum fragmentation metrics and their use in optical channel allocation algorithms," in *Fotonica*, 2017, pp. 1–4.

[17] F. Arpanaei et al., "Three-dimensional resource allocation in space division multiplexing elastic optical networks," *Journal of Optical Communications and Networking*, vol. 10, no. 12, pp. 959–974, 2018.

[18] C. Natalino et al., "The Optical RL-Gym: An open-source toolkit for applying reinforcement learning in optical networks," in *International Conference on Transparent Optical Networks*, 2020, Mo.C1.1.

PAPER F

Fragmentation- and QoT-Aware RBMSA with Spectrum Defragmentation in Dynamic Multi-Band Elastic Optical Networks

Ehsan Etezadi, Farhad Arpanaei, Carlos Natalino, Erik Agrell, Paolo Monti, José Alberto Hernández, Marija Furdek

Submitted to the Journal of Lightwave Technology in May 2025

The layout has been revised.

Abstract

Multi-band elastic optical networks (MB-EONs) transmit information in multiple bands to increase the available capacity. However, they suffer from QoT degradation caused by the inter-channel stimulated Raman scattering effect, which requires addressing through tailored resource assignment. Additionally, dynamically arriving and departing optical connection requests generate SF, where spectrum resources become scattered into non-continuous chunks and aggravate SBR even when the total available bandwidth is sufficient. To jointly address these challenges, we propose an SF- and QoT-aware algorithm for RBMSA, along with proactive spectrum defragmentation (SD), referred to as *SFQA-defrag*. The algorithm considers SF metrics and QoT levels of available channels across multiple candidate paths to ensure spectrum allocations that meet the QoT requirements while minimizing the SF. The SD process proactively reorganizes spectrum allocation to restore continuity, thus reducing fragmentation and lowering the SBR. The *SFQA-defrag* algorithm is evaluated against benchmark algorithms using three reference backbone topologies. The results demonstrate that it significantly reduce SBR and SF compared to benchmarks, albeit with a slight increase in the average path length.

1 Introduction

The growing demand for bandwidth, driven by high-bit-rate applications such as video streaming, cloud services, and IoT, along with the continuous emergence of new services, requires dynamic and resource-efficient optical network operations [1]. This increasing demand is rapidly surpassing the capabilities of traditional C-band elastic optical networks (EONs) [2]. Multi-band elastic optical networks (MB-EONs) provide an economical way to significantly enhance data transmission capacity by utilizing multiple wavelength bands across the optical spectrum, such as L, C, S, E, O, and U bands [3]. Within each band, the optical spectrum is divided into frequency slots of fine granularity, and a channel is formed by grouping one or more contiguous slots allocated along the path carrying a modulated optical signal. Each channel operates through a dedicated BVT, which enables flexible modulation and bit rate adaptation based on the signal quality of the lightpath. The versatility of this architecture ensures that the next-generation EON can accommodate varying traffic patterns and future growth, making it an indispensable infrastructure for enabling communication and driving innovation across industries [4]. However, the shift from conventional routing, modulation and spectrum assignment (RMSA) in EONs to routing, band, modulation format and spectrum assignment (RBMSA) in MB-EONs introduces additional complexity due to the necessity of choosing wavelength bands alongside paths, spectrum and modulation formats. Additionally, the QoT of optical lightpaths varies across wavelength bands due to nonlinear impairments. A further challenge arises from the inefficient use of transceiver (TRx) capacity, especially when low-bit-rate service requests are provisioned on dedicated lightpaths, leading to underutilized spectrum resources. Moreover, the dynamic nature of service requests leads to spectrum fragmentation (SF), where spectrum resources become fragmented into small, disjoint, and non-contiguous segments across the links [5]. This can result in inefficient network capacity utilization and higher blocking probabilities for the incoming service requests. Thus, effective resource allocation strategies in MB-EONs must consider QoT and SF simultaneously. These strategies should also incorporate traffic grooming, which aggregates multiple low-bit-rate service requests onto existing lightpaths with available capacity, minimizing the need for deploying new TRx.

To alleviate the impact of fragmentation, SF-aware RBMSA algorithms leverage information on spectrum resource utilization to minimize service blocking ratio (SBR) [6]. In addition to the preemptive, SF-aware service provisioning, SF can also be addressed through spectrum defragmentation (SD) [5]. The goal of SD is to reallocate lightpaths such that the spectral gaps are consolidated and aligned more effectively across network links, consequently allowing for the accommodation of more services and improving overall spectrum utilization. SD approaches can be categorized into two main types: reactive and proactive [7]. Reactive approaches are triggered by service-blocking events, whereas proactive approaches are executed without waiting for blocking to occur, typically by monitoring network performance metrics to determine the good timing for SD or by performing it periodically. While SD has been shown to reduce SBR, it also introduces a reconfiguration overhead, undesirable for network operators. Depending on the specific SD approach, this overhead may involve terminating, reallocating, and reestablishing selected lightpaths. The frequency of SD cycles and the number of reallocations within each cycle are key metrics used to assess SD overhead [8]. This indicates that potential improvements in SBR and the associated overhead must be jointly considered when designing and evaluating SD approaches.

In addition to SF, another aspect to consider for the resource allocation in MB-EONs is the variation of the QoT in the optical lightpaths. This variation stems from NLI, including Kerr effects and the ISRS phenomenon, which results in self-phase modulation, cross-phase modulation, and power depletion from shorter to longer wavelengths when resources outside the C-band are used [9], [10].

QoT-aware provisioning can reduce SBR and enhance spectrum usage efficiency by assigning spectrum resources that support the highest possible modulation, based on the physical-layer quality of each channel [11]. It evaluates the QoT of predefined channels, each composed of a fixed number of frequency slots, and selects the ones offering the best transmission quality. However, this approach may inadvertently exacerbate SF. This occurs because channels with the best QoT may not always be continuous across the entire source-destination path. Also, fulfilling the requested bit rate of a service request often necessitates allocating multiple non-contiguous spectrum segments, leading to several isolated channels in the same path. This issue is particularly pronounced in multi-band scenarios such as C+L+S-band networks, where differences in QoT caused by ISRS are substantial.

To address the issues mentioned above in a resource-efficient way, it is essential to balance the trade-offs between SF and QoT management in dynamic MB-EONs, and to solve the SF- and QoT-aware routing, band, modulation format and spectrum assignment (RBMSA) problem jointly. In [12], we proposed a first heuristic algorithm for the SFQA RBMSA for C+L+S-band dynamic MB-EONs. The algorithm considers two SF metrics along with the QoT of available channels on different candidate paths to determine the most suitable path and channel.

In this paper, we extend that work by proposing an enhanced algorithm referred to as *SFQA-defrag*, which integrates the SFQA RBMSA with proactive SD. The *SFQA-defrag* algorithm incorporates the occupancy state information into the path and channel selection processes. Additionally, *SFQA-defrag* includes traffic grooming during service provisioning and traffic re-grooming during SD cycles, to further improve spectrum utilization and reduce the SBR.

The physical layer model used in this study considers the impact of ISRS on both ASE noise and NLI, enabling an accurate QoT estimation across different bands [11]. Finally, the NoC metric used to evaluate SF is refined to better reflect the impact of SF across neighboring links where services are allocated over discrete channels. The performance of *SFQA-defrag* is evaluated through extensive simulations on three real-world network topologies: Japanese backbone (JPNB), United States backbone (USB), and Spanish backbone (SPNB). The results show that *SFQA-defrag* significantly outperforms benchmark algorithms that consider only QoT or SF metrics, achieving lower SBR in dynamic MB-EONs.

The rest of the paper is organized as follows. Section 2 reviews the state of the art for the resource management methods in dynamic MB-EONs. Section 3 presents the system model and physical layer assumptions. Section 4 describes *SFQA-defrag*. Section 5 outlines the simulation settings, while Section 6 evaluates the algorithm's performance. Finally, Section 7 concludes the paper.

2 Related Work

The resource allocation problem in MB-EONs is particularly challenging due to the presence of physical-layer impairments, such as ISRS. Conventional RMSA techniques, primarily developed for single-band scenarios, fall short in capturing these additional impairments and constraints, making new approaches essential to meet the required QoT levels in MB-EONs. The authors in [13] extend the RMSA problem to the RBMSA problem for the first time and present a basic GSNR-aware provisioning strategy based on the generalized Gaussian noise model, which enables more accurate QoT estimation and efficient spectrum utilization. To improve performance and reduce blocking probability, the authors in [14] develop a family of band allocation algorithms that adapt to the characteristics of service requests, such as route length and bit rate. The main idea is that selecting bands based on individual service attributes leads to more effective spectrum utilization. The authors in [15] investigate the impact of increased configuration granularity in next-generation

BVTs for flexible-grid elastic optical networks. They consider practical bandwidth variable transponders implementations, by optimizing configuration selection for data rate and bandwidth combinations.

In recent years, substantial research has focused on SF and its mitigation, utilizing integer linear program (ILP) models, (meta) heuristics, and machine learning-based techniques. The study in [16] models the proactive parallel lightpath reconfiguration problem in EONs as an ILP formulation and analyzes its computational complexity. The work in [17] explores heuristic methods for hitless bandwidth defragmentation, such as spectrum sweeping and hop tuning. In [8], SD is conducted periodically, with lightpath selection for reallocation based on service parameters. A deep reinforcement learning-based framework is developed in [18], which jointly manages when to initiate SD, which lightpaths to reconfigure, and how to reassign spectrum resources. However, most of these studies are limited to the C band and rely on fixed reach and capacity values, primarily due to the lack of efficient, low-complexity methods for QoT estimation. To the best of our knowledge, few studies focus on fragmentation management in multi-band scenarios. Some address SF-aware service provisioning, while others explore SD in multi-band optical networks.

On the SF-aware RBMSA side, the authors in [19] propose a Q-learning-based dynamic routing algorithm for C+L-band EONs, considering fiber impairments such as ISRS. The algorithm incorporates SF effects and spectrum constraints, employing first-fit, last-fit, and exact-fit allocation strategies. In [20], the authors tackle the trade-off between SNR and spectrum efficiency in C+L-band optical networks by proposing a resource allocation approach using C+L optical cross-connects with all-optical wavelength converters. Their method minimizes link load, manages SNR impacts, and reduces SF. Similarly, the authors in [21] introduce a survivability-focused RBMSA algorithm for C+L band EONs, addressing challenges such as ISRS, SF, and service disruptions caused by link failures.

Regarding SD, [22] presents an adaptive cross-layer bandwidth defragmentation algorithm to reduce bandwidth fragmentation arising from mismatches between services and channels in multi-band optical networks. Additionally, a signal-quality-aware proactive SD scheme for C+L-band EONs is presented in [23]. This approach minimizes SF and maintains QoT during spectrum retuning using machine learning-based QoT estimation. It incorporates nonlinear-

Table 1: Literature on resource allocation for MB-EONs considering impairments and SF. **SFA**: spectrum fragmentation-aware, **EGGN**: enhance generalized Gaussian noise, **TGR**: traffic grooming and re-grooming,

Reference	**SFA-RBMSA**	**SD**	**EGGN model**	**C+L+S-band**	**C+L-band**	**TGR**
[19]	✓	×	×	×	✓	×
[20]	✓	×	×	×	✓	×
[21]	✓	×	×	×	✓	×
[22]	×	✓	×	×	✓	✓
[23]	×	✓	×	×	✓	×
This study	✓	✓	✓	✓	✓	✓

impairment-aware SD algorithms to enhance spectrum utilization while addressing ISRS effects.

Table 1 summarizes the most relevant studies in the literature, specifically those addressing impairment considerations and fragmentation management in MB-EONs. To the best of our knowledge, no existing work has accounted for all impairments, including the ISRS effect in ASE and NLI noise, while simultaneously integrating SF-aware resource allocation with proactive SD. Our study addresses this gap by employing a comprehensive physical layer model that supports SF management, and QoT-aware service provisioning. In addition, we extend the analysis beyond the conventional C+L band systems considered in prior studies to include the S band, enabling performance evaluation over a broader optical spectrum.

3 System Model and Physical Layer Assumptions

In this section, we present the system model employed in this work. We outline the node functionality and network infrastructure, present the methodology used for QoT estimation, and describe the SF metrics employed in our approach. In this study, the GSNR is used as the indicator of QoT, accounting for both linear and nonlinear noise components.

3.1 Node and Network Architecture Model

We consider a network that comprises a set of nodes and links, representing a dynamic MB-EON scenario where service requests continuously arrive and depart. Transmission can take place in multiple bands, utilizing pre-defined channels. Each channel comprises six spectrum slots and has a total bandwidth of $6 \times 12.5 = 75$ GHz. For each service request, we must determine a path from the source to the destination node and a set of channels along that path that collectively meet the requested bit rate. Multiple channels may be allocated to a single service request depending on its needed bit rate, but they must all follow the same path. Additionally, the continuity constraint dictates that the channels assigned to a particular service must be the same across all links along the chosen path. The channels assigned to a path do not need to be contiguous, as each channel utilizes a separate BVT. Furthermore, we assume bidirectional traffic model, where both directions of a service request share the same path and modulation format.

Each node in the network is equipped with C+L+S-band BVTs and ROADMs, enabling reconfigurable add/drop operations across multiple bands. The in-line amplifier sites are equipped with C-band EDFAs for the C-band channels, L-band EDFAs for the L-band channels, and TDFAs for the S-band. The ASE-shaped noise is considered for the idle channels to guarantee the power profile consistency [24], [25]. Moreover, the in-line amplifier sites are equipped with DGEs to ensure optimal launch power for each span based on the fast power optimization strategy proposed in [11]. Furthermore, the BVTs at each node support flexible modulation format selection, soft-decision forward error correction, and variable bit rate operation [26] Based on the GSNR of each channel, the transmission rate of each TRx can be adaptively tuned by adjusting its modulation format. This flexibility is provided by uniform standard quadrature amplitude modulation with adaptive variable code-rate, probabilistic constellation shaping, or time-domain hybrid-format technologies [27].

The ability to vary the transmission rate at the TRx level enables traffic (re-)grooming at the optical, rather than the IP/MPLS layer. The optical layer traffic (re-)grooming is managed by an orchestrator that controls both the IP/MPLS and optical layer software-defined networking (SDN) controller agents. Consequently, when a new request arrives, the spare capacity of the already established lightpath between the same source and destination is utilized; if this spare capacity is insufficient to meet the required bit rate, a new lightpath must be deployed.

3.2 QoT estimator

For GSNR calculation, we apply an enhanced generalized Gaussian noise (EGGN) semi-closed form model to estimate the NLI noise power, including the Kerr effects and ISRS [28], [29]. The EGGN is versus the classical GGN. EGGN includes an extra term that corrects for the modulation format dependence, improving the accuracy of nonlinear interference modeling. This model was validated through field trial experiments [30]. According to the concept of incoherent GN model for uncompensated optical transmission links [31], the end-to-end GSNR for a lightpath on channel i can be derived as follows:

$$GSNR^{i}_{\mathrm{LP}}|_{\mathrm{dB}} = 10 \cdot \log_{10}\left[\left(\Sigma_{s\in S}\sigma^{s} + \sigma^{-1}_{\mathrm{TRx}}\right)^{-1}\right] - \sigma_{\mathrm{Flt}}|_{\mathrm{dB}} - \sigma_{\mathrm{Ag}}|_{\mathrm{dB}}, \quad (\mathrm{F.1})$$

$$\sigma^{s} = \left(\frac{P^{s+1,i}_{\mathrm{tx}}}{P^{s,i}_{\mathrm{ASE}} + P^{s,i}_{\mathrm{NLI}}}\right)^{-1} \quad (\mathrm{F.2})$$

Moreover, $P^{s+1,i}_{\mathrm{tx}}$ is the launch power at the beginning of span $s+1$, $P^{s,i}_{\mathrm{ASE}} = n_{\mathrm{F}} h f^{i} (G^{s,i} - 1) R_{\mathrm{ch}}$ is noise power caused by the DFA equipped with DGE, and the NLI noise power ($P^{s,i}_{\mathrm{NLI}}$) is calculated from (2) in [28]. n_{F}, h, f^{i}, $G^{s,i} = P^{s+1,i}_{\mathrm{tx}}/P^{s,i}_{\mathrm{rx}}$, S, and R_{ch} are the noise figure of DFA, the Planck constant, the channel frequency, the center frequency of the spectrum, the DFA gain, the set of spans, and the channel symbol rate, respectively. $P^{s,i}_{\mathrm{rx}}$ is the received power at the end of span s. σ_{TRx}, σ_{Flt}, σ_{Ag} are the transceiver SNR, the SNR penalty due to wavelength selective switches filtering, and the SNR margin due to aging.

Using F.1, GSNR is calculated for any lightpath from an arbitrary source to an arbitrary destination in the network. Subsequently, for each of the K shortest paths, the feasible modulation format for every channel along the path is pre-calculated by comparing the estimated GSNR of each channel to the modulation format thresholds defined in the literature [4]. The pre-computed modulation format levels are then used during the RBMSA decision

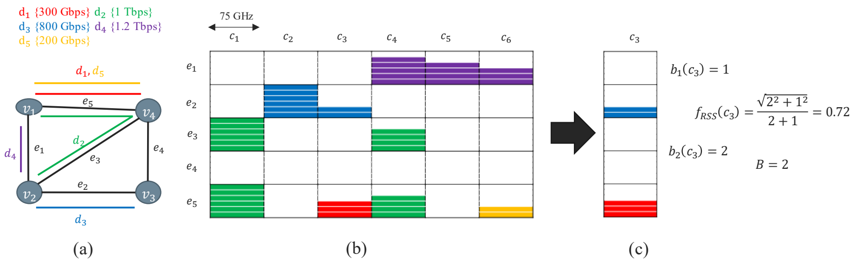

Figure 1: An example with a subset of five network links supporting five services (a). The spectrum occupancy state (b). Calculation of the root of sum of squares (RSS) metric value for channel 3 (c).

process to efficiently evaluate which path–channel combinations can satisfy a given bit rate request, reducing the computational overhead during service provisioning.

3.3 Spectrum fragmentation (SF) metrics

Various metrics have been proposed in the literature to quantify SF within an EON, enabling network operators to monitor and optimize spectrum resource utilization [32]. Our proposed fragmentation-aware method utilizes two key SF metrics, i.e., NoC and RSS, designed to gauge fragmentation of spectrum channels along the network links. Since the spectrum contiguity constraint is not required, as explained in Sec. 3.1, we adjust these metrics to focus solely on measuring the fragmentation of channels across neighboring links. Figure 1 illustrates a simple network example with four nodes, labeled v_1 to v_4, and five links, denoted by e_1 to e_5. Each link has six available channels, denoted by c_1 to c_6. Five active services, denoted by d_1 to d_5, are established in the network, and their respective channel allocations is shown in Fig. 1(b). Note that some channels are fully occupied, while others have spare capacity available for incoming service requests. Let us denote the sizes of the B free blocks on all links for a channel c by $b_1(c), \ldots, b_B(c)$. The RSS metric can then be defined as follows:

$$f_{RSS}(c) = \frac{\sqrt{\sum_{i=1}^{B} (b_i(c))^2}}{\sum_{i=1}^{B} b_i(c)} \tag{F.3}$$

Figure 1(c) illustrates the value of the RSS metric for channel c_3 as defined in (F.3).

NoC quantifies the SF level of a channel across the network. It is calculated per channel by assessing the occupancy state of that channel on all links in the network. The NoC for a given channel on a link is defined as the number of times the channel's state on that link differs from the state of the same channel on its adjacent links. The total NoC for a channel is then obtained by summing these values across all links.

In the example shown in Fig. 1(b), no service occupies channel c_3 on link e_3. Looking at its neighbors, we see that services occupy c_3 on links e_2 and e_5 while links e_1 and e_4 have c_3 unoccupied. So, there are cuts between links e_3 and e_2, as well as links e_3 and e_5. Therefore, the NoC for channel c_3 on the link e_3 is 2. The NoC value for channel c_3 on all the links can be calculated analogously, and the total NoC is obtained by summing these values, resulting in a total of 12 for this channel.

4 The Spectrum Fragmentation- and QoT-Aware (SFQA) RBMSA Algorithm with Spectrum Defragmentation (SD)

In this section, we introduce the proposed algorithm for SFQA RBMSA with proactive SD in MB-EON. We start by detailing the RBMSA algorithm, followed by a presentation of the proactive SD algorithm, and then provide a complexity analysis to evaluate their computational cost.

4.1 Spectrum Fragmentation- and QoT-Aware (SFQA) RBMSA

The core idea of the *SFQA* RBMSA algorithm is to reduce the SBR by jointly considering QoT and SF during path and channel selection. For each service request, the algorithm prioritizes paths and channels that support the highest possible modulation format while also minimizing SF. The pseudocode is presented in Algorithm 4.

Inputs include the service request d, a set of candidate paths P between the source node s and the destination node d, the complete set of usable

	c_1	c_2	c_3	c_4	c_5	c_6
e_1	0	0	0	1	1	1
e_2	0	1	1	0	0	0
e_3	1	0	0	1	0	0
e_4	0	0	0	0	0	0
e_5	1	0	1	1	0	1

(a)

	c_1	c_2	c_3	c_4	c_5	c_6
$v_1 - v_2$	6	6	6	5	4	4
$v_1 - v_3$	6	6	6	5	4	4
$v_1 - v_4$	6	6	5	4	4	3
$v_2 - v_3$	6	6	6	6	5	4
$v_2 - v_4$	6	6	5	5	5	4
$v_3 - v_4$	6	6	6	5	4	3

(b)

	c_1	c_2	c_3	c_4	c_5	c_6
$v_1 - v_2$				$(d_4, 0)$	$(d_4, 0)$	$(d_4, 1)$
$v_1 - v_3$						
$v_1 - v_4$			$(d_1, 2)$			$(d_5, 1)$
$v_2 - v_3$		$(d_3, 0)$	$(d_3, 4)$			
$v_2 - v_4$						
$v_3 - v_4$						

(c)

Figure 2: The channel occupancy matrix O (a), the modulation format table M (b), and the channel state S (c) for the simple network example in Fig. 1

channels across all frequency bands $\mathcal{C}$, the pre-calculated modulation format tables M for all paths and channels, the channel occupancy matrix O, the matrix showing the remaining capacity of the established channels S, and the selected spectrum fragmentation metric T.

To illustrate these variables, an example based on the network topology in Fig. 1 is shown in Fig. 2. Figure 2(a) shows the O matrix where 1 indicates that a channel is fully or partially occupied by a service on a link, while 0 otherwise. Figure 2(b) presents the M table, which contains the modulation format levels for K paths between each source–destination pair and for all channels. For simplicity, the example shows only the values corresponding to the shortest path of each pair. The modulation format levels in the M table range from $m = \{1, 2, 3, 4, 5, 6\}$, corresponding to bit rates from 100 Gbps to 600 Gbps. For instance, a value of 6 for a given channel means that the channel can support up to 600 Gbps. Some services may not fully utilize a channel's capacity depending on their bit rate requirements. For example, service d_3, which requires 800 Gbps, occupies the full capacity of channel c_2 and uses only 200 Gbps of channel c_3. The remaining capacity of partially used channels is tracked in the S matrix, as shown in Fig. 2(c). Each entry in the S matrix is a tuple that indicates the service request occupying the channel and the remaining capacity of its corresponding BVT on that path. In this case, the unused 400 Gbps on channel c_3 between nodes v_2 and v_3 represents an active BVT that can be used by future incoming service requests.

The algorithm's outputs are the selected path and a list of new channels that collectively meet the requested bit rate. If no suitable channels are found, the service request is blocked. The constraints are that all channels assigned to a service must follow the same path, and the continuity constraint requires that the same set of channels be available on every link along that path.

Algorithm 4: The spectrum fragmentation- and QoT-aware (SFQA) algorithm

```
Input: d, P, 𝒞, M, O, S, T
Output: C_s
C_s ← ∅; // channels selected for the service request
br ← the bit rate of d
for each p in P do
    r ← br
    for each c in S of p do
        rc ← free capacity on channel c
        if rc > 0 then
            C_s ← C_s ∪ {c}
            r ← r − β ∗ rc
            if r <= 0 then
                update the channel state S
                return p, C_s
        C_s ← ∅
    for each p in P do
        for each c in 𝒞 do
            if O(e, c) == 0 for all e in p then
                if T is RSS then
                    FS(p, c) ← F_new(p, c) − F_current(p, c)
                else if T is NoC then
                    FS(p, c) ← F_current(p, c) − F_new(p, c)
    P_sorted ← sort P by descending modulation level M(p, c), then FS(p, c)
    for each p in P_sorted do
        C_sorted ← sort channels on p by descending M(p, c), then FS(p, c)
        r ← br
        for each c in C_sorted do
            C_s ← C_s ∪ {c}
            r ← r − β ∗ M(p, c)
            if r <= 0 then
                update the channel occupancy matrix O
                update the channel state S
                return p, C_s
        C_s ← ∅
    return C_s
```

The algorithm operates in three phases. In phase one, the algorithm checks whether a service request can be accommodated using existing established channels, i.e., using traffic grooming. If grooming is not successful, the algorithm proceeds to phase two where it computes the fragmentation score (FS) for all candidate paths and available channels. Finally, in phase three, the algorithm selects a path and the corresponding channels based on the modulation format and the computed FS values. More details about each phase are provided next.

In phase one (lines 3–13), upon arrival of service request d, the algorithm starts by analyzing all candidate paths between the source and destination nodes. For each candidate path $p \in P$, the algorithm initializes a temporary variable r with the required bit rate of the service request (line 4). It then iterates through the set of established channels along p stored in S. For each channel c, the algorithm retrieves the remaining free capacity rc and checks whether it is greater than zero (lines 6–7). If a channel has available capacity, it is added to the set of selected channels and $\beta \times rc$ is subtracted from r (lines 8–9), where β is the unit of capacity per modulation level (set at 100 Gbps in our work). This indicates how much of the service request bit rate can be covered by reusing that channel. If there is sufficient free capacity on existing channels to accommodate the entire request, the updated value of r drops to zero or less (line 10), triggering an update in S and returning the selected path p along with the set of reused channels C_s (lines 11–12). If no path can fully accommodate the service request using existing channels, the algorithm proceeds to the second phase.

The second phase (lines 14–20) starts by identifying the free channels along each candidate path using the occupancy information from the O.

For each candidate channel, the algorithm calculates the difference in FS obtained by assigning the channel to the service request F_{new}, relative to the current value F_{current} (lines 17–20). If RSS is used as the metric, F_{current} and F_{new} are determined by (F.3). If the metric is NoC, then F_{current} and F_{new} correspond to the respective NoC values for channel c. Since low SF corresponds to either a high RSS or a low NoC value, the FS must be defined differently for the two metric to represent improvements in SF consistently. With the RSS metric, the FS is defined as $FS = F_{\text{new}} - F_{\text{current}}$, whereas with NoC, $FS = F_{\text{current}} - F_{\text{new}}$. The algorithm is designed to select the channels with the highest FS values, as they correspond to the greatest reduction in SF.

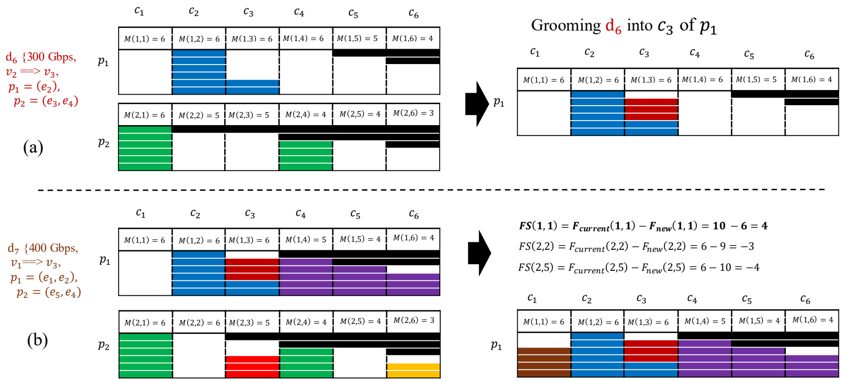

Figure 3: An example of the SFQA algorithm provisioning a new service via traffic grooming (a), and by establishing a new lightpath (b).

The third phase of the algorithm identifies the best path-channel(s) combination that satisfies the service request. The list of candidate paths is sorted (P_{sorted}) in the descending order of the highest supported modulation format, recorded in $M(p, c)$ (line 21). In case of ties, paths are further ranked based on the highest FS of their candidate channels.

For each path in P_{sorted}, the available channels are then sorted in the descending order of their modulation format level (line 23), or the FS value if the modulation levels are the same. The sorted channels are then iteratively selected to support the current request (lines 26–27) until the requested bit rate is fully served and r becomes zero or less (line 28). At this point, the channel occupancy matrix O is updated to reflect the new allocation. S is also adjusted to reflect the remaining free capacity on the selected channels (lines 29–31). However, if there are not enough channels along a path to meet the requested bit rate, the selected channels are cleared, and the algorithm proceeds to the next path (line 32). Should none of the paths provide sufficient channels to satisfy the request, the algorithm returns an empty set C_s, indicating that the service request d cannot be accommodated and is therefore blocked (lines 32–33).

Figure 3 provides an illustrative example of the *SFQA* algorithm for the network topology from Figure 1, where two candidate paths are considered for each incoming service request. The modulation format level for each path–channel pair is shown as $M(p, c)$. The blacked-out parts in each channel indicate capacity that cannot be utilized due to the limitations of the selected modulation format. For example, if the modulation format level is 4, then 4 out of 6 capacity units can be used, and the remaining 2 are marked in black.

In Fig. 3(a), when service request d_6 arrives, requiring 300 Gbps between nodes v_2 and v_3, the algorithm first attempts to groom the traffic by checking whether any of the established channels along the candidate paths p_1 and p_2 have sufficient free capacity. Since p_1 is the shorter path, p_1 is checked first. Channel c_3 of sufficient free capacity, allowing the service to be supported without activating a new channel. Figure 3(b) depicts the arrival of service request d_7, requiring 400 Gbps from v_1 to v_3. While two paths are available, neither has an established channel with enough capacity to accommodate d_7. Hence, a new lightpath is needed. Channels c_1 on p_1 and c_2 and c_5 on p_2 are available. The algorithm calculates the FS for each channel based on the NoC metric, as shown on the right side of Fig. 3(b). For example, for channel c_1 on path p_1, the fragmentation score is computed as $FS(1,1) = F_{\text{current}}(1,1) - F_{\text{new}}(1,1) = 4$. This score reflects the reduction in SF if c_1 is used by d_7. Among the candidates, c_1 on p_1 and c_2 on p_2 offer the same highest modulation format level, so c_1 on p_1 is selected due to its superior FS.

4.2 Proactive spectrum defragmentation

The proposed SD algorithm proactively initiates SD cycles, which can be triggered periodically or when a performance indicator threshold is exceeded. The pseudo-code for an SD cycle of *SFQA-defrag* is presented in Algorithm 5. The main objective of the SD algorithm is to reduce spectrum fragmentation by reorganizing the channels which improve the SF most significantly. Rather than reallocating entire services, individual service channels are considered for reallocation the fact that multiple non-contiguous channels can be assigned to a single service and reallocated independently.

The algorithm receives as input the set of active services whose channels are candidates for reallocation, D, the maximum number of service channels allowed for reallocation, N, the list of the channels $\mathcal{C}$, pre-calculated modulation format table M, the channel occupancy matrix O, the channel state matrix S, and the selected spectrum fragmentation metric T to be used.

Algorithm 5: The spectrum defragmentation (SD) cycle

Input: D, N, $\mathcal{C}$, M, O, S

$MovedCount \leftarrow 0$;
$D_s \leftarrow \varnothing$; `// service selected for reallocation`
for *each* d *in* D **do**
  for *each* c *in channels of* d **do**
    if *there is a channel* c' *on the same path that can be re-groomed with* c *by checking* S **then**
      Re-groom c and c'
      Update S
      Update O
      $MovedCount \leftarrow MovedCount + 1$;
    if $MovedCount \geq N$ **then**
      break ; `// Stop if the maximum allowed movements are reached`
$DO \leftarrow \varnothing$;
for *each* d *in* D **do**
  for *each* c *in channels of* d **do**
    if c *is fully occupied by* d **then**
      if T *is RSS* **then**
        $DS(p_d, c) \leftarrow F_{\text{removed}}(p_d, c) - F_{\text{current}}(p_d, c)$
      else if T *is NoC* **then**
        $DS(p_d, c) \leftarrow F_{\text{current}}(p_d, c) - F_{\text{removed}}(p_d, c)$
      if $DS(p_d, c) > 0$ **then**
        $DO \leftarrow DO \cup (c, d, DS(p_d, c))$
$DO_{\text{sorted}} \leftarrow$ sort DO by descending $DS(p, c)$,
$RS_{\text{best}} \leftarrow 0$;
$c_{\text{target}} \leftarrow \varnothing$;
for *each* $(c, d, DS(p_d, c))$ *in* DO_{sorted} **do**
  for *each* c' *in* $\mathcal{C}$ **do**
    if $O(e, c') == 0$ *for all* e *in* p_d **then**
      if $M(p_d, c') >= M(p_d, c)$ **then**
        if T *is RSS* **then**
          $RS(p_d, c') \leftarrow F_{\text{new}}(p_d, c') - F_{\text{current}}(p_d, c')$
        else if T *is NoC* **then**
          $RS(p_d, c') \leftarrow F_{\text{current}}(p_d, c') - F_{\text{new}}(p_d, c')$
        if $RS(p_d, c') > RS_{best}$ **then**
          $RS_{\text{best}} \leftarrow RS_d(i)$
          $c_{\text{target}} \leftarrow c'$
  if $RS_{best} \geq DS(p_d, c)$ **then**
    move channel c to c_{target}
    update the channel occupancy matrix O
    update the channel state S
    $MovedCount \leftarrow MovedCount + 1$;
  if $MovedCount \geq N$ **then**
    break ; `// Stop if the maximum allowed movements are reached`

SFQA-defrag comprises three parts. The aim of the first is to re-groom traffic by consolidating partially occupied channels and freeing up resources. In the second part, the best service channel for reallocation is identified. In the third, the algorithm seeks the best target channel to reassign the selected service channel. More details on each part are provided next.

The first step iterates through all active services and their associated channels. For each service channel c, it checks whether another channel c' on the same path can be re-groomed with it, based on the remaining capacity recorded in S (lines 36–38). If re-grooming is possible, the channels are consolidated and channel c' is freed up. The O and S are updated to reflect new allocations, and the counter of the number of moved service channels is incremented (lines 39–42). Re-grooming is preferred because it releases resources. In contrast, channel reallocation merely relocates a channel to a position that is more favorable in terms of SF. If the number of moved service channels reaches the maximum allowable limit N, the algorithm stops (lines 43–44). Otherwise, it moves to the second part.

The second part identifies the best service channels for reallocation. The defragmentation options are stored in set DO, initially empty (line 45). The algorithm calculates the defragmentation score (DS) for the fully occupied channels, i.e., channels of fully utilized capacity on a given path. This ensures that only channels with no remaining capacity are considered for reallocation, avoiding unnecessary movement of partially utilized channels that could accommodate additional services (lines 46–48). For each eligible service channel, the algorithm calculates the value of DS by hypothetically removing the channel and computing the difference in the SF metric before F_{current} and after its removal F_{removed} (lines 49–52). The goal is to identify channels whose removal would improve the overall fragmentation state of the spectrum. The definition of the DS depends on the selected SF metric. If RSS is used, higher values indicate lower SF. The score is computed as $F_{\text{removed}} - F_{\text{current}}$. A positive value means that removing the channel leads to an increase in RSS, and thus, a decrease in SF. In contrast, when NoC is used, lower values indicate less fragmentation. The score is calculated as $F_{\text{current}} - F_{\text{removed}}$. A positive value in this case implies a reduction in SF. Therefore, in both cases, the algorithm selects the reallocation that yields the highest DS. Only service channels with a positive DS value, i.e., indicating that their removal would reduce SF, are added to DO, along with their corresponding service and computed score (lines 53–54). This list is then sorted in descending order based on the DS values, so that the channels offering the highest potential improvement in SF are considered first (line 55)

In the third phase, the algorithm begins by initializing two variables: one to keep track of the best SF improvement score found, and another to store the corresponding target channel (lines 56–57). For each candidate service channel in the sorted DO, the algorithm searches along the same path for alternative channels that are currently free and compatible, meaning they can support the modulation format of the candidate service channel, based on the values in the M table (lines 58–61). Each eligible target channel is then evaluated by computing the reallocation score (RS), which measures the change in SF if the service channel were moved to that channel. To calculate RS, the algorithm hypothetically assumes that the candidate target channel is chosen for reallocation and the service channel is moved to it. The RS value is calculated as the difference in the SF metric before and after this hypothetical movement. Depending on the chosen SF metric, the algorithm selects the reallocation option that yields either a higher value (for RSS) or a lower value (for NoC) (lines 62–65). Next, the algorithm compares the calculated RS for the current target channel with the highest score found so far (line 66) and updates the best target channel, denoted as c_{target}, if the new RS value is better (lines 67–68).

After evaluating RS for all available target channels and identifying the best option, the algorithm compares the RS with the DS of the candidate service channel (line 69). This comparison determines whether removing the service channel and moving it to a new channel would yield a benefit in terms of the SF metric. If no improvement is achieved, the movement is not executed. If there is a gain in the SF metric, the selected service channel, c, is reallocated to the target channel. The counter for the number of moved service channels is incremented, and the channel occupancy (O) and channel state (S) matrices are updated (70-73). The algorithm continues until the maximum number of allowed reallocated service channels, N, is reached, at which point the SD cycle terminates (lines 74–75).

Figure 4 illustrates an example of a SD cycle based on the network state shown in Fig. 1, after accommodating service requests d_6 and d_7. In the first phase, the algorithm scans all active services and their corresponding channels to identify candidates for traffic re-grooming. Services d_5 and d_1

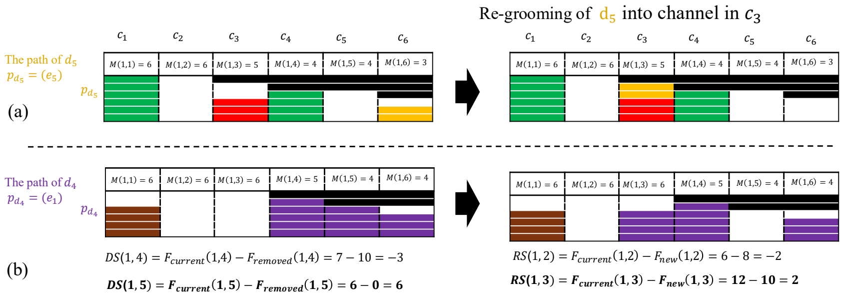

Figure 4: An example of defragmentation done via traffic re-grooming (a), and by reallocating a service channel (b).

share the same path, and channel c_3 has sufficient capacity to accommodate d_5. Consequently, the service channel of d_5 is consolidated to channel c_3. As a result, the original service channel of c_6 is released (Fig. 4(a)).

In the second phase, the algorithm identifies candidates for reallocation (Fig. 4(b)). For simplicity, only service channels c_4 and c_5 of node d_4 are considered in this example. The DS value is computed for these channels based on the NoC metric. As a result, c_5 is selected for reallocation due to its higher DS value.

In the third phase, the algorithm searches for the best target channel along the path of d_4, considering free channels that support the modulation format of c_5. Channels c_2 and c_3 meet these criteria. For each candidate target channel, the algorithm calculates RS, as shown on the right side of Fig. 4(b). The RS is computed based on the NoC metric, ultimately selecting c_3 as the target channel.

4.3 Complexity Analysis

In the worst-case scenario, when phase 1 of the *SFQA* algorithm fails to accommodate the incoming request through grooming, the algorithm proceeds to evaluate all path–channel combinations. This includes checking the modulation format level from the M look-up table and sorting the available channels for each of the $|P|$ candidate paths. The total time complexity can be expressed as:

$$T_{\text{SFQA}} = O\big(|P||\text{S}|\big) + O\big(|P|\,|C|\big) + O\big(|P|\,|C|\log|C|\big)$$

which simplifies to by considering $\max|\mathrm{CS}| = |C|$

$$T_{\mathrm{SFQA}} = O\big(|P|\,|C|\,\log|C|\big).$$

For the *SFQA-defrag* algorithm, the worst-case time complexity of the SD cycle, assuming no early termination, can be expressed as:

$$\begin{aligned} T_{\mathrm{SD}} = {} & O(|D|\,C_d) + O(|D|\,C_d) \\ & + \; O\big(|D|\,C_d\,\log(|D|\,C_d)\big) + O(|D|\,C_d\,|C|), \end{aligned}$$

where $|D|$ is the number of demands and C_d the number of channels per demand. Noting that $C_d \le |C|$, this expression simplifies to

$$T_{\mathrm{SD}} = O(|D|\,|C|^2).$$

Despite these worst-case bounds, both *SFQA* and *SFQA-defrag* maintain lightweight computational complexity, making them suitable for real-time spectrum reallocation in dynamic MB-EON environments.

5 Simulation Setting

This study explores C+L+S-band EONs with a total bandwidth of 20 THz, distributed as 6 THz for the C-band, 6 THz for the L-band, and 8 THz for the S-band, divided into 268 channels, each occupying 75 GHz (6×12.5 GHz). A 400 GHz guard band is maintained between adjacent bands. Simulations are conducted on three topologies: the JPNB (12 nodes and 17 links), the USB topology (14 nodes and 22 links), and the SPNB topology (30 nodes and 56 links) [11]. The maximum span length is set to 80 km. The analysis considers six modulation formats, from PM-BPSK to PM-64QAM, operating at 64 Gbaud, with supported bit rates ranging from 100 Gbps (PM-BPSK) to 600 Gbps (PM-64QAM). In our simulation, we set $\beta = 100$ Gbps, corresponding to the granularity of modulation level.

The network utilizes EDFAs with noise figures of 4.5 dB and 5 dB for the C- and L-bands, respectively, and a TDFA with a 6 dB noise figure for the S-band. Standard single-mode fiber with a zero-water peak is assumed, with spectrum continuity constraints applied for channel assignments along given paths.

Service requests are characterized by randomly generated end nodes, uniformly selected, and bit-rates uniformly distributed between 50 Gbps and 600 Gbps, with a granularity of 50 Gbps. The arrival of service requests follows a Poisson process with an average arrival rate of $\lambda = 25$ requests per unit time. The service request holding time is modeled as a negative exponential distribution with an average of $1/\mu$ unit time. Consequently, the offered traffic load is expressed as λ/μ normalized traffic units (NTUs). Given that the average bit-rate of a single request is 325 Gbit/s, a traffic load of 100 NTUs corresponds to approximately 32.5 Tbps of offered traffic load. The offered traffic load is approximately adjusted to achieve a SBR between 0.01% and 1% for the proposed *SFQA-defrag* algorithm. Each simulation run processes two million service requests employing the *SFQA* algorithm for each request. The parameter K, representing the number of pre-computed shortest paths, is fixed at 3. The proposed defragmentation algorithm is implemented within the Optical RL-Gym framework for efficient evaluation and comparison [33].

This study considers two variations of the *SFQA* algorithm, differentiated by the SF metric used. The version employing the NoC metric is termed *SFQA-NoC*, while the version using the RSS metric is referred to as *SFQA-RSS*. When the RBMSA algorithm is combined with proactive SD, the resulting algorithms are named *SFQA-defrag-NoC* and *SFQA-defrag-RSS*. Specifically, *SFQA-defrag-NoC* applies the NoC metric in both the RBMSA and SD processes, while *SFQA-defrag-RSS* uses the RSS metric. The SD period is set to 10 service request arrivals, with a maximum of $N = 10$ allowed reallocations for proactive SD. These values are chosen to have a balance between SBR gain and SD overhead [8].

To evaluate the performance of the proposed algorithm, we compare it with three benchmark algorithms: *QA*, which considers only the QoT of the channels during resource assignment [11]; *FA-NoC* and *FA-RSS*, which rely solely on fragmentation metrics, specifically the NoC and RSS, respectively; and *SAP*, a baseline approach that selects the shortest path first and then identifying the channel supporting the highest efficient modulation format along that path. For all methods, when identical modulation formats or SF metrics are encountered, channels with the lowest frequency are prioritized.

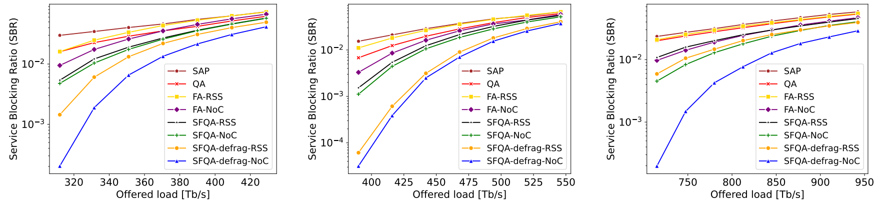

(a) JPNB topology **(b)** USB topology **(c)** SPNB topology

Figure 5: The service blocking ratio (SBR) for the three topologies under exam.

6 Numerical results

Figures 5a, 5b, and 5c show the SBR for various strategies under different offered traffic loads for the JPNB, USB, and SPNB topologies, respectively. The results show that *QA* consistently outperforms *SAP* by 23.7%, 19%, and 10% for the JPNB, USB, and SPNB topologies, respectively. This indicates that prioritizing physical-layer knowledge in the service provisioning process leads to improved performance. Furthermore, it becomes clear from the figures that the algorithms *FA-NoC* and *FA-RSS*, which incorporate only SF metrics into the decision-making process, outperform *SAP* across all topologies.

The *SFQA* algorithm, which jointly considers QoT and SF, achieves superior performance compared to all benchmark algorithms. Specifically, the *SFQA-NoC* algorithm slightly outperforms *SFQA-RSS*, and significantly surpasses *QA* and *FA-NoC* by 23% and 22% on average across all traffic loads for the JPNB topology. A similar trend is observed for the USB topology, where *SFQA-NoC* outperforms *QA* and *FA-NoC* by 28% and 19% on average, with performance levels close to *SFQA-RSS*. However, a different trend is seen for the SPNB topology, where *SFQA-NoC* outperforms *SFQA-RSS* by 22%. Additionally, in the SPNB topology, *SFQA-NoC* outperforms the *QA* and *FA-NoC* algorithms by 39% and 22%, respectively. The overall superior performance of the *SFQA* algorithms over *QA* highlights the benefits of incorporating occupancy state information into the path and channel selection processes. Also, jointly considering both QoT and SF metrics leads to more informed routing and allocation decisions, resulting in improved resource utilization compared to strategies focusing on only one aspect.

Figure 5 also presents the SBR results for *SFQA-defrag-RSS* and *SFQA-*

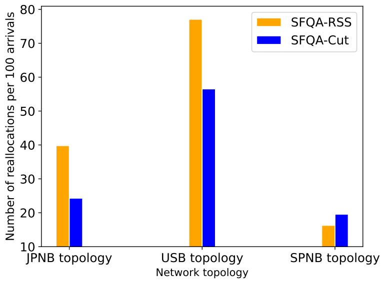

(a) Number of reallocations

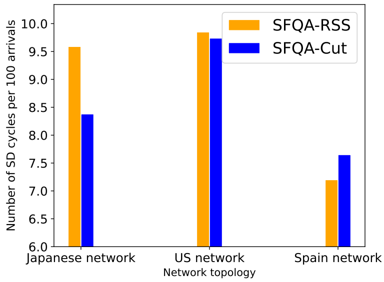

(b) Number of completed SD cycles

Figure 6: Spectrum defragmentation (SD) overhead for three network topologies.

defrag-NoC, which combine RBMSA with the proposed proactive SD method. These algorithms outperform their counterparts, i.e., *SFQA-defrag-NoC* and *SFQA-defrag-RSS* show 41.2% and 20% improvements over *SFQA-NoC* and *SFQA-RSS*, respectively, for the JPNB topology. Similar improvements (i.e, 43% and 41%) are observed for the USB topology. For the SPNB topology, the improvements are 44% and 18%. It is important to note that SD introduces additional overhead in terms of the number of reallocations and completed SD cycles, which are crucial factors in evaluating SD algorithms. Figure 6 illustrates the average number of channel reallocations and completed SD cycles for the network topologies under exam. The performance gains of *SFQA-defrag-NoC* come at a cost of 8.3 completed SD cycles and 23.8 reallocations (per 100 arrivals) for the JPNB topology. The numbers for *SFQA-defrag-RSS* become 9.5 SD completed cycles and 39.6 reallocations. Given that we start one SD cycle every ten service arrivals, and we allow at most N = 10 reallocations per cycle, the theoretical maximum number of SD cycles per 100 arrivals is 10, resulting in potentially 100 total reallocations. However, these limits are never reached regardless of the topology. The number of SD cycles and reallocations varies across the three network topologies, depending on their specific characteristics, such as path diversity and link distribution, which influence the level of fragmentation and modulation format of the channels. These factors affect how often reallocation opportunities arise and how effective they are in reducing SF.

The effects of SF metrics on the performance of the proposed algorithms

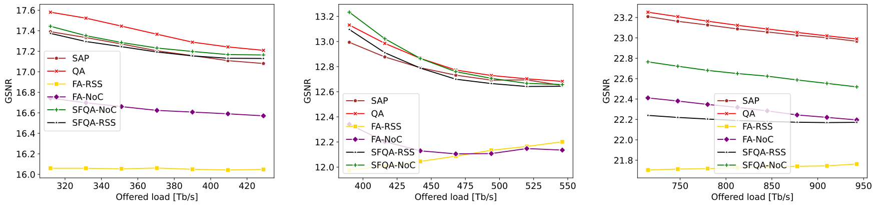

(a) JPNB topology **(b)** USB topology **(c)** SPNB topology

Figure 7: The average generalized signal to noise ratio (GSNR) for the three topologies under exam.

in terms of SBR can be analyzed by comparing the performance of *SFQA-defrag-RSS* and *SFQA-defrag-NoC*, as shown in the Fig. 5. In all three topologies, *SFQA-defrag-NoC* consistently outperforms *SFQA-defrag-RSS*, suggesting that the NoC metric better represents the level of SF in the network. However, the SD overhead must also be considered (Fig. 6). In the JPNB topology, *SFQA-defrag-NoC* is superior to *SFQA-defrag-RSS* by 29% while requiring fewer reallocations and SD cycles. In the USB topology, both algorithms perform similarly in terms of SBR and SD cycles, though *SFQA-defrag-RSS* reallocates 26% more service channels. For the SPNB topology, *SFQA-defrag-NoC* demonstrates significantly better SBR performance than *SFQA-defrag-RSS* by 46%, albeit reallocating 15.7% more service channels with 6% more SD cycles. A similar trend is observed in the RBMSA algortihms without SD, where *SFQA-NoC* shows better performance than *SFQA-RSS*, and *FA-NoC* outperforms *FA-RSS*. These results highlight that the NoC metric is better suited than RSS for capturing SF in MB-EONs where services are allocated over discrete channels.

Figure 7 shows the average GSNR levels across different scenarios for the topologies under exam. Since paths are not changed during the reallocation process in *SFQA-defrag*, their GSNR levels are close to those of the corresponding *SFQA* algorithms and are therefore not shown in the figure. Among all the algorithms, *QA* achieves the highest GSNR, surpassing the *SFQA* variants by 1%, 0.5%, and 4% for the JPNB, USB, and SPNB topologies, respectively. However, this improvement in signal quality does not translate into better performance in terms of SBR. On the contrary, the SBR results presented earlier show that the *SFQA* algorithms significantly outperform *QA*.

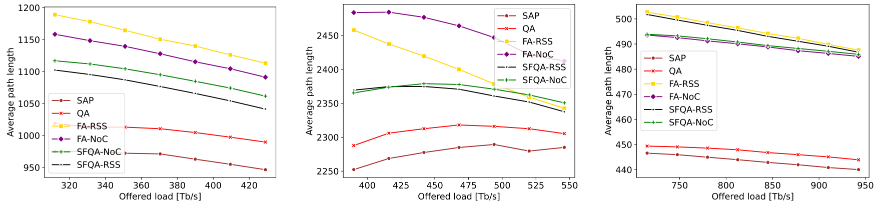

(a) JPNB topology **(b)** USB topology **(c)** SPNB topology

Figure 8: The average path length for the three topologies under exam.

This implies that while *QA* selects the best channels in terms of GSNR levels, its failure to consider SF of the channel grid leads to degraded performance compared to the *SFQA* algorithms. This observation highlights the importance of incorporating occupancy state and SF information into the routing and spectrum allocation process, rather than relying solely on physical-layer quality parameters. Also, the worst GSNR levels are observed for *FA-NoC* and *FA-RSS*, which rely solely on fragmentation metrics and disregard QoT of the channels.

Figure 8 shows the average path lengths for different scenarios under various loads for all topologies under exam. As seen in the figure, the benefit of *SFQA* in terms of SBR comes at the cost of longer paths. Specifically, the *SFQA-NoC* algorithm exhibits (on average) paths that are 8% and 13% longer than those obtained with the *QA* and *SAP* algorithms for the JPNB topology, 2% and 4% longer for the USB topology, and 9% and 10% longer for the SPNB topology. This behavior arises because *SFQA* prioritizes SF reduction when selecting paths and channels. As a result, it may bypass the shortest path in favor of routes that offer better spectrum availability, ultimately lowering the SBR. As expected, the *SAP* algorithm performs best in this metric, as it prioritizes shorter path lengths over other metrics.

7 Conclusion

This paper presents a heuristic algorithm for routing, band, modulation format, and spectrum assignment in multi-band elastic optical networks, leveraging quality of transmission-aware knowledge and spectrum fragmentation (SF) metrics, such as NoC and root of sum of squares (RSS). The proposed approach integrates proactive spectrum defragmentation (SD) and traffic grooming for incoming service requests, alongside traffic re-grooming during SD cycles, to enhance spectral efficiency.

Simulation results across three network topologies demonstrate that the proposed algorithm significantly reduces service blocking ratio compared to benchmark algorithm by up to 44%, on average for topologies, while improving SF metrics. This improvement comes at the cost of a modest increase in average path length, which is observed to rise by up to 13%. Additionally, the analysis highlights the importance of selecting appropriate SFs, as *SFQA-defrag-NoC* outperforms *SFQA-defrag-RSS* for all the topologies. These results emphasize that incorporating fragmentation and occupancy information into the resource allocation process can lead to more effective spectrum utilization than relying solely on physical-layer quality indicators.

References

[1] P. A. Baziana, "Optical data center networking: A comprehensive review on traffic, switching, bandwidth allocation, and challenges," *IEEE Access*, vol. 12, pp. 186 413–186 444, 2024.

[2] W. Klaus et al., "The role of parallelism in the evolution of optical fiber communication systems," *Proceedings of the IEEE*, vol. 110, no. 11, pp. 1619–1654, 2022.

[3] T. Hoshida et al., "Ultrawideband systems and networks: Beyond C + L -band," *Proceedings of the IEEE*, vol. 110, no. 11, pp. 1725–1741, 2022.

[4] F. Arpanaei et al., "Enabling seamless migration of optical metro-urban networks to the multi-band: Unveiling a cutting-edge 6D planning tool for the 6G era," *Journal of Optical Communications and Networking*, vol. 16, no. 4, pp. 463–480, 2024.

[5] B. C. Chatterjee et al., "Fragmentation problems and management approaches in elastic optical networks: A survey," *IEEE Communications Surveys & Tutorials*, vol. 20, no. 1, pp. 183–210, 2018.

[6] B. Bao et al., "SDFA: A service-driven fragmentation-aware resource allocation in elastic optical networks," *IEEE Transactions on Network and Service Management*, vol. 19, no. 1, pp. 353–365, 2022.

[7] R. Wang and B. Mukherjee, "Provisioning in elastic optical networks with non-disruptive defragmentation," *Journal of Lightwave Technology*, vol. 31, no. 15, pp. 2491–2500, 2013.

[8] J. Comellas, L. Vicario, and G. Junyent, "Proactive defragmentation in elastic optical networks under dynamic load conditions," *Photonic Network Communications*, vol. 36, no. 1, pp. 26–34, 2018.

[9] P. Poggiolini, "A generalized gn-model closed-form formula," *arXiv preprint arXiv:1810.06545*, 2018.

[10] D. Semrau, R. I. Killey, and P. Bayvel, "A closed-form approximation of the gaussian noise model in the presence of inter-channel stimulated raman scattering," *Journal of Lightwave Technology*, vol. 37, no. 9, pp. 1924–1936, 2019.

[11] F. Arpanaei, M. R. Zefreh, Y. Jiang, *et al.*, "Synergizing hyper-accelerated power optimization and wavelength-dependent qot-aware cross-layer design in next-generation multi-band eons," *arXiv preprint arXiv:2411.02911*, 2024.

[12] E. Etezadi, F. Arpanaei, C. Natalino, *et al.*, "Joint fragmentation-and qot-aware rbmsa in dynamic multi-band elastic optical networks," in *2024 24th International Conference on Transparent Optical Networks (ICTON)*, IEEE, 2024, pp. 1–5.

[13] N. Sambo, A. Ferrari, A. Napoli, *et al.*, "Provisioning in multi-band optical networks," *Journal of Lightwave Technology*, vol. 38, no. 9, pp. 2598–2605, 2020.

[14] F. Calderón, A. Lozada, P. Morales, *et al.*, "Heuristic approaches for dynamic provisioning in multi-band elastic optical networks," *IEEE Communications Letters*, vol. 26, no. 2, pp. 379–383, 2021.

[15] J. Müller, G. Di Rosa, O. Jovanovic, *et al.*, "Physical-layer-aware multi-band optical network planning framework for rate-adaptive transceivers," *Journal of Optical Communications and Networking*, vol. 16, no. 5, B71–B80, 2024.

[16] M. Zhang, C. You, and Z. Zhu, "On the parallelization of spectrum defragmentation reconfigurations in elastic optical networks," *IEEE/ACM Transactions on Networking*, vol. 24, no. 5, pp. 2819–2833, 2016.

[17] M. Zhang, Y. Yin, R. Proietti, Z. Zhu, and S. B. Yoo, "Spectrum defragmentation algorithms for elastic optical networks using hitless spectrum retuning techniques," in *2013 Optical Fiber Communication Conference and Exposition and the National Fiber Optic Engineers Conference (OFC/NFOEC)*, IEEE, 2013, pp. 1–3.

[18] E. Etezadi, C. Natalino, R. Diaz, *et al.*, "Deep reinforcement learning for proactive spectrum defragmentation in elastic optical networks," *Journal of Optical Communications and Networking*, vol. 15, no. 10, E86–E96, 2023.

[19] J. L. Ravipudi and M. Brandt-Pearce, "Impairment-and fragmentation-aware dynamic routing, modulation and spectrum allocation in c+ l band elastic optical networks using q-learning," *Optical Switching and Networking*, vol. 47, p. 100 717, 2023.

[20] Y. Teng, H. Yang, Q. Yao, *et al.*, "Srs-proactive-aware resource allocation based on all-optical wavelength converters in c+ l band optical networks," *Journal of Lightwave Technology*, 2024.

[21] Y. Liu, N. Feng, L. Shen, J. Lv, D. Yan, and J. Zhao, "Fragmentation and isrs-aware survivable routing, band, modulation, and spectrum allocation algorithm in multi-band elastic optical networks," *Applied Sciences*, vol. 14, no. 11, p. 4755, 2024.

[22] J. Liu, Z. Xi, and R. Gu, "Adaptive cross-layer bandwidth defragmentation for multi-band optical network," in *2023 Asia Communications and Photonics Conference/2023 International Photonics and Optoelectronics Meetings (ACP/POEM)*, IEEE, 2023, pp. 1–5.

[23] R. K. Jana, B. C. Chatterjee, A. P. Singh, *et al.*, "Machine learning-assisted nonlinear-impairment-aware proactive defragmentation for c+ l band elastic optical networks," *Journal of Optical Communications and Networking*, vol. 14, no. 3, pp. 56–68, 2021.

[24] F. Arpanaei et al., "Launch power optimization for dynamic elastic optical networks over C+L bands," in *International Conference on Optical Network Design and Modelling (ONDM)*, Coimbra, Portugal, 2023, ISBN: 978-3-903176-54-6.

[25] V. Curri, "Multiband optical transport: A cost-effective and seamless increase of network capacity," in *OSA Advanced Photonics Congress 2021*, Optica Publishing Group, 2021, NeTu2C.3.

[26] Infinera Blog, *What the heck are modem SNR and holistic co-design?* `https://www.infinera.com/blog/what-the-heck-are-modem-snr-and-holistic-co-design/tag/optical/`, Accessed April 2024.

[27] J. Cho et al., "Probabilistic constellation shaping for optical fiber communications," *Journal of Lightwave Technology*, vol. 37, no. 6, pp. 1590–1607, 2019.

[28] P. Poggiolini et al., "Closed form expressions of the nonlinear interference for UWB systems," in *European Conference on Optical Communications (ECOC)*, 2022, Tu1D.1.

[29] M. R. Zefreh et al., "A GN-model closed-form formula supporting ultra-low fiber loss and short fiber spans," *ArXiv*, vol. /abs/2111.04584. 2021.

[30] Y. Jiang et al., "Experimental test of closed-form EGN model over C+L bands," in *European Conference on Optical Communications (ECOC)*, 2023, pp. 254–257.

[31] P. Poggiolini et al., "The GN-model of fiber non-linear propagation and its applications," *Journal of Lightwave Technology*, vol. 32, no. 4, pp. 694–721, Feb. 2014, ISSN: 1558-2213.

[32] M. Quagliotti et al., "Spectrum fragmentation metrics and their use in optical channel allocation algorithms," in *Fotonica*, 2017, pp. 1–4.

[33] C. Natalino, T. Magalhães, F. Arpanaei, *et al.*, "Optical networking gym: An open-source toolkit for resource assignment problems in optical networks," *Journal of Optical Communications and Networking*, vol. 16, no. 12, G40–G51, 2024.